Analyzing Runoff Dynamics of Paved Soil Surface Using Weighable Lysimeters

vorgelegt von
Dipl.-Ing.
Yong-Nam Rim
aus Pyongyang, Korea (DVR)

Von der Fakultät VI - Planen | Bauen | Umwelt
der Technischen Universität Berlin
zur Erlangung des akademischen Grades
Doktor der Ingenieurwissenschaften
- Dr. -Ing. -

genehmigte Dissertation

Promotionsausschuss:

Vorsitzender: Prof. Dr. Bernd-Michael Wilke
Berichter: Prof. Dr. Gerd Wessolek
Berichter: Prof. Dr. Wilfred Endlicher

Tag der wissenschaftlichen Aussprache: 28.04.2011

Berlin 2011

D83

Danksagung

Mein größter Dank gilt Prof. Dr. Gerd Wessolek, dass er mir als "Außenstehender" die Möglichkeit gab, an seinem Fachgebiet wissenschaftlich arbeiten zu können. Danke für das Verständnis, die herzliche Förderung und das mir stets entgegengebrachte Vertrauen. Dank ihm weiß ich, was wissenschaftliches Arbeiten heißt und wie man es anfängt.

Weiterer Dank gilt Prof. Dr. Wilfred Endlicher für die Bereitschaft, meine Arbeit zu begutachten, vor allem dafür, dass er mir als Sprecher des gesamten Graduiertenkollegs wertvolle Impulse gab und mich motivierte, förderte und mir eine außergewöhnliche Sichtweise des Forschens vermittelte.

Ich danke Dr. Thomas Nehls ganz herzlichst dafür, dass er mit Geduld, Verständnis und breiter Diskussion meine Forschungsarbeit angeleitet, mit offenen Ohren meiner wenigen Kenntnis großes Selbsbewusstsein geschenkt und mich die ganze Strecke lang herzlich begleitet hat.

Ohne die wissenschaftstechnische und praktische Wegleitung durch Dr. Steffen Trinks wäre das Projekt so nicht zustande gekommen. Ich danke ihm für die tatkräftige Unterstützung, besonders während der Anfangsphase meiner Arbeit.

Weiterhin danke an Dr. Norbert Litz für die Verfügbarkeit der Lysimeterstation und Dr. Norbert Markwardt für die Kooperation beim technischen Aufbau der Anlage. Mein Dank gilt auch an Herrn Michael Facklam, Karl Bötscher und Frau Ute Lesner für die Hilfe an den regnerischen und windigen Tagen während des Aufbaus und der Fertigstellung der Lysimeteranlage sowie an Dr. Björn Kluge, Alexandra Toland und Dr. Andrè Peters für die vielen Diskussionen und Anregungen.

Allen Doktoranden des DFG-Graduiertenkollegs "Stadtökologische Perspektiven 780/3" gilt mein Dank für die gemeinsame, freudige Zeit der Ausbildung zu "Stadtexperten".

Schließlich danke ich meinen Eltern und Schwester für das Vertrauen, das lange Warten, Geduld und all das, was ich heute bin, ganz besonders für die stetige Zuversicht über meine Entscheidung.

Preface

I studied the urban water balance, especially the runoff dynamics of permeable pavements. My work was initiated within the Graduate School "Perspectives on Urban Ecology" (DFG-GRK 780/3). This interdisciplinary research program has been supported by German Science Foundation (Deutsche Forschungsgemeinschaft) and represented by Prof. Dr. Wilfred Endlicher at the Department Gerography of Humboldt Universität zu Berlin. DFG-GRK 780/3 has included projects in social and natural sciences and started in 2002 at Humboldt Universität zu Berlin, Technische Universität Berlin, and Freie Universität Berlin. Since then, the three phases concentrated on different topics:

Cohort 1 (2002–2005): Perspectives on Urban Ecology I - The Example of the European Metropolis of Berlin

Cohort 2 (2005–2008): Perspectives on Urban Ecology II - Shrinking cities: structural changes as opportunities for the development of urban nature and enhanced environmental quality for city dwellers

Cohort 3 (2008–2011): Perspectives on Urban Ecology III - Optimizing urban nature development–Dynamic change of nature functions and the urban environment of city dwellers.

The aim of my (third) cohort (2008–2011) was to understand the functions of ecological processes in the city impacting the quality of life for urban human population. Scenarios take into account the profound issues of change in climate, demographics, economy, and all their consequences for nature and environment in metropolitan areas. The chosen interdisciplinary approach integrated the following research clusters:

Cluster 1 - Optimize ecological functions and biodiversity of urban roadsides

Cluster 2 - Reuse of former housing estates and urban brownfields

Cluster 3 - Strategies for temporarily used urban sites

Cluster 4 - Psychological health and mental state of urban dwellers

My work, as a part of cluster 1, was developed from the two predecessor projects in the graduate school. Dr. Thomas Nehls investigated the properties of paved urban soils and the sorption and transport of heavy metals (Nehls, 2007). Dr. Eva Klingelmann studied leaching of the pesticide glyphosate from

urban pavements (Klingelmann, 2009). Both studies suffered from the lack of process-based hydrologic model for paved soils in their solute transport simulations. Therefore, I started with the aim to develop such a process-based model from lysimeter experiments. I hope that the expanded understanding of urban runoff processes contributes to the improvement of life circumstances for urban dwellers.

December 2010.

Summary

Soil hydrology investigates the dynamic equilibrium between precipitation, runoff, evapotranspiration, and infiltration processes at the soil surface. Although it is known that these dynamic processes also play a role for fully and partly paved soil surfaces, the departments of urban water managements have mostly understood surface hydrologic processes in terms of simplified and empiric model. The runoff coefficient for the design storms allows the quantification of the occurring surface runoff water. Such a rational approach was the basic concept for flood-oriented urban design.

In consideration of urban adaption strategies to climate change and water shortages, it becomes clear that process-based models are necessary in order to predict the availability of water resources with high temporal and spatial resolution. Surface water is no more to get lost, but to be available for utilization. This clearly reflects the paradigm change to the resource-oriented handling with the rainwater in urban areas.

Many studies investigated the effective parameters for describing runoff behaviors only based on the runoff measurement from the paved surfaces. However, in order to develop a process-based model, the observation and the measurement of all water balance components in their relationship are necessary.

The aim of the study is to develop a process-based model for runoff dynamics. For the representative elementary area of paved soil surfaces, the water balance processes were measured under varying natural hydrologic conditions, using the weighable paved lysimeter system. In order to observe the runoff dynamics even from small events, a new runoff setup, called the weighable tipping bucket (WTB), was developed.

Based on the measurement from the weighable lysimeter system, a model for intensity-dependent surface storage and runoff was developed. The surface hydrologic parameters for two typical pavement types, Bernburg mosaic cobblestone and Concrete paving slab, were determined. The fundamental knowledge is to be established in order to understand and describe the functions of pavement as one compensation factor for urban water budget. The upper boundary conditions of the lysimeter attempted to simulate the real urban soil surfaces. The urban water budget processes were continuously observed for the climate and hydrologic conditions of Berlin, Germany for the period between May 2009 and April

2010. The components, such as precipitation, evaporation, runoff and groundwater recharge were measured with the resolution of 0.1 mm/min. The annual runoff coefficients were ca. 16 % and 27 %, respectively, for Bernburg mosaic cobblestone and Concrete paving slab. These results were considerably smaller than the results predicted from the standard regulations (e.g. DWA-Regeln). The surface storage and the rainfall event intensity were derived as the main factor from the analysis of runoff-producing rainfall events.

The process-based model of runoff dynamics describes the runoff coefficient in relationship with the rainfall event intensity, r, the surface storage, V_s, the runoff-producing intensity, r_o, the final infiltration rate, b, and the infiltration exponent, n.

$$RC = f(r) = \left(1 - \frac{V_s}{P \cdot \left(1 - \frac{r_o}{r} \cdot tanh\,\frac{r}{r_o}\right)}\right) \cdot \left(1 - \frac{R - R^{\frac{1}{n}}}{(1-n) \cdot (1 - R^{\frac{1}{n}})}\right)$$

The surface storage determines the total potential of pavement for the infiltration capacity through the rainfall event. The smaller the rainfall event intensity, the more effective the buffer function of the surface storage becomes. Hence, the runoff behavior of small and middle-strong precipitation events clearly differs from that of storm events. While the runoff coefficient for the small events rapidly increases together with the increasing intensity, the runoff coefficients remains relatively constant for the storm events with great intensity, depending of the paving materials.

Throughout the adaption of these models to the observed precipitation events, the average effective values for the surface hydrologic parameters are determined for the two pavements. The surface storages amounted to ca. 0.9 mm and 0.4 mm, the runoff-producing intensities to ca. 0.02 mm/min and 0.01 mm/min, the final infiltration rates to 0.016 mm/min and 0.012 mm/min, and the infiltration exponents to ca. 2.5 and 0.7, respectively, for Bernburg mosaic cobblestone and Concrete paving slab.

In this study, a process-based model concept for describing the dynamic runoff behaviors of paved soil surfaces was developed for the first time and applied to two different pavement types. The improvement of the lysimeter technique by using a weighable tipping bucket enabled the high-resolution measurement of runoff processes. A technical and analytical method could be established to derive the surface hydrologic parameters for further paving materials. This is important for the quantification and improvement of retention capacity for new materials in the sense of pavement renewing potential. For example, during the

measurement period, the utilization of the mosaic cobblestones has shown 1.7-fold smaller runoff in comparison with the concrete paving slabs. The model clarified that the surface storage has to be adjusted to the characteristics of regional precipitation frequency in order to minimize the runoff water.

The process-based model allows assessing the uncertainty of the prediction from the simplified empiric models. It can be applied to the various climate conditions.

Zusammenfassung

Die Bodenhydrologie untersucht die dynamischen Gleichgewichte zwischen Niederschlag sowie Abfluss-, Verdunstungs- und Infiltrationsprozessen an Bodenoberflächen. Zwar spielen diese dynamischen Prozesse auch für die versiegelten und teilversiegelten Flächen eine Rolle, allerdings fasst die Siedlungswasserwirtschaft die entsprechenden Prozesse bislang in vereinfachten empirischen Modellen zusammen. Der Abflussbeiwert für maximale Bemessungsregen ermöglicht die Quantifizierung des anfallenden Wassers. Das Model bildet so die konzeptionelle Grundlage für die entwässerungskomfort- und hochwasserschutzorientierte Stadtplanung.

Im Zuge der Diskussion um die urbane Anpassungsstrategie an den Klimawandel und die Wasserknappheit wird deutlich, dass prozessbasierte Modelle benötigt werden. Damit kann die Verfügbarkeit vom Niederschlagsabflusswasser auch unter sich ändernden klimatischen Bedingungen räumlich und zeitlich hochaufgelöst berechnet werden. Während also Wasser in der Vergangenheit "anfiel", wird es in Zukunft "verfügbar" sein. Dies spiegelt deutlich den Paradigmenwechsel hinzu einem ressourcen-orientierten Umgang mit dem Regenwasser in der Stadt wider.

Zahlreiche Studien ermittelten effektive Parameter zur Beschreibung des Abflusses nur aus Abflussmessungen auf versiegelten Flächen. Für die Entwicklung eines prozessbasierten Modells wird jedoch die Erfassung aller Wasserhaushaltskomponenten im Zusammenhang nötig.

Das Ziel der Arbeit ist, ein prozessbasiertes Modell für die Beschreibung des dynamischen Abflussverhaltens zu entwickeln. Die Arbeit untersucht dafür den Wasserhaushalt teilversiegelter repräsentativer Elementarflächen unter natürlich variierenden Niederschlagsbedingungen mittels hochauflösender wägbarer Lysimeter. Um die Dynamik der Abflussprozesse auch für kleine Niederschlagsereignisse untersuchen zu können, wurde ein neues Messinstrument, die wägbare Kippwaage, entwickelt.

Daraus wurde ein Modell für die intensitätsabhängige Oberflächenspeicherung und Abfluss abgeleitet. Die oberflächen-hydrologischen Parameter für die am häufigsten benutzten urbanen Flächenmaterialien wurden bestimmt. Damit soll die Grundlage geschafft werden, die Funktion der teilversiegelten Flächen als Ausgleichsraum für das Stadtklima herauszuarbeiten. Unter der realitätsnahen Ver-

wirklichung der oberen Randbedingung der Lysimeter wurde das durchgängige urbane Wasserhaushaltsgeschehen für das Klima- und Niederschlagsverhältnis vom Berlin gemessen. Im Untersuchungsjahr zwischen Mai 2009 und April 2010 wurden die Wasserhaushaltskomponenten, Niederschlag, Verdunstung, Abfluss und Grundwasserneubildung, sowohl für Bernburger Mosaikpflaster als auch für Großbetonsteinplatte mit einer Auflösung von minimal 0.1 mm/min aufgezeichnet. Dabei wurde ein Oberflächenabfluss von insgesamt ca. 16 % des Niederschlags für das Bernburg Mosaik und ca. 27 % für die Großbetonsteinplatte ermittelt. Diese Werte sind deutlich geringer als die Werte, die mittels Abflussbeiwerten aus Regelwerken prognostiziert wurden. Durch Analyse der abflusswirksamen Ereignisse wurden der Oberflächenspeicher und die Intensität der Niederschlagsereignisse als bestimmende Faktoren abgeleitet.

Das prozess-basierte Modell des dynamischen Oberflächenabflusses beschreibt den Abflussbeiwert in Abhängigkeit von der Niederschlagsintensität, r, dem Oberflächenspeicher, V_s, der abflusswirksamen Intensität, r_o, der Endinfiltrationsrate, b und dem Infiltrationsexponent, n.

$$RC = f(r) = \left(1 - \frac{V_s}{P \cdot \left(1 - \frac{r_o}{r} \cdot tanh\,\frac{r}{r_o}\right)}\right) \cdot \left(1 - \frac{R - R^{\frac{1}{n}}}{(1-n)\cdot(1-R^{\frac{1}{n}})}\right)$$

Der Oberflächenspeicher bestimmt die Abflusswirksamkeit und den gesamten Prozess des Abflusses. Die Pufferfunktion des Oberflächenspeichers ist umso effektiver, je kleiner die Niederschlagsintensität und je größer die Endinfiltrationsrate ist. Daher unterscheidet sich das Abflussverhalten während schwacher bis mittelstarker Ereignisse deutlich vom Abflussverhalten bei Starkregenereignissen. Während der Abflussbeiwert für die schwachen bis mittelstarken Niederschlagsereignisse mit steigender Intensität rasch steigt, bleibt er für größere Intensitäten materialabhängig relativ konstant.

Durch die Anpassung dieses Modells an die beobachteten Ereignisse wurden die mittleren wirksamen oberflächen-hydrologischen Parameter für die zwei Pflasterarten bestimmt. Der Oberflächenspeicher beträgt ca. 0,9 mm bzw. ca. 0,4 mm, die abflusswirksame Intensität ca. 0,02 mm/min, bzw. ca. 0,01 mm/min, die Endinfiltrationsrate 0,016 mm/min bzw. 0,012 mm/min und der Infiltrationsexponent ca. 2,5 bzw. ca. 0,7 jeweils für das Bernburg Mosaik bzw. die Betonsteinplattepflaster.

In dieser Arbeit wurde erstmals ein prozessbasiertes Modell für die Beschreibung des Oberflächenabflussverhaltens teilversiegelter Flächen entwickelt und auf zwei verschiedene Teilversiegelungsarten angewendet. Durch die Erweiterung

der Lysimetertechnik um die wägbare Kippwaage zur hochauflösenden Erfassung des Oberflächenabflusses wurde eine technische und analytische Methodik für die Ableitung der Flächenparameter auch anderer Versiegelungsmaterialien entwickelt. Damit können die Retentionskapazitäten neuer Materialien im Sinne des Belagsänderungspotenzials gemessen und verbessert werden. Zum Beispiel führte die Gestaltung teilversiegelter Flächen mit Bernburger Mosaik im Vergleich zu Betonsteinplatten im Beobachtungszeitraum zu einem 1,7-fach verringerten Abfluss. Das Modell verdeutlicht, dass der Oberflächenspeicher auf die Niederschlagsverteilung abgestimmt werden muss, um den Oberflächenabfluss zu minimieren.

Das prozessbasierte Modell ermöglicht die Abschätzung der Unsicherheiten der Prognosen vereinfachter empirischer Modelle. Das Modell kann weiterhin auf unterschiedliche Klimabedingungen angewendet werden.

Contents

List of Figures

List of Tables

List of Abbreviations

Abbreviation	Meaning
a	infiltration capacity parameter
A	size of catchment area [ha]
b	final infiltration rate for saturated soil [mm/min]
CPS	concrete paving slab
d	seam portion
ΔW	changeable water storage in soil [mm]
E_s	evapotranspiration of sealed area [mm]
E_u	evapotranspiration of unsealed area [mm]
ET	evapotranspiration [mm]
F	actual retention capacity [mm] or [l/ha]
GW	groundwater recharge [mm]
I	infiltration depth [mm] or [l/ha]
$i(t)$	infiltration function [mm/min]
i_r	average infiltration capacity [mm/min]
MCS	Bernburg mosaic cobblestone
n	infiltration exponent
n	number of rainfall event
n	event number
$NF(r)$	cumulative event frequency function
$\mathbb{P}$	set of rainfall events
P	precipitation depth [mm] or [l/ha]
P_a	initial loss [mm]
P_e	effective precipitation [mm]
$\mathbf{P}_n$	n^{th} event as set element, characterized by intensity r_n, depth P_n, duration t_n, or rainfall pattern

P_u	effective rainfall depth while soil is unsaturated [mm]
$PF(r)$	cumulative precipitation frequency function
$\mathbb{P}[r]$	set of rainfall events of intensity r
$P(r)$	total precipitation sum of $\mathbb{P}[r]$
P_s	effective rainfall depth after soil is saturated [mm]
$p(t)$	precipitation intensity [mm/min]
Q	actual runoff sum [mm] or [l/ha]
$q(t)$	runoff intensity [mm/min]
r	rainfall event intensity
r_o	runoff-producing intensity [mm/min]
RC	runoff coefficient
RC_e	effective runoff coefficient
RC_u	runoff coefficient during unsaturated infiltration process ($t_c < t < t_s$)
RC_e	runoff coefficient during saturated infiltration process ($t \geq t_s$)
RO	runoff sum [mm] or [l/ha]
T	precipitation duration [min]
t_c	time point of runoff beginning
T_c	runoff concentration duration [min]
TB	tipping bucket
T_d	precipitation separation criterion (time span between rainfall events) [min]
T_e	effective precipitation duration ($t_p - t_c$) [min]
t_p	time point of precipitation ending
t_s	time point of saturation
V_s	surface water storage or surface storage [mm]
V_p	porous volume of paving material [mm]
V_{sm}	porous volume of seam material [mm]
V_r	infiltrated water of initial loss [mm]
WTB	weighable tipping bucket

Part I

Introduction

Chapter 1

Background and Motivation

1.1 Background of Pavement Hydrology

Functions of Pavements

Pavements have been used to seal streets and roads for 4000 years. They fulfill important functions as technical infrastructure in cities. Pavements allow city dwellers to emancipate from the natural circumstances such as muddy soils in rainy weather. Paved ways are drained, in order to provide a profound, dry, and reliable way for fast transport of goods and people. Usually, during construction, also a leveling of the way is gained. These were the main purposes to build roads in ancient times e.g. the "Via Militaris" in the Roman Empire, as well as "Autobahnen" nowadays (see Fig. 1.1).

Paved streets and ways canalized movements and transport, they connected and divided the parts of the city. Therefore, pavements structured the city, and due to numerous design possibilities, they forged the architectural identity for the cities.

From the hygienic viewpoints, pavements in connection with sewage systems contributed to clean housing and helped to minimize epidemics like cholera. After all, soil sealing enables convenient city life and urban prosperity, nevertheless, it also provides ecological habitat functions for plant and animals.

Effects of Soil Sealing

In Berlin, the degree of soil sealing is nearly 34 % of the urban landscape. 11 % are covered by buildings, 13 % are sealed without buildings, and 10 % are streets. Depending on the quarter, soil sealing varies between 20 % and 66 %, however, around two thirds of this is always made up of public streets and walkways which are considered as "partly sealed areas" (Senatsverwaltung Berlin für Stadtentwicklung, 2001).

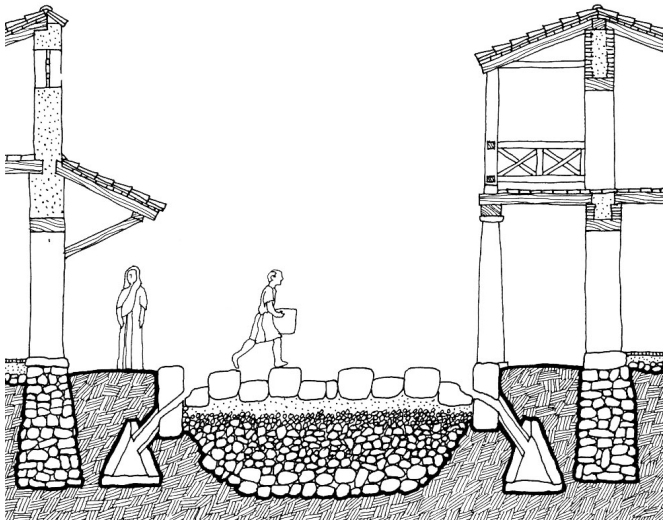

(a) Ancient Roman street.

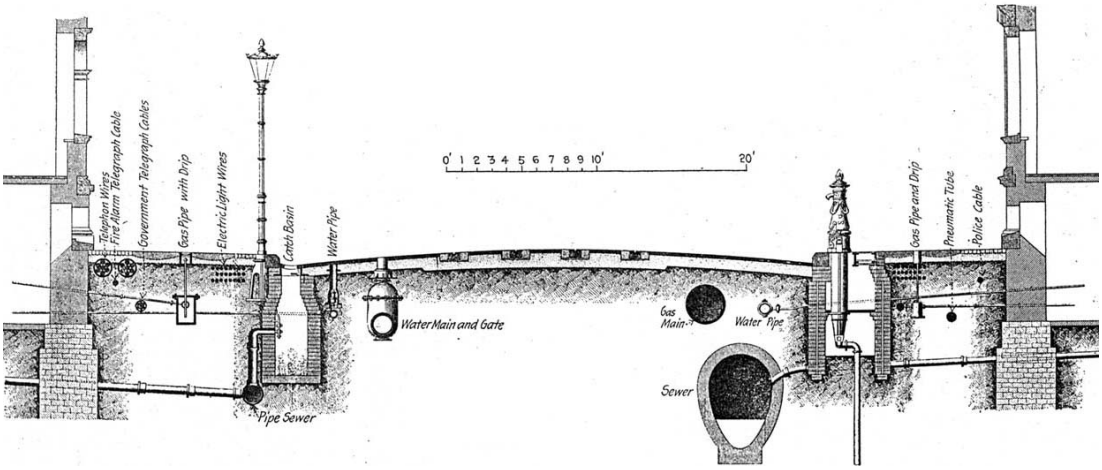

(b) Berlin street from 19^{th} century.

Figure 1.1: Typical road cross sections (a) from Roman times (Fusch,2010: online. http://cc.owu.edu) and (b) from Berlin 19^{th} century (Schladweiler et al. 2010: online. http://sewerhistory.org). Note that the sewage system is an important feature of soil sealing.

Soil sealing is highly anthropogenic in many respects: the spatial distribution and vertical construction of paved surface, the material properties that compose the pavement and the hydrological aftereffects on the urban watershed. Soil sealing induces alterations of nature in urban areas, leading to a number of ecological and economic problems for city dwellers and the surrounding population. Thus, urban environment obtains completely a different circumstance in result (Nehls et al., 2006).

Despite such a high degree of soil sealing, it has not yet gained a significant importance for the sense of common social perception. Therefore the Federal Law for Soil Protection has not yet defined soil sealing as soil impairment. Soil sealing is mentioned in the law only as one of several possibilities for blocking harmed soil material, in order to prevent its mobilization by wind and water erosion or inflow of harmful substances from the atmosphere into the groundwater zone (Wessolek, 2001). However, the impact of soil sealing has been recognized for long time in respects of extreme urban water balance, urban heat stress, and quality of urban water resources.

Firstly, soil sealing has a crucial effect on the urban water balance due to interruption of the water exchange process between pedosphere and atmosphere. It is known that the average runoff can increase enormously through soil sealing, while infiltration is confined to remain as optimal as in natural soils (Fig. 1.2). For paved soil surfaces, the reduction of evaporation is a significant problem for urban micro-climates in the summer period. The reason is presumably the small storage capacity of paved surfaces (Flötter, 2006; Göbel et al., 2007; Starke, 2010). The evaporation can be exponentially increased by increasing the soil opening ratio (also called "seam portion"). Therefore, purposeful selection of pavements and suitable implementation can positively affect the urban water balance and climate, e.g. through the use of porous pavements with big seam portions and high surface storage (Nakayama and Fujita, 2010).

Secondly, it is evidenced that the surface water resource of urban area is reducing due to the modified urban water budget. This leads to distinctive temperature fluctuation with heightened average. The affected urban heat balance results clearly in high heat stress (Endlicher, 2008). Compared to the unsealed surrounding areas, the average annual temperature increases by 0.5 to 1 K with absolute maximum differences of up to 10 K (Kuttler, 1998). This so called *"urban heat island effect"* leads to human health problems and to increased macroeconomic costs in these areas (Tol, 2002; Townsend et al., 2003). The urban heat island effect cannot be completely avoided by desealing measures, but its impact on the human population can be decreased by using water-sharing pavements.

Thirdly, problems of surface water dynamics lead to further troubles for urban water quality (Heinzmann, 1998; Akan and Houghtalen, 2003). Because the urban soils are persistently exposed to emissions and immissions, the seam materials– the soil between the paving stones on pavements–which acts as flow path for infiltration and capillary rising, is strongly modified over the years with urban

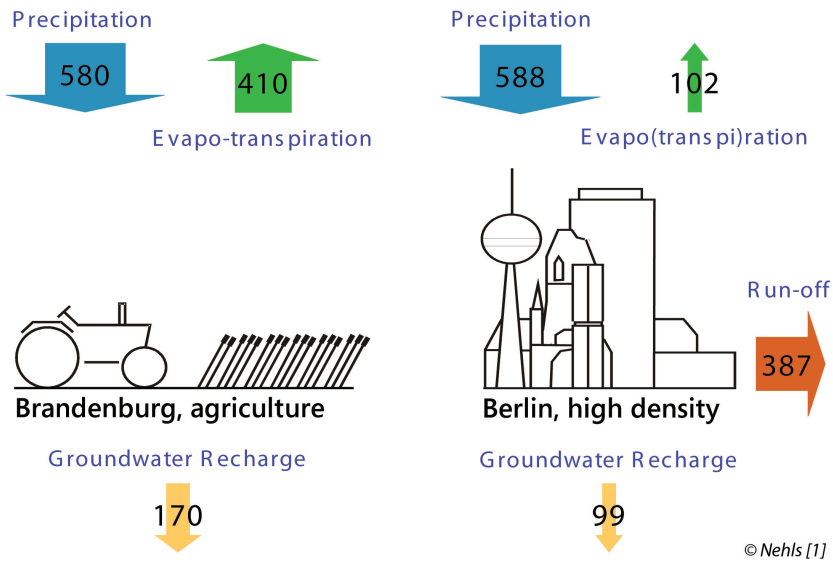

Figure 1.2: Urban water balance for Berlin compared to its suburbs (units are in millimeters) (Nehls et al., 2006). The annual water balance of the urban area has been modified drastically by soil sealing. A Goal of urban water management is to decrease runoff and increase the infiltration capacity. Hereby, enhancing the surface storage capacity, we can control the urban water balance depending on rainfall event frequency.

dirt, e.g. foliage, cigarette butts, food residues, animal faeces, oil, and industrial particles containing (e.g. soot, abrasions from tires and brakes) (Dawson, 2008). Thus, increased runoff consequently mobilizes contaminants on urban soil surface. In Berlin, at least the traffic is a source of contaminations, e.g. heavy metals and organic contaminants like PAHs. Although pesticides were developed for agricultural use, they are used in cities in terms of weed control on pavements (Klingelmann, 2009). Therefore, pavements allow infiltration of pollutants like heavy metals or pesticides, which are released from traffic or actively applied.

Future Design of Urban Catchment as Sewer System

Given the consequences of soil sealing, the improvement of rainwater infiltration and the surface retention, the enhancement of the evaporation, and the decrease of runoff are the main goals of ecological urban water management. For paved surfaces, the water storage capacity serves as water retention; hence, it plays a key role in studying pavement hydrology. In order to understand water resource control in urban areas, it is also necessary to know how the region-specific small precipitation events participate in the whole water budget process, as well as storm events. This is especially essential knowledge, given the variation of precipitation frequency with climate change (Arnbjerg-Nielsen and Fleischer, 2009;

Faram et al., 2010). Water budget components may be considered as dynamic processes. This can help us select suitable paving types, e.g. cobblestones and concrete paving slabs with sufficient openings, in order to reach the goals mentioned above.

A typical urban landscape mostly consists of street canyon, building facades and roof surfaces, and urban greens. There are modern urban strategies such as the innovative adiabatic cooling technology for indoor space and the greening technology for building facades and roofs, not to mention about the efforts to retain natural urban greens (Dreiseitl and Grau, 2009).

Because, from economic and social reasons, those innovative ambitioned technologies are not always and everywhere possible in the city areas–especially for the big cities such as Berlin, more technical adaption and fundamental knowledge are necessary to control the urban water resources.

Design of sewer systems needs to challenge with the existing uncertainty of basic data and to differentiate its safety concept. The pavements are considered a crucial part of urban sewer system, especially in the background of the future demographic development and the predicted climate change. The illustration of the detailed runoff transportation in urban areas and its interplay with the precipitation will become more and more a routine-task for model calibration and plausibility. Therefore, a process-based modeling of urban catchment gradually becomes indispensable task of pavement hydrology (Pecher and Hoppe, 2011).

1.2 Aims and Hypothesis

A goal of conventional urban water management was the fast drainage of surface flow to protect the urban catchment area from floods. Another goal was to control water pollution for urban water systems by separating runoff completely from the original water cycle. These led to the development of hydrological approach aimed at removing surface water as fast and far as possible towards outlet channels and wastewater treatment plants. Urban sewer systems were designed and continuously improved for the cases of storm events. This approach allowed cities to develop rapidly till the middle of last century (Geiger et al., 2009).

However, after the 1950s, the significant disadvantage of this approach was recognized in the point of economical and ecological view for residential water engineering and management systems. After the "Separated Rainwater Management" had been established and practiced for several decades, many regions and communities are nowadays working to decentralize municipal rainwater management so that sustainable urban development is ensured by a more holistic approach to urban water resources (Pecher and Hoppe, 2011).

Many numerical models and operational tools were developed for describing the urban water catchment area more precisely in order to reconnect the urban

surface flow with natural water cycle. These attempts still could not go beyond the principles of its regional redistribution and reallocation. The design storms–a rainfall event of specified size and return frequency (i.e., a storm what has the likelihood of occurring once every 10 or 100 years) that is used to calculate the runoff volume and peak discharge rate–are still the key input factor for dimensioning the rainwater management system (ATV-DVWK, 1992; IPS, 2005; Kwon, 2008; Sieker et al., 2009; Bronstert et al., 2006).

From an urban hydrologic viewpoint, permeable pavement is preferable to total sealing because it provides improved water retention capacity. Here, the surface water storage is a key parameter. It is presumably used up differently for the rainfall events, depending on the pavement types. For instance, small rainfall events result in much different surface water behavior than the design storm events. This behavior finally influences on the annual water balance (Ferguson, 2005).

Several studies have indicated that permeable pavements impacts dynamically on water balance processes according to soil hydrologic and climatic conditions (Flötter, 2006; Glugla and Krahe, 1995; Schramm, 1996). The dynamic runoff behaviors were described by using operational algorithms, but not able to be mathematically interpreted. The infiltration process was a complex interaction of many sub-processes that are too complicated to mathematically describe.

The previous models developed for urban water balance embed the classical approaches which do not parameterize the reaction of disturbed urban surfaces such as the rational runoff approach and SCS approach. The concept family of Horton's infiltration was the first attempt at modeling dynamic water infiltration, but it had been originally used for modeling large natural watershed areas (see Chap. 2.1).

There is still the question how far the paved soils can show the potential for the improved urban water balance and which surface parameter is the most important for explaining the runoff dynamics. Surface storage capacity is likely to include parameters such as seam portion, porosity of pavement and initial soil conductivity. But its clear influence on runoff and infiltration has not yet been derived (Borgwardt, 2006).

The main hypothesis of the work is that the paved soil surface can play a positive role for the improvement of the urban water balance, when they are adjusted to the regional precipitation characteristics. Furthermore, this dynamically depends on the interplay between the soil surface and the rainfall event parameters.

The final aim of the study is to develop a process-based model for runoff dynamics of paved soil surfaces. A paved weighable lysimeter system will be designed and constructed, especially for runoff measurement from the representative elementary area of two typical pavements of Berlin: Bernburg mosaic cobblestone and Concrete paving slab. The annual water balance process will be analyzed profoundly in the relationship with the precipitation frequency. After the runoff

and the infiltration processes are physically described, the surface storage and the runoff coefficient will be clarified as function of rainfall intensity and surface hydrologic parameters. By applying these model concepts to the measured data from experiment period between 2009 and 2010, the surface hydrologic parameters for the two typical pavement types will be determined. In sum, it is aimed to gain the basic knowledge needed to improve urban water resource management by better controlling urban surface water resources.

Chapter 2

Urban Soil Water Budget - State of the Art

Over the last 20 years, a number of studies on urban water budget have been carried out. Experimentally, these studies have been based on either lysimeter or lab studies according to research object and extent. Lysimeter studies (also known as "*Lysimetery*") have enabled researchers to look at the physical and hydrological phenomena in soils as a whole, incorporating the true complexity of paved soils, while lab studies have focused on certain individual processes. Since priority of these studies was given to flood protection and the related economic interests, the studies, primarily runoff studies, have focused on the cases of storm events. Results from these studies provided the technical specifications and standards with maximum runoff coefficient and minimum conductivity of most paving materials. From this state of knowledge, urban planning and water engineering have resulted in economic and ecological risks. The potential of partly paved surfaces are underestimated and the sewer infrastructures are overdimensioned (DIN 1986-3, 1986; ATV-DVWK, 1992; Sieker et al., 2003; DWA-A, 2005; Borgwardt et al., 2000; ATV-DVWK, 2000; DWA-A, 2006).

In this chapter, some selected lysimeter studies are reviewed. Their results are analyzed in comparison to the hydrologic potential of paved surfaces for urban water budgets. Overviews of some runoff and infiltration models will provide a fundamental conceptual model of surface water processes.

2.1 Lysimeter Studies on Urban Water Balance

Glugla and Krahe (1995) studied urban runoff generation from the hydrologic-economic and resource-emphasized aspects. They considered the role of regional typical small events for surface retention and evaporation. For regions of Berlin, they clarified that the surface storage capacity of sealed areas presumably played a decisive role for the total continuous water supply of the inner-city system of

Table 2.1: Surface hydrologic parameters for pavements of cobblestone and paving slab from Leipzig by Schramm (1996). i_r = final infiltration rate, RC_{max} = max. runoff coefficient, V_s = surface storage, and d = seam portion.

Paving material	Event parameters	RC_{max} [%]	i_r [mm/min]	V_s [mm]	d [%]
Concrete cobblestone	r = 0.6 mm/min, T = 60 min	82.0	0.10	1.6	27
	r = 1.15 mm/min, T = 30 min	90.1	0.10		
Concrete paving slab	r = 0.58 mm/min, T = 61 min	84.0	0.09	1.5	7
	r = 1.18 mm/min, T = 30 min	93.0	0.08		

water channels. For pavement with a seam portion of 5 %, they found that the paving material demonstrated a surface storage of 0.3 mm (= 0.3 L/m^2), while the seam soil showed a surface storage of 0.2 mm. Their key finding was that the potential surface storage of permeable pavements should increase with increasing seam portion and it enhances the evaporation amount. "Bargrov-relation" was introduced to calculate the annual evapo(transpi)ration of impervious and pervious soil surfaces.

Schramm (1996) simulated an extensive urban surface system with 20 types of permeable pavements in Leipzig, Germany. Some pavements are from the turn of the century, as a part of an effort to ensure that the experiment took place under very realistic soil in-situ conditions. He considered the precipitation characteristics as a runoff parameter and described the rainfall-runoff relationship of 20 pavements according to event intensity and duration as well as seam portion. He found that the relationship between runoff and rainfall event intensity tended to be a logarithm function which was derived by simple descriptive method.

Tab. 2.1 shows the surface hydrologic parameters of concrete cobblestone and paving slab which were included in his permeable pavements. Two kinds of storm events were simulated, in which both rainfall intensity and duration were controlled. Despite the difference of seam portion by 20 %, the experiment resulted in very similar values of infiltration (0.08–0.10 mm/min) and surface storage (1.5–1.6 mm). The max. runoff coefficient were fewer dependent of seam portion. Quardrpling of intensity resulted in increasing of runoff coefficient RC_{max} only by ca. 10 %.

Table 2.2: Water balance for pavements of Bernburg mosaic cobblestone and Concrete paving slab from Berlin by Wessolek (1993, 1994). Water balance data are based on the measurement between 1986 and 1987. RO = runoff, GW = groundwater recharge, and ET = evapotranspiration. Units are in %.

Paving material	Period	RO	GW	ET
Berburg mosaic cobblestone	summer	60	23.1	16.9
	winter	45.8	48.3	5.9
	annual	54.3	33.3	12.4
Concrete paving slab	summer	73.8	12.2	14
	winter	63.8	31.6	4.5
	annual	69.7	20	10.3

The rainfall events, simulated by a sprinkling system, were too artificial to imitate real hydrologic conditions. The runoff water was pumped from the surface by pressure pipe and its amount was weighed. This should clearly have led to an unclear interpretation of infiltration in this experiment, which was calculated as the rest amount of runoff (the difference between the volume of water applied and the runoff collected). It was also not possible to make a statement about small event runoff.

Wessolek carried out one of the first paved lysimeter experiments, with pavements that included concrete paving slabs, grass pavers, cobblestones and asphalt, in Berlin-Jungfernheide, Germany (Wessolek, 1993, 1994; Wessolek and Facklam, 1997). An extensive overview of physical-chemical composition of seam materials and hydrological properties was completed. They pointed out that the bigger the seam portion was, the greater the infiltration capacity per day (155 cm/day for grass paver, 58 cm/day for cobblestone, 9 cm/day for paving slab, and less than 1 cm/day for asphalt). Infiltration performance measured by lysimeter was always better than that measured by infiltrometer in realistic street areas (see Tab. 2.3.

Based on the experiments from the years 1985/1986 (Wessolek, 1993, 1994), he calculated the annual water balance for the total precipitation depth of 631 mm. For cobblestone pavements, the rate of groundwater recharge was 33 %, the runoff coefficient was 54 %, and the evaporation rate was 12 %. For paving slab

Table 2.3: Surface hydrologic parameters for pavements of Bernburg mosaic cobblestone and Concrete paving slab from Berlin by Wessolek (1993, 1994); Wessolek and Facklam (1997). r_0 = runoff-producing intensity (which is strong enough to produce runoff), RC_{max} = max. runoff coefficient, V_s = surface storage, $i_r\,(lab)$ = final infiltration rate under lab condition, $i_r\,(lysimeter)$ = final infiltration rate under lysimeter condition, $i_r\,(innercity)$ = final infiltration rate under actual inner city condition, and d = seam portion.

Paving material	r_o [mm/min]	RC_{max} [%]	V_s [mm]	i_r (lab) [mm/min]	i_r(lysimeter) [mm/min]	i_r(inner city) [mm/min]	d [%]
Berburg mosaic cobblestone	0.09	66	1.5 - 2.0	0.90	0.40	0.016	20 - 30
Concrete paving slab	0.02	88	0.3 - 0.8	0.23	0.06	0.011	2 - 5

pavements, the rate of groundwater recharge was 20 %, the runoff rate coefficient 70 %, and the evaporation rate was ca. 10 % as Tab. 2.2 shows. As for the reason of the relatively high infiltration rate despite soil sealing, the high wetting capacity of pavements and the large number of days with low precipitation depth have been mentioned. He attempted to clarify the seam portion as a relevant infiltration factor for paved soil surfaces, but no clear relationship could be found (Wessolek and Facklam, 1999).

Illgen et al. (2007) developed an ambitious monitoring program to evaluate the infiltration and runoff parameters of various paved surfaces. Under laboratory conditions, he used a lysimeter-like system and a sprinkling system. Tipping buckets were main instrument used to quantify the water mass. The experiment surface was paved with non-porous as well as porous concrete blocks. The used sub-base structure was more typical for newly constructed areas other than for the normal traditional city areas. In order to simulate the clogging effects of aging seam material, silica powder was distributed on the paved surface. He found that the infiltration performance of the same pavement shows a broad variability at different monitoring points. For example, the infiltration rate at the center of a parking lot was much smaller than that at the boundary area. In general, though, a relative high infiltration rate was measured at many locations with pavements that are generally assumed to be hardly permeable. He found that the final infiltration (saturated infiltration) normally began to settle within 60 min rainfall duration.

A significant relationship between rainfall intensity and infiltration performance was found, while the surface slope of paved surfaces was of less importance in explaining runoff generation. For pavements with a gravel sub-base, the runoff rate was very low as 25–50 l/s·ha (equal to ca. 0.15–0.3 mm/min) under rainfall intensity of 1000 l/s·ha (equal to ca. 6 mm/min). One of the key findings was that there was also a relationship between rainfall intensity and infiltribility, especially, for non-clogged surface. There was little such relationship for the considerably clogged surfaces. This can be traced back to non-intensity-dependent final infiltrability for cases of the older paved soils.

Borgwardt (2006) tried to find the relationship between infiltration performance and the pavement aging process. For the experiment duration of 10 years, he analyzed the modification of infiltration performance with many concrete pavements. The increasing percentage of coarse particle size of less than 0.0063 mm from 10 % to 50 % caused a rapid decrease in saturated hydraulic conductivity from 55 mm/min to 5 mm/min.

Over the 10 year period, the total infiltration performance was reduced by 20 % in concrete blockstone pavements. He found that increasing the seam portion from 5 % to 30 % should have led to a 10-fold increasement of infiltration. However, a generalized relationship was difficult to define. Therefore, he suggested that the correct selection of seam material was much more meaningful than the increase of seam portion and that seam materials with suitable composition provide an enormous potential to unburden the existing draining system.

Flötter (2006) accomplished one of the most recent lysimeter systems with pavements in Hamburg, Germany. His work contributed to the technical progress of urban lysimetry. His aim was to study the runoff and infiltration behavior of three typical surface materials (concrete cobblestone, concrete paving slabs and water-bound surfaces) with a standard sub-base structure. He investigated also the soil physical and hydrological properties of seam material. He observed the water balance between 1996–2006, so that the aging process through material modification could also be considered. His methodology indicated the importance of high mass resolution for runoff studies. Then he made a statement of intensity-dependent runoff dynamics by means of an operational calculation.

The most problematic aspect of this experiment was the low temporal resolution. He did not accurately calculate the rainfall parameters, since he could not make a statement about runoff behavior for the small rainfall events that might be typical for the region. This should have led to a statement of insufficient analysis about surface storage. Tab. 2.4 and Tab.2.5 show some aspects of his results about the water balance components and the surface hydrologic parameters.

Starke (2010) used a special lysimeter-like experiment system with pavement in order to directly measure real urban evaporation. He quantified the vaporing water mass with a tunnel-wind system. This system was equipped with moisture sensors. The tunnel-wind system redirected the steaming water from pavement along the moisture sensors to determine the evaporation volume. His pavement

Table 2.4: Water balance for pavements of concrete cobblestone and paving slab from Hamburg by Flötter (2006). *RO* = runoff, *GW* = groundwater recharge, and *ET* = evapotranspiration. Units are in [%].

Paving material	Period	*RO*	*GW*	*ET*
Concrete cobblestone	summer	17.8	67.8	14.4
	winter	8.1	88.6	3.4
	annual	12.0	80.0	8.0
Concrete paving slab	summer	43.6	46.9	9.5
	winter	38.9	59.4	1.8
	annual	41.0	54.0	5.0

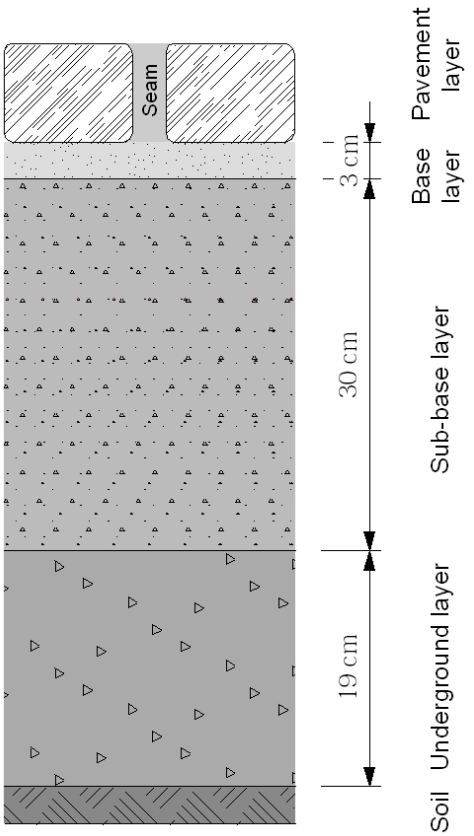

Figure 2.1: An example of standard vertical structure of sidewalk: Lysimeter surface scheme used by Flötter (2006). In practice, many walkways get along without such sophisticated sub-base structures. The sideway vertical structure and construction vary regionally.

Table 2.5: Surface hydrologic parameters for pavements of concrete cobblestone and paving slab by Flötter (2006). r_0 = runoff-producing intensity (which is strong enough to produce runoff), RC_{max} = max. runoff coefficient, i_r = infiltration capacity, V_s = surface storage, and d = seam portion.

Paving material	Time elapsed	r_o [mm/min]	RC_{max} [%]	i_r [mm/min]	V_s [mm]	d [%]
Concrete cobblestone	after installation	0.2	85	1.32	0.24	4.9
	after 4 years	0.16	88	0.27		
Concrete paving slab	after installation	0.15	91	0.33	0.17	1.75
	after 4 years	0.007	95	0.01		

had a rather innovative sub-base structure with a very high porous volume (ca. 51 L). His key finding was that the dynamics of evaporation performance of porous pavement demonstrated a strong dependency on the rainfall event. The higher surface storage capacity the pavement had, the more effectively it could even out the extreme evaporation fluctuation.

Using non-weighable lysimeters with 13 pavements (each with a surface size of $4\,m^2$) in Berlin-Dahlem Germany, Rim (2008) found that the runoff concentration time was strongly dependent on rainfall event intensity. The pavements seemed to have a constant surface storage. Thus, he confirmed that the surface storage could parametrize the paved surface more accurately than the seam portion. With regard to the methodology, representative elementary surfaces were needed in order to reach high temporal runoff characteristics. For several years, Schmidt (2001) investigated the annual urban water balance for the Berlin region with non-weighable paved lysimeters. He made a subject of discussion that the actual urban water problem whould not be about the low infiltration, but about enhancing urban evaporation performance, and suggested that the latter will need to stand in the spotlight in urban hydrological design.

Additionally, many laboratory experiments took place with different aims. Objectives that could not be reached by means of lysimeters, could be studied in the laboratory experiments. These experiments investigated, e.g., infiltration and macro pore systems of sealing materials. Paradoxically, lysimeter studies always led to much higher values of hydraulic conductivity than the lab experiments. Most technical specifications and standards are still based on results of laboratory experiments. Finally, one can claim that there have not been as many lysimeter studies for paved soils as laboratory experiments. The lysimeter techniques have not been able to simulate adequately the interplay between water budget subprocesses.

2.2 Models for Runoff and Infiltration Processes

Many soil hydrologic models have been developed in the last century and used for studies of water processes at the soil surface. The most essential characteristics distinguishing these models are the temporal and spatial dimensions of the water infiltration concept used.

Water balance models are normally used to assess the long-term hydrologic process. But the hydrologic processes during a rainfall event are difficult to determine with significant precision (Niemczynowicz, 1999). Therefore simplified parameters such as the runoff coefficient and degrees of sealing are well established in practical application in order to quantify the storm water process (DWA-A, 2005). In order to include extensive hydrologic parameters in descriptions of hydrologic processes, SCS developed the CN (curve number) system. Process-based models such as Green-Ampt's Model, Philip's Equation and Schwartzendruber's Principle were derived and adapted the infiltration curve as a function of time (Green and Ampt, 1912; Philip, 1957a; Schwartzendruber, 1974).

Water Balance

The water budget at the soil surface includes water income, water outcome, and changeable water storage for a closed viewing system such as an urban catchment area. Regarding the long-term water balance, the whole water balance normally balances out, that is, the changeable water storage becomes negligible for the long-term water budget. The water budget can be described by the water balance equation (see. Eq. 2.1), which enables inflows and outflows to be balanced for a given elementary area.

$$P = E_u + E_s + I_u + I_s + RO_u + RO_s + \Delta W \tag{2.1}$$

P : precipitation [mm]
E_u : evapotranspiration of unsealed area [mm]
E_s : evapotranspiration of sealed area [mm]
I_u : Infiltration of unsealed area [mm]
I_s : Infiltration of sealed area [mm]
RO_s : Runoff of sealed area [mm]
RO_u : Runoff of unsealed area [mm]
ΔW : changeable water storage in soil [mm]

For a short-term water balance, water storage (ΔW) plays a role, as shown in Eq. 2.1. Due to to capillary rising capacity, ΔW is an important water resource factor that influences the urban micro-climate for city dwellers.

Rational Method

The concept of the runoff coefficient stems from the "Rational Method" of Emil Kuichling from the year 1889 (McCuen, 2004). This is the most commonly used uncalibrated equation in which the peak discharge relates mathematically to rainfall depth and drainage area. The value of the runoff coefficient is a function of the land use, covering condition, soil group, and watershed slope. This method has been applied mostly to small watersheds such as urban areas.

$$Q = RC \cdot A \cdot P \tag{2.2}$$

Q : runoff depth [mm] or [l/ha]
RC : runoff coefficient [%]
A : size of catchment area ha]
P : precipitation depth [mm] or [l/ha]

The runoff coefficient concept proceeds from the simple assumption that a catchment area allows falling water to infiltrate and run off independent of the rainfall process and that this relationship remains constant. This assumption is suitable only if the soil condition fulfills at least requirements of soil saturation. In most precipitation events, however, the RC cannot remain constant. Therefore some other concepts have been developed, such as the unit-hydrograph method or the SCS method. In combination with these, the RC formed a basic runoff calculation model.

SCS Rainfall-Runoff Depth Relation

In the practice of watershed management, the"SCS (Soil Conservation Service) Rainfall-Runoff Relationship" has been frequently used since the 1960s for calculating runoff discharge, due to its universal and practical approaches. Watershed parameters such as surface storage and soil moisture are included within the model.

In this model, surface water storage is presumed to have a strong influence on initial loss. Runoff is considered as water in excess of the infiltration that results from surface saturation. Fig. 2.2 the decomposition of rainfall into direct runoff (Q), initial lost (P_a, called also initial abstraction), and actual retention (F).

The SCS method separates the total rainfall into these three components and starts from the following relationship between them:

$$F = (P - P_a) - Q \tag{2.3}$$

It is assumed that runoff will not occur until the initial abstraction has been satisfied. The ratio of available water for runoff ($P - P_a$) to available storage

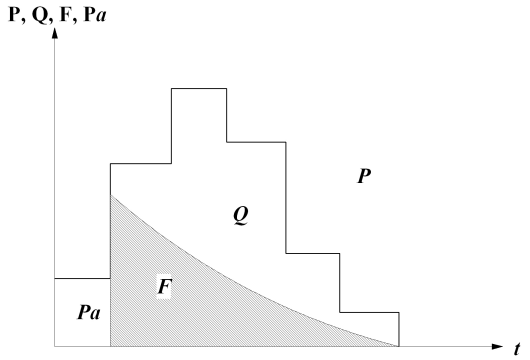

Figure 2.2: Decomposition of rainfall event by SCS rainfall-runoff relationship (McCuen, 2004).

V_s represents the proportion of water available for runoff per unit of available storage. In the model, it is presumed that there may be a rationality that this ratio $(P - P_a)/V_s$ equals the proportion of water that runs off per unit of water retained.

$$\frac{P - P_a}{V_s} = \frac{Q}{F} \tag{2.4}$$

Rearranging Eq. 2.3 into Eq. 2.4 to solve for Q yields

$$Q = \frac{(P - P_a)^2}{(P - P_a) + V_s} \tag{2.5}$$

The storage (V_s) should be influenced by factors such as land use, interception, infiltration, depression storage and antecedent moisture. These factors simultaneously affect the initial lost. Therefore much empirical evidence was used to support the assumption that there might be a relationship between P_a and V_s as following:

$$P_a = 0.2 \cdot V_s \tag{2.6}$$

Substituting Eq. 2.6 into Eq. 2.5 yields the following equation with only one unknown S:

$$Q = \frac{(P - 0.2\,V_s)^2}{P + 0.8\,V_s} \tag{2.7}$$

SCS developed the CN (curve number) system to make the easy use of Eq. 2.7 possible. CN includes the relationship:

$$V_s = \frac{1000}{CN} - 10 \tag{2.8}$$

The SCS rainfall-runoff relationship has been used primarily for big natural watersheds. In the 1980s, *SCS-TR 55*, a variation of *SCS* was released with the new adapted *CN* for urban areas.

Nevertheless, the suitability of the rational assumptions of Eq. 2.6 are still questionable, because of the assumption that the initial abstraction remains constant for the varying rainfall events in a given catchment. In other words, it should not change with the intensity of the rainfall event. The equation solely suggests that the soil surface includes a minimum storage capacity propor-tional to total surface storage to hold rainwater back, independent of rainfall processes. In order to meet a reasonable assumption about surface runoff, a greater understanding about the infiltration process is needed.

Nearly all infiltration equations suggest an infiltration rate with a rapid initial decline and a final approach to a constant. Most equations are based on empirical experiments. The initial infiltration process is especially complicated and difficult to describe.

Horton's Infiltration Model

Since the 1940s, possibly the best known and most widely used and process-based method for computing infiltration and runoff is the "Horton's infiltration model", developed in 1937 (Eq. 2.9). His idea of storm runoff as an excess of rainfall over infiltration capacity is called "Hortonian overland flow" or "infiltration excess overland flow". Horton used rainfall excess in short form. He strictly used the term "infiltration capacity" instead of "infiltration rate".

$$f = f_c + (f_o - f_c) \cdot e^{-k \cdot t}\,, \tag{2.9}$$

where f = infiltration capacity [inches/hour] at time t [hour], f_o = infiltration capacity at time $t = 0$; f_c = minimum constant infiltration capacity; and k is constant for a given curve (Beven, 2004).

The "Horton Infiltration Equation" has been employed to calculate runoff and infiltration for big natural watersheds, especially in combination with the unit-graph theory of LeRoy K. Sherman (1932) (McCuen, 2004). A number of well-known hydrological simulation models make use of the Horton model in obtaining an assessment of infiltration and runoff rates (Green, 1986).

The impression has persisted that the Horton model is an empirical relationship because his equation sums up all processes affecting the rate of infiltration capacity change. However, the Horton Infiltration Equation results in a decline towards a constant, which is similar to the pattern of change in infiltration capacity in other equations such as Green and Ampt's curve (Green and Ampt, 1912) and Phillip's curve (Philip, 1957b).

Philip's Infiltration Model

By combining "Darcy's law"

$$q = -K\frac{\partial H}{\partial z} \tag{2.10}$$

and the "Continuity equation"

$$\frac{\partial \theta}{\partial t} = -\frac{\partial q}{\partial z}\,, \tag{2.11}$$

a general flow equation can be expressed as following:

$$\frac{\partial \theta}{\partial t} = -\frac{\partial}{\partial z}(K\frac{\partial \psi}{\partial z}) - \frac{\partial K}{\partial z}\,, \tag{2.12}$$

where q = the flux which at the soil surface equals the infiltration rate, H = total hydraulic head which is the sum of the pressure head (Hp) and the gravity head (Hg), K = the hydraulic conductivity, θ = the soil moisture, and t = time. Phillip solved Eq. 2.12 in a form of physically-based converging power series which describes cumulative infiltration I as a function of time t (Philip, 1957a) and then suggested a simplified formula for practical purposes (Philip, 1957b). Thus, the cumulative infiltration is

$$I = St^{1/2} + b \cdot t \tag{2.13}$$

and the infiltration rate is

$$i = \frac{\partial I}{\partial t} = \frac{1}{2}St^{-1/2} + b \tag{2.14}$$

The sorptivity S reflects the soil's ability to absorb water by matrix forces during the initial stages of infiltration. b is essentially the saturated conductivity at which soil finally arrives after a long infiltration duration.

Rubin's Experiments and Schwartzendruber's Infiltration Model

Rubin (1966) implemented a fundamental research for the development of the theory of water uptake during rainfall infiltration (also called rain-pond infiltration). He divided the water uptake process into 3 infiltration sub-processes:

(i) non-ponding infiltration, involving rain not intense enough to produce ponding;

(ii) pre-ponding infiltration due to rain that can produce ponding but that has not yet done that;

(iii) and rain-pond infiltration, characterized by ponded water.

The first two processes are intensity-controlled and the latter is pressure-controlled, i.e. by the depth of water above soil surface. During non-ponding infiltration, the soil surface has a limiting saturation moisture content specific to the rainfall intensity, and the hydraulic conductivity gradually approaches the rainfall intensity. During pre-ponding infiltration, the rain intensity exceeds the infiltration rate, and the soil's infiltration capacity is about to be reached.

In addition, he found that the decreasing infiltration flux curve under a constant rate of water application is not the same as that obtained when surface ponding is imposed from $t = 0$ onward (Rubin, 1966). (In order to assure the absence of hysteresis, a rainfall event was considered only if its intensity was an increasing function of time. In my study the annual rainfall time series have to be very precisely separated into rainfall events series so that the rainfalls with decreasing intensity can be excluded.)

Schwartzendruber (1974) attempted to develop an empirical equation to describe the intensity-dependent water uptake process investigated by Rubin (1966). He proposed the following mathematical description:

$$i = at^{-n} + b\,, \tag{2.15}$$

where i is infiltration rate, a and n are curve parameters specific to soil surface properties, and b is the saturated hydraulic conductivity. This was only an implicit expression of water uptake as a function of time, which includes both seepage and surface storage filling. Nevertheless, based on this knowledge, he then derived an equation to calculate the cumulative runoff under a constant rainfall flux (Swartzendruber and Hillel, 1975):

$$w = (r - b) \cdot (T - T_1)\,, \tag{2.16}$$

where w is cumulative runoff, r is rainfall intensity, T is modified time, and T_1 is the modified time at which the surface storage V_s is ponded. He presumed that there was a static depth of water V that could be stored on the surface of the infiltration plot before overflow would start to release any further cumulative water excess as runoff from the plot. This static surface storage might exist even on a smooth surface because sufficient water is needed to drive the cumulative runoff from surface.

Part II

Materials and Method

Chapter 3

Developing the Paved Weighable Lysimeter System

This chapter gives a detailed description about the weighable lysimeter system with permeably paved surface, and represents the most important stage in this work. It has been implemented for 2 years in Berlin, Germany. Our lysimeters were developed to enable measurements

- of all components of the urban water budget,
- within a realistic walkway structure, and
- under completely natural hydrologic conditions.

It was essential that the system be able to

- measure the water budget components independently of each other,
- allow observation of the components correlatively with each other in a dynamic process,
- ensure high mass and temporal resolution.

Using weighable lysimeters with permeably paved surfaces, the measurements of runoff generation, infiltration capacity, and evaporation performance have to be acquired continuously in time series for the whole experiment period. In addition, the measurement system has to be capable of determining the soil hydrological parameters such as surface storage and saturated hydraulic conductivity.

3.1 General Aspects of Lysimeters

Determination of the water budget components by lysimeter

In general, a lysimeter system is used to acquire water budget components of top soil zone. The acquisition takes place by weighing the amount of water moving into and out of the system. According to the European definition, a lysimeter is a vessel container with local soil placed with its top flush and the ground surface for the study of several phases of the hydrological cycle, e.g. infiltration, runoff, evapotranspiration, soluble constituents removed in drainage, etc (Diestel et al., 1993; DVWK, 1996; Fank et al., 2004; Berger and Cepuder, 2007; European Lysimeter Plattform, 2008).

Seepage water can be sampled for detection of material flux within the soil. The lysimeter body is filled with original or artificial soils and its surface must match the surrounding surface. The lysimeter surface can be free, planted or paved. Large-capacity lysimeters can provide a realistic approximation of any soil section for investigating the physical and chemical interactions taking place between atmosphere, pedosphere, and biosphere, observed under natural conditions. In Europe, there are 82 lysimeter stations and 40 of which are in Germany. Over 90 % of them are installed for studies of forestry, agriculture and disposal sites (Lanthaler, 2006).

A lysimeter measures the weight change of the lysimeter body. The sign of these values can express water inflows, like precipitation (P), or water outflows, like evapotranspiration(ET) in connection with other water budget components, like groundwater recharge (GW) and runoff (RO).

Eq. 3.1 shows a common water balance equation in lysimeter:

$$P = RO + GW + ET + \Delta W\,, \tag{3.1}$$

where P = precipitation, RO = runoff, GW = groundwater recharge, ET = evapotranspiration, and ΔW = changable water storage. ΔW is calculated from rearranging Eq. 3.1. During a precipitation event

$$\Delta W = P - RO - GW, \tag{3.2}$$

if evaporation is likely negligible ($ET = 0$). In this case, ΔW gives the value of incoming water infiltrating through paved soil surface.

During the dry period ($P = 0$ between precipitation events)

$$\Delta W = -ET - GW\,. \tag{3.3}$$

In this case ΔW represents, with a negative value, the outgoing water evaporating from the paved surface.

Problems

Little is known about weighable lysimeters with pavements. The ones used in the past were for isolated studies, each aimed at addressing a unique aim, and an established system for manufacturing and using paved lysimeters has not yet been developed. From the reviews about lysimeter and water budget studies in Section 2.1, two significant problems can be brought out about the state of the art:

(i) In most water budget studies, infiltration was simply calculated as the difference of precipitation and runoff without exact evaluation of infiltration accuracy through direct measurement. The evaporation was also computed by an empirical formula. Therefore, those studies could make a statement about the annual water balance or water balance of a certain water regime, but not a sophisticated statement about water budget processes. The reason is that estimation of runoff are more reliable, due to the high and simple accuracy of runoff measurement techniques, than those of infiltration, which is normally too complicated to determine directly under real conditions.

(ii) Studies that attempted to include process-based observation (e.g. for runoff dynamics) often employed the sprinkling tests in most cases. Sprinkling tests are suitable only for figuring out the peak discharges and runoff behavior of storm events. The sprinkling technique has not gone so far as to exactly reproduce small events that are frequently observed in reality. Thus, in order to consider the varying water processes of small events, the experiment absolutely needs to be based on the given natural precipitation events.

Since the aim of this study is to accurately describe the surface water behavior, the following problems can arise for the experimental design:

- Lysimeter surface has to imitate all the characteristics of real urban soil surfaces,
- Runoff delaying has to be avoided, and
- The neighborhood and boundary effects has to be avoided.

One remarkable characteristics of this study is that the experiment is running in field conditions with paved soils that can match very closely to real urban surfaces. Many experiments with strictly defined boundary conditions in laboratories could refer only to the runoff behavior of paving materials, but not the runoff dynamics of paved soils, including seam materials. The experimental design was strongly focused on enhancing the temporal resolution and avoiding unnecessary intermediate storage such as runoff delays within the gutter (called gutter errors).

3.2 Measurement of the Water Budget Components

3.2.1 Lysimeter Setup

In order to monitor every water budget phenomena a weighable lysimeter system with pavement was constructed in the field of UBA (Federal Agency for Environment) and installed in Berlin Marienfelde, in the southern part of Berlin (see Fig. 3.1).

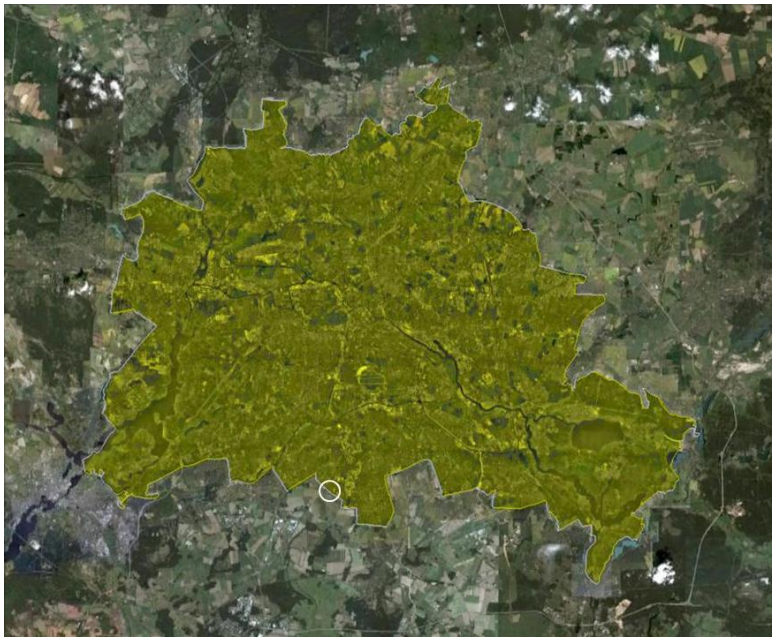

Figure 3.1: Lysimeter location in Marienfelde, southern Berlin, Germany.

The lysimeter system consists of 2 paved lysimeters, 2 FAO reference lysimeters (Fig. 3.2), and a climate station that existed already for the whole UBA field. The paved lysimeter, used here for studying the urban water budget, can measure all components of a water budget (precipitation, infiltration, evaporation, runoff, and groundwater recharge) separately. Infiltration is not only estimated as the difference between precipitation and runoff, but can also be directly measured due to the high resolution of lysimeter. Evaporation can also be directly determined. By using FAO lysimeters, the system is able to monitor the potential evapotranspiration throughout the experiment. One rain gauge system is installed based on the model of Hellmann (W.M.O., 2006). Further significant aspect of system is the weighable runoff measurement set-up (see Chap. 4).

The lysimeter bodies stand in the basement where all actions are monitored (see Fig. 3.4). Fank et al. (2004) once suggested that the invisible lysimeter is the

Figure 3.2: Lysimeter site in the experiment field of UBA (Federal Agency for Environment): The area surrounding the lysimeters is paved with identical pavement. The metal ring imposed at the lysimeter surface edge protects the runoff gutter from rain. Note that the Hellmann rain gauge installed at 30 cm level from the soil surface.

best one, that is, the lysimeter surface has to match the surface of the surrounding ground in order to avoid the so called "island effect". Thus, the experiment area of 20 m^2 was also paved with concrete paving slabs.

The lysimeter surface has a size of 1 m^2. The bodies stand in 1.5 m depth. The lysimeter containers are stainless steel and sit on a large scale with a resolution of 100 g/sec (Fig. 3.3).

The paved lysimeter bodies are filled with construction sand (mine-washed sand materials from the sand mine factory Firma Kluge from Brandenburg Berlin, grain size 0–2 mm) to a depth of 1.3 m and with gravels for the remaining 0.2 m (Fig. 3.5). This gravel layer serves as a capillary blocking layer in the lower lysimeter boundary to prevent against water loss from gathering seepage water.

To measure the groundwater recharge, the suction plates are set with a sub-pressure of 0.63 m provided by water column, which corresponds to the matrix potential of 1.8 pF. The seepage water can be measured with a resolution of 0.005 g. A geotextile material (a protection fleece from the factory Firma Naue with product label: Secutex 301GRK 5) is placed over the suction plates, serving as the leading capillary layer that completely gathers the seepage water (Fig. 3.6). The seepage water is completely captured with four suction plates and measured at groundwater recharge (Fig. 3.7).

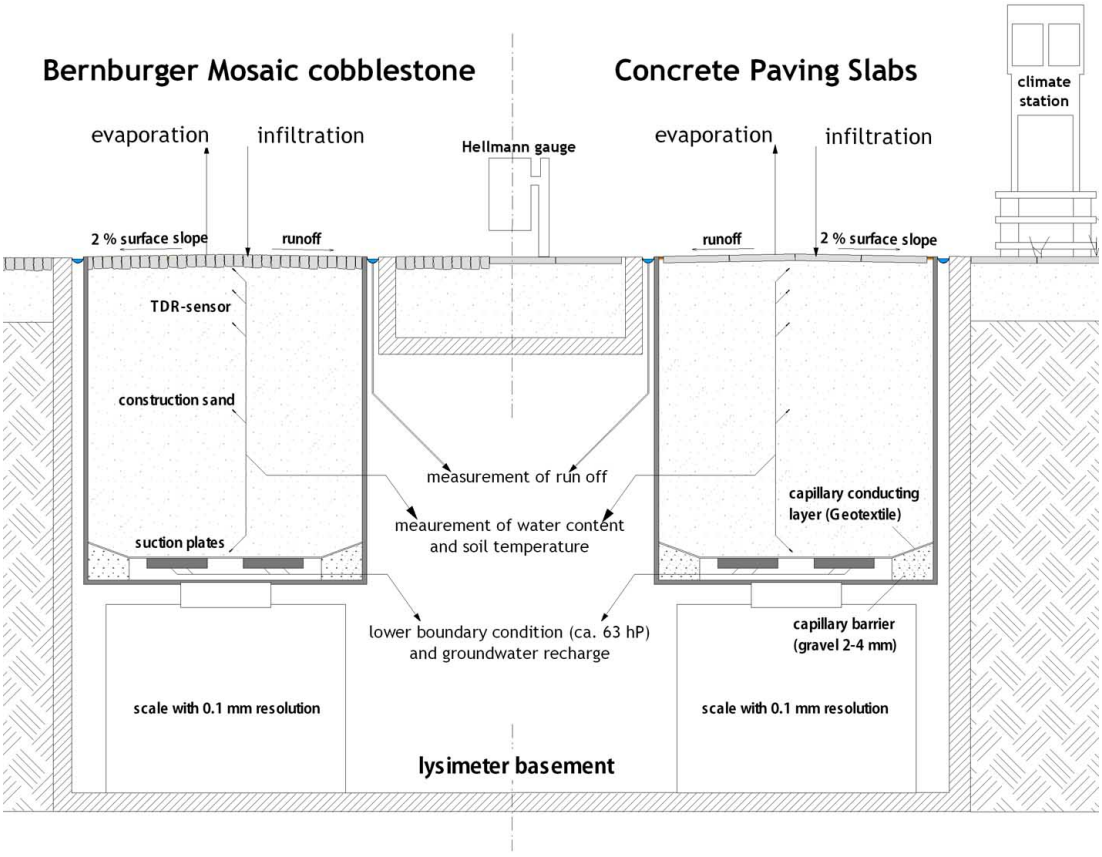

Figure 3.3: Scheme of paved weighable lysimeter.

Figure 3.4: Lysimeter basement.

Figure 3.5: Sand-bedding as pavement base.

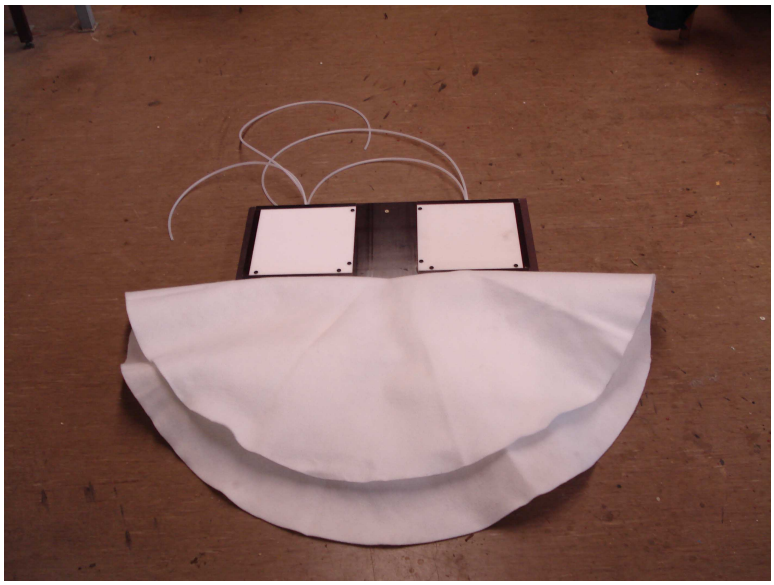

Figure 3.6: Gathering seepage water at the lower boundary: Fleece material as capillary conducting layer above the suction plates and the gravel layer.

Figure 3.7: Capillary blocking layer from gravel prevents the eventually ponded water at lysimeter bottom from rising up.

Figure 3.8: Water column and runoff discharge pipe: the water column provides suction plates with a sub-pressure of ca. 63 hP. The runoff discharge pipe carries the runoff down from the runoff gutter.

3.2.2 Pavement Assembly with "Berlin's Sidewalk"

The permeable pavement serves as materials for walkway, parking slots, sports grounds, streets, and roads with small burdening. In experiment, the walkway variation, so called "Berlin's Walkway", has been chosen, which consists of "Burnburg mosaic cobblestones" and "Concrete paving slabs". "Burnburg mosaic cobblestones" is pavement with several natural stones from the region of a former mine in Bernburg, eastern Germany. The reason for this choice lies in the common use of these walkway materials in Berlin and many parts of Germany.

Fig. 3.9 presents lysimeter surface with "Bernburg mosaic cobblestone" and "Concrete paving slab". These surrounding stainless steel rings protect the runoff gutter from collecting direct rainfall onto it. The pavement materials differ from each other in terms of the following properties:

(i) Concrete surface is normally much more porous than natural stones. According to the studies of Wessolek and Facklam (1997), the porosity and field capacity of cobblestone are 3.9 Vol.% and less than 0.5 Vol.%, respectively, while those for concrete are 5.1 Vol.% and 1.0 Vol.%.

(ii) The seam portion of cobblestone pavements is normally much bigger than that of concrete pavements. In terms of heat and temperature behavior, pavements show very different daily fluctuations depending on the seam portion (Starke, 2011; Wessolek and Facklam, 1997).

For calculating the seam portion, Rim (2008) suggested a procedure. This procedure yields the seam portion of max. 45 % for pavements from Bernburger mosaic cobblestone (MCS) and max. 10 % for pavement from concrete paving slabs (CPS).

The upper surface and sub-base of lysimeter pavements attempt to imitate the actual streets of Berlin. Each lysimeter has a a slope of about 2 % from the middle point to surface border. In real urban conditions the common gradient for road construction is between 1 % and 5 %. Due to practical reasons and the best construction practices, the gradient of 2 % was here chosen (Niesel, 2002).

In Fig. 2.1 an example of the standard vertical structure of a street and walkway is shown. In this work, no such sub-base structure was used for the following reasons:

(i) the new seam materials decline somehow in porosity after extended use (Borgwardt et al., 2000) and reach a clogging -state quickly;

(ii) in practice, a sub-base is commonly not needed in the construction of walkways, and the walkway is instead bedded directly in base sand by a vibratory plate machine; and

(iii) well-structured sub-bases with high retention capacity do occur, but are evidenced not to increase surface evaporation considerably (Starke, 2010).

(a) Bernburg mosaic cobblestones *(MCS)*.

(b) Concrete paving slabs *(CPS)*.

Figure 3.9: Lysimeter surface with the materials of "Berlin's Walkway".

Table 3.1: Parameter of lysimeter pavements. Almost identical seam material and sub-base structure are used for both pavements of Bernburg cobblestone and concrete paving slabs. The surfaces differ rather due to the surface properties like seam portion and pavement size. The seam materials were collected from different sites in Berlin.

layer	Properties	Bernburg mosaic cobblestone	Concrete paving slabs
Paving material	seam portion [%]	40	7
	surface slope [%]	2	2
	size [cm•cm•cm]	min. 4 • 4 • 4 max. 6 • 6 • 6	30 • 30 • 4
Seam material (0 - 1 cm)	seam width [mm]	5 - 10	2 - 7
	thickness [mm]	10	
	ρ_B [10^3g/cm^3]	1.49**	
	sand [%]	89.68* / 86.27 **	
	silt [%]	8.39* / 12.73 **	
	clay [%]	1.98* / 1.00 **	
	humus [%]	2.88	
Sub-base material (1 - 5 cm)	thickness [mm]	40	
	ρ_B [10^3g/cm^3]	1.61**	
	sand [%]	95.23**	
	silt [%]	4.37**	
	clay [%]	0.43**	
	humus [%]	0.37**	
Base material (> 5 cm)	ρ_B [10^3g/cm^3]	1.51	
	sand [%]	100	

ρ_B:dry bulk density, * by Wessolek and Facklam (1997), ** by Nehls et al (2006)

3.2.3 General Runoff Assembly

Throughout the study, runoff measurement will be the key method for measuring changes in the water balance. In general, the runoff process for paved catchment areas consists of runoff generation at the surface and runoff transport along the flow path. According to the complexity of soil and surface flow path properties, both processes will shape a causal relationship that is known as "runoff concentration". Here, the runoff generation process considerably influences the runoff transport process.

Two rainfall-runoff relationships are of great interest:

(i) the total runoff depth and

(ii) the runoff peak discharge.

The first relationship is primarily dependent on the infiltration capacity of the catchment surface, while the latter is additionally dependent on the concentration process. The smaller the catchment surface size is, the more clearly the runoff generation can be observed.

Hence, owing to the small area of the lysimeter surface ($1\,m^2$), the observed runoff process presumably represents the runoff generation process. The abovementioned runoff depth and the peak discharge can be described in high accuracy. Therefore, lysimeter surface can be defined as a "representative elementary surface".

As the runoff from the paved surface at the beginning of a rainfall event proceeds in interplay with the initial infiltration of short duration, a good temporal resolution is important. For this reason, our weighable lysimeter can provide the option to precisely monitor the initial infiltration process. Further, the evaporation of short duration that follows immediately after the rainfall event can be persued in a high timely manner.

In Fig. 3.10, seam material is being compressed by pouring water onto it in order to consolidate the soil surface without using a vibratory plate machine. In this figure the produced runoff is streaming downwards to the runoff gutter, which is set up directly along the surface edge. This allows the run-off to be immediately shunted to a separate discharge pipe.

Fig. 3.11 illustrates the runoff collection process through the runoff gutter. The collected runoff water goes to the tipping bucket, which be used to can quantify the unit volume of water.

No water is lost in this procedure. The lysimeter wall and drain gutter are made of high-grade stainless steel. . The amount of runoff water that is retained in the gutter is called the runoff gutter error. In our system it amounts to max. 150 ml that corresponds to 0.15 mm and the delaying time span is not more than 10 minutes (see Chap. 5.1).

Figure 3.10: Water pouring to consolidate the seam material and runoff water flowing to runoff gutter. The runoff gutter is fixed along the lysimeter side wall.

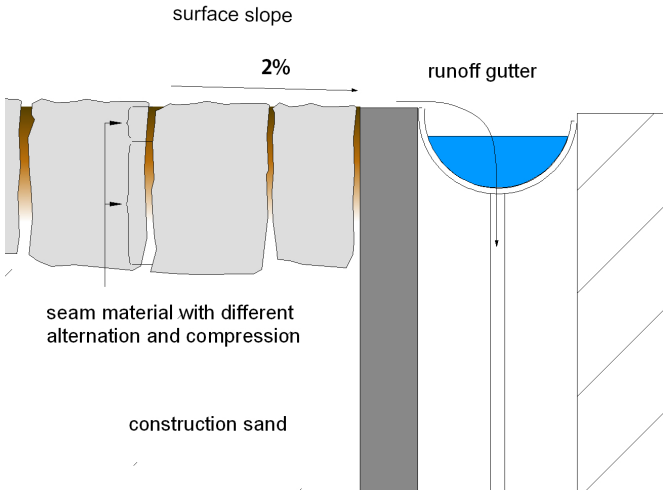

Figure 3.11: The upper surface (at least the top 1 cm) of pavement is the most altered and compressed soil in real urban streets. The soil zone of next 4 cm below that is less compressed. Runoff water is collected in the runoff gutter and flows to the runoff tipping bucket in the lysimeter basement.

3.3 Data Acquisition and Handling

Data streaming

From April 2009 to October 2010, the rainfall, infiltration, runoff, evaporation and groundwater recharge were continuously monitored from 4 lysimeters in a temporal resolution of 3 seconds. The collected water balance data were summed up and analyzed in a resolution of 1 minute. Thus, for this work the temporal data analysis will be primarily based on units of millimeters per minute [mm/min].

All acquired data were directed to a central computer by multiple transmitting via serial ports RS 232c. Because the multiple serial transmission could fail in weather-related stress from the resolution of 1 second, all data input is configured to the 3 seconds resolution, even though the system is capable of 1-second resolution.

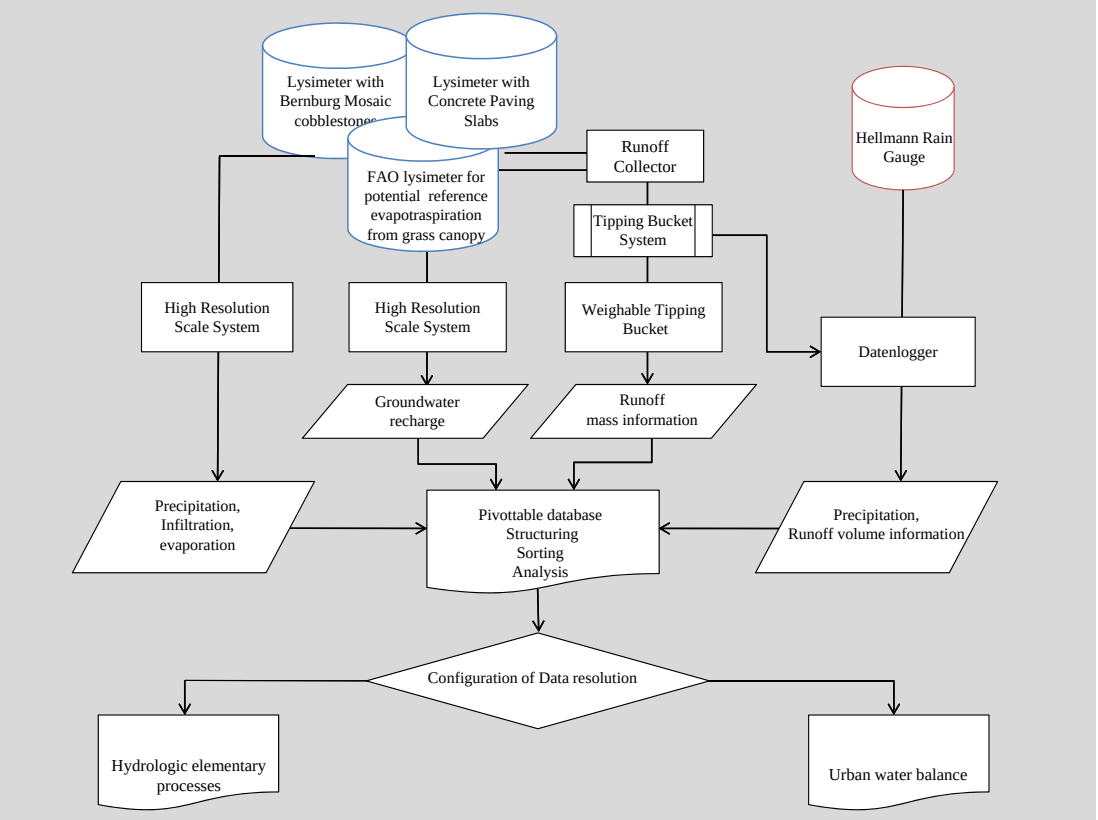

Figure 3.12: Lysimeter data stream: Evaporation, infiltration and groundwater recharge are balanced by precision digital scales (manufactured by Sartorius AG, Germany). Runoff generation is measured by a weighable tipping bucket. All data streams are transfered to the central computer via RS-232C, handled and stored within the Pivot database .

Scales and Equipments

In the experiment, a complex system of balancing equipments was needed to measure all water budget components separately. Precipitation amounts were determined primarily with the Hellmann rain gauge (W.M.O., 2006), which works along with the embedded precision tipping equipment (often called the tipping bucket). Lysimeters are theoretically also able to measure the precipitation depth according to an objective target, too. Here, the precipitation data determined by lysimeter were used as controlling data for the data correctness as gauged by the Hellman model when suspected data errors happeneds to arise.

The employed Hellmann gauge counts a unit volume each time the falling rain fills the tipping bucket. This unit volume is the volumetric amount of water that the tipping bucket releases by changing its position. The Hellmann gauge used has a $200\,cm^2$ apparatus surface and a tipping volume corresponds to 2 ml, allowing a measurement resolution of 0.1 mm (equals to $= 0.002\,L/0.02\,m^2$) (see Fig. 3.13).

The tipping signal is registered in a Combilog 1020 (data logger for Hellmann gauger and runoff gutter). The Combilog 1020 is able to register and process the series of tipping signals with its own CPU. This runs continuously with its own battery. By this device the automatic measurement is ensured even in bad weather situations.

Similarly, the runoff measurements were also made using a tipping-based volume scale (tipping bucket). The runoff tipping bucket used (manufacturer: UMS GmbH, Germany, 2006) has a unit tipping volume of 100 ml. As the lysimeter surface surface area is $1\,m^2$, the runoff measurement resolution also comes to 0.1 mm (equal to $0.1\,L/1\,m^2$). Fig. 3.8 and Fig. 4.2 show the introduced tipping bucket subjected to a runoff system..

Using a tipping bucket, an exact value of water mass can normally be gained. The disadvantage is the undefinable temporal resolution. The bigger the tipping volume becomes, the more often this problem. In the case of the runoff tipping bucket in our system, the low temporal resolution can give an misleading statement about time-related runoff processes. Many small events can get lost without being included in sample groups if the runoff water was less than one tipping volume (100 ml). To handle this problem, we developed an improved setup called a weighable tipping bucket (*WTB*).

A *WTB* is a combination of a normal digital scale and tipping equipment connected through a trasit lever. A *WTB* demonstrates a mass resolution of 0.0005 mm by doubling the 1 g step of scale with lever structure. In the Chap. 4 more is discussed about *WTB*.

As for the lysimeter balance, a huge industrial balance was used which can functionally hold the entire weight of ca. 8000 kg from sand and water. Nevertheless, the precipitation, infiltration and evaporation could be measured very sufficiently with resolution of 0.1 mm. This resolution is the ratio of the balance

Figure 3.13: Hellmann gauge in 30 cm level from the paved surface in lysimeter station.

resolution to surface area (equal to $100\,\mathrm{g}/1\,\mathrm{m}^2$. In contrast to the tipping bucket, the lysimeter balance can theoretically demonstrate weight value in 1-second intervals. A sensitive lever of the lysimeter balance is equipped with a metal rod, which transmits the mechanical movement due to weight change towards a precise digital scale.

The seepage water, gathered by the suction plates and capillary conducting layer, arrives at the seepage water container through the water column. The digital scale for measurement of groundwater recharge can give groundwater weight values at a resolution of 0.005 mm.

Data Handling

The central monitoring computer manages a data base that allows

- automatic structuring, sorting and navigating;
- automatic event separation and analysis; and
- real-time axis dimension.

For data handling, tools like Labview, Visual-Basic, and PIVOT table database were used (Jamal and Hagenstedt, 2004; Schwenk and Schuster, 2009). Using the visual programming software Labview, the ten RS 232C ports were scanned through every 3 seconds. The Visual-Basic (VBA) algorithm mainly recomposes

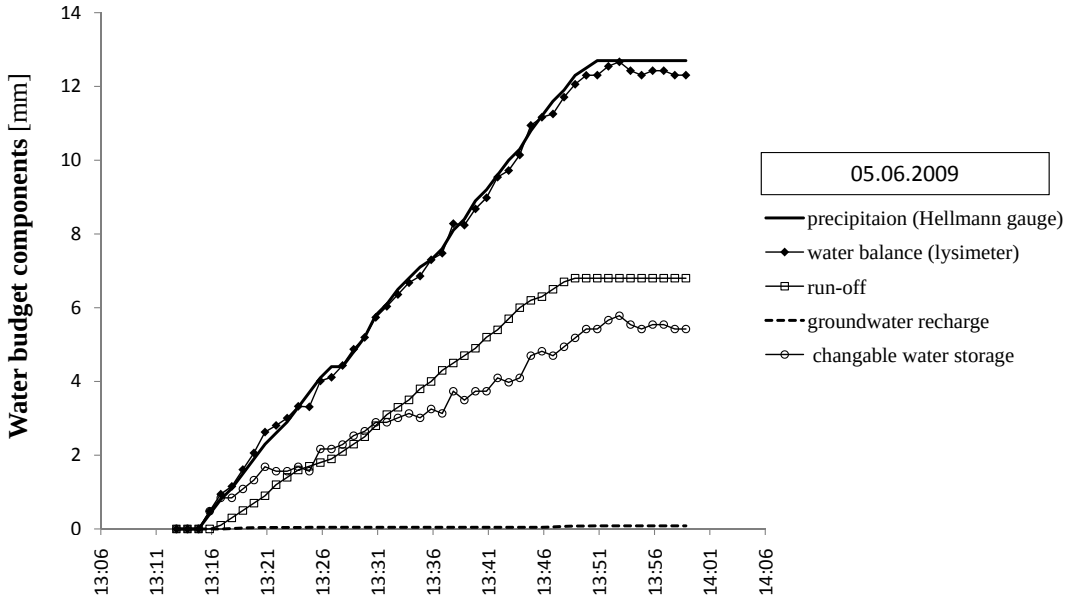

Figure 3.14: Precipitation event measured by Hellmann gauge and paved weighable lysimeter. Note the good agreement between the cumulative values of precipitation from Hellmann gauge and of the water balance from lysimeter for an event on June 5^{th}, 2009.

the synchronized mass values from the digital scales and non-synchronized volume values from the tipping buckets together on the real-time axis. Eventually the clocking failure of the logger system needs to be corrected by this VBA-tool. Because clocks from different logger systems do not match each other perfectly, this synchronization is indispensable. After this treatment the real-time data can flow into the Pivot-database.

A pivot database is a navigable table-database in which analysis resolution can be automatically configured. By setting up different resolutions, one can alternate the viewing dimension, e.g. from the annual water balance to a single hydrologic event. Furthermore, since it based on MS Excel, no special knowledge is needed for use. Thus the personnel-independent expansion and continuation of the database is simple and effective.

Fig. 3.14 shows result of a sprinkling test. The rainfall depth is calculated from the independent measurement of runoff, infiltration. Hellmann gauge gives almost as same precipitation as lysimeter. Due to wind influence, lysimeter data contains fluctuation. The difference between both measurement is less than 0.2 mm during the ca. 40 min sprinkling duration–(12.5 mm by Hellmann, 12.3 mm by lysimeter)

Chapter 4

A New Technical Approach for Measuring the Runoff Dynamics

The high temporal and quantitative resolution of runoff measurement is of significant interest. In this study, a runoff setup was installed with a runoff gutter, discharge pipe, and tipping bucket (TB). The common tipping buckets have a good volumetric accuracy in volume resolution and are capable of quantifying the highest rainfall intensities over a range of expected flows. However, this leads to the varying temporal resolutions for different flow intensities, and in particular results in low resolutions for small flow events. Therefore, their applicability to runoff measurements and other hydrological process studies is limited, especially when the dynamics of both small and large flow events will be described.

To solve this problem, an improved technique for runoff dynamics was added to the TB. It is accomplished by coupling the TB to a digital balance, called a weighable tipping bucket (WTB). The improved volume and temporal resolution of the WTB and the associated data processing concepts are demonstrated. A systematic uncertainty of TB measurements compared to WTB measurements is calculated. The impact of the increased resolution on our understanding of runoff dynamics on paved urban soils are discussed, exemplary for the runoff and the initial loss of a paved urban soil.

4.1 General Aspects of Runoff Measurements

The dynamics of the urban water balance are not completely understood (Ragab et al., 2003). Measuring runoff from permeable paved urban soils in a high temporal and quantitative resolution is the prerequisite for the formulation of a process-based surface water model. Such a model, based on meteorological data and pavement characteristics, would be capable of predicting changeable

runoff behavior for the changing rain volume and intensity distribution due to climate change as forecasted (Arnbjerg-Nielsen, 2006). Such models are therefore of interest for the development of climate change adaptation strategies for urban areas, such as drainage adjustment (Arnbjerg-Nielsen and Fleischer, 2009; Faram et al., 2010), the use of runoff water as an urban cooling resource for improved evapotranspiration (Nakayama and Fujita, 2010) or risk assessment for increased infiltration (Göbel et al., 2007; Nehls et al., 2007).

Importance of small events In this study, the water balance of pavements is measured using 1 m^2 weighable lysimeters (Rim et al., 2009). On the lysimeter surfaces, small rain events lead to small absolute runoff flows. However, these have to be detected. For understanding the processes that influence runoff generation from paved soil surfaces, small rain events are of the same or even greater importance than storm events for two reasons:

(i) Figure 4.1 demonstrates the long-term precipitation event sum distribution. It highlights the contribution of small precipitation events to the cumulative sum of precipitation in the study area. Similarly, precipitation events with small intensities contribute substantially to the total sum of precipitation (see Chap. 5.2). At the station Berlin-Marienfelde, 5 %, 50 % and 95 % of the cumulative rainfall is generated by rain fall events with intensities smaller than 0.0076, 0.0263 and 0.1886 mm/min respectively.

(ii) The runoff (RO) is a non-linear function of precipitation sum (P) and intensity (Sen and Altunkaynak, 2006). This means that different runoff generation processes might be of differing effectiveness for different rainfall amounts and intensities. Therefore, one needs to study runoff for both small and heavy rainfall events.

The functional principle of a TB is to count how often the two buckets with known unit tipping volume are filled and self-emptied. This principle has been used since the 1950s and is often used in hydro-meteorological instrumentation such as rain gauges (W.M.O., 2006) or stem flow meters (White and Rhodes, 1970). Tipping buckets have also been regularly employed for runoff measurements since the early 1960s (Pillsbury et al., 1962; Edwards et al., 1974; Khan and Ong, 1997). In addition, they are, used in wick samplers and lysimeters for the measurement and sampling of seepage water and for multi-compartment sampling (Meissner et al., 2010).

TBs are robust, reasonably-priced devices for the discontinuous detection of flow events with a wide spectrum of flow intensities and a high temporal resolution at the flow intensities for which the bucket was dimensioned (Habib et al., 2001). During instrumentation of our lysimeters, we became aware that the traditional TB is not appropriate for providing constant measurements, at high temporal and volumetric resolution, of runoff with both very low and very high flow intensities. Below is an explanation of why it is not suitable as it is and how

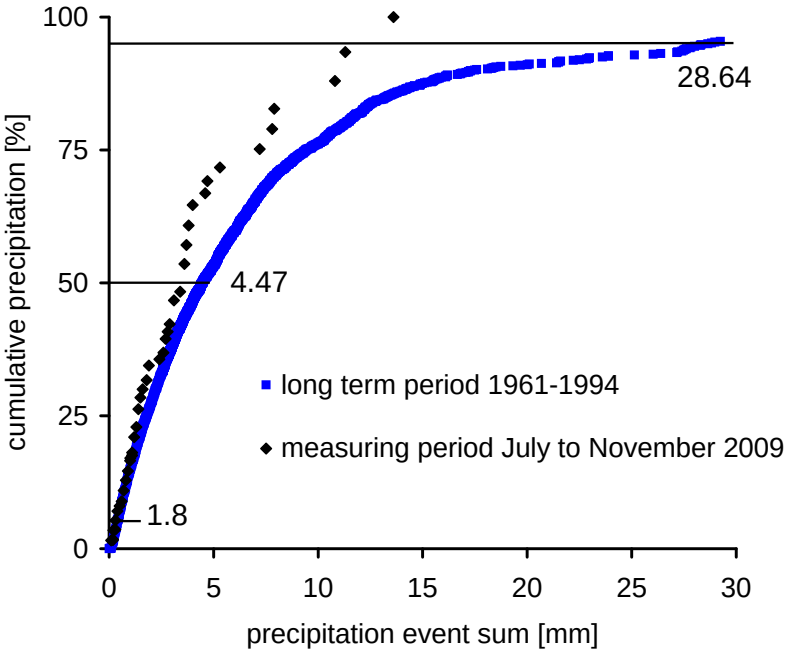

Figure 4.1: Contribution of individual precipitation event sums (separated by a dry period $T_d = 10\,\text{min}$) to the cumulative sum of precipitation at the station Berlin-Marienfelde, 1961–1994 (solid line, N=11363) and of the rain events during the observation period of this study, July, 8$^{\text{th}}$ to November, 30$^{\text{th}}$, 2009 (dashed line, N=154). The 5 %, 50 % and 95 % quantiles are marked for the period 1961–1990.

we improved the system.

Limited volumetric and temporal resolution of tipping buckets Before the first tipping and after the last tipping, the TB delivers no information about the water level in the bucket and about the current flow into or out of the bucket. Therefore, the TB is not appropriate for accurately determining the duration of flow events. There is no information on the real beginning of the flow event from the tipping signals, as the first drops of the event do not necessarily lead to a tipping signal; even if the first drop did lead to a tipping, we would not know that it was the first drop. In addition, there is no information about the water left in the bucket from the previous flow events.

Similarly, the time of the end of a flow event cannot be determined exactly, because it is not known when the flow stopped unless the last drop caused a tipping (and also then we cannot know that is was the last drop).

The problem of incorrect flow event durations gets more important with decreasing flow intensities for a given bucket volume. If flow event sums are smaller than the bucket volume, individual flow events are no longer detectable.

The starting point of a flow event can be extrapolated from the behavior of the flow during the reliable TB measuring period, especially when the rise of the flow intensity at the beginning of the event is very steep. However, this is already an interpretation of measured data and not a true measurement.

The TBs are usually dimensioned to detect the highest of an expected range of flow intensities. This is done by choosing the bucket size according to the expected flow rate and the maximum possible tipping frequency. Then, TBs provide proper information, especially during high flow events, after the first tipping and before the last tipping of the buckets. This duration is the "reliable TB measurement period".

Because of the distinct volume of the bucket, low flow intensities lead to low temporal resolutions, and high flow intensities lead to high temporal resolutions. The problem of the resulting high measurement uncertainties is discussed by Yu et al. (1997). If, as in this study, a wide range of flow intensities are of the same interest as great events, TBs are inappropriate measuring devices in terms of temporal resolution.

Further, different flow events cannot be detected with an adequate, a priori chosen temporal resolution. This is a disadvantage of the TBs concerning the harmonization of measurements of different water balance elements in the same catchment. The bucket volume could be decreased to increase the resolution for small events, but that would decrease the maximum detectable flow rate of the TB. Also, the filling of the bucket needs to take a sufficiently long time compared to the duration of a complete tipping (Yu et al., 1997). Otherwise, the TB overflows without quantification of the flow.

It can be argued that the water balance for the TB itself is closed over long periods. Water that is left in the bucket after an event will be added to the next event. Using this argument, TBs have been employed for runoff studies aimed at the measurement of annual mean runoff amounts for paved urban soils (Wessolek and Facklam, 1997; Wessolek, 2008). However, for systems in which the tipping bucket cannot be sealed against the atmosphere, as in our setup, water could be lost from the bucket due to evaporation. Even small evaporated amounts may then sum up to substantial losses at the end of the observation period.

The traditional TB had to be improved to be applicable for our studies of runoff generation and runoff dynamics from paved urban soils. The volume resolution given by the bucket size of the TB had to be improved substantially, without decreasing the capacity to detect high flow events. By increasing the volume resolution of the TB, we were able to also increase its temporal resolution.

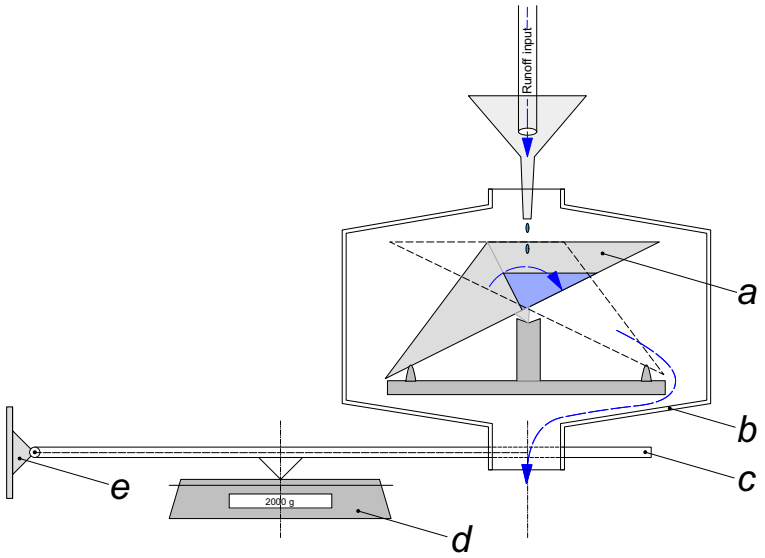

Figure 4.2: Scheme of the weighable tipping bucket system. The blue arrow indicates the way the water has to go when leaving a) the tipping bucket and b) the box. The other parts of the set-up are c) the lever connected to the balance by a screw, d) the balance and e) the pivot.

4.2 Weighable Tipping Bucket

WTB Setup

In the lysimeter basement, runoff water is collected by a tipping bucket (Pulsameter MC 1, UP Umweltanalytische Produkte GmbH, Cottbus, Germany) with a bucket volume of 0.1 L which is equivalent to 0.1 mm of runoff from the paved surface. During calibration, the average of the two bucket volumes ($\bar{V}_{\mathrm{B}}$) was measured as 0.098 L (standard error = 0.002 L).

The TB has been coupled to a digital balance (Acculab VIC-4KG, Sartorius AG, Goettingen, Germany) with a resolution of 1 g. The TB is mounted at the end of a lever with the length l_1, which is pivoted at the another end (Fig. 4.2). This leverage construction was needed in order to discharge the TB without making the digital balance wet. At the distance $l_2 = 0.51 \times l_1$, a screw transmits the force to the digital balance. The distance l_2 was estimated during calibration of the balance system using 100 g test weights. The calibration of the balance has been repeated at the end of the measuring period. The drift of the balance was lower than 1 g. However, we enhanced twice the resolution of the balance at its detection limit.

The screw connects the balance to the leverage and allows the TB to adjust horizontally, which is a prerequisite for the proper functioning of the TB. Due to the leverage effect, the accuracy of the WTB system as a whole is $V_{\mathrm{min}} \approx 0.001$ L.

The signals from both the TB and the WTB are recorded by data loggers (see Chap. 3.3). The temporal resolution of the TB varies with the runoff intensity; the maximum flow intensity detectable by the TB is 15 mm/min. Due to some technical reasons described above, in this study the temporal resolution of the data logger connected to the balance is 3 s.

Data Processing Concept

To correct the leverage effect, the weights detected by the digital balance were multiplied by the factor 0.5 in order to get the actual water weight in the tipping bucket. The TB signals were processed as follows: the first tipping is accounted for as $0.5\,\bar{V}_{\mathrm{B}}$, every following tipping is accounted for as $\bar{V}_{\mathrm{B}}$. After the last tipping, another $0.5\,\bar{V}_{\mathrm{B}}$ is added to the sum of tippings before. This evenly distributes the water left in the bucket after the last tipping of an event and the water collected before the first tipping of the subsequent event to all of the individual events.

The sum of a runoff event measured by the TB is therefore

$$RO_{\mathrm{TB}} = \frac{n\bar{V}_{\mathrm{B}}}{A} \quad (n \in \mathbb{N}) \quad [\mathrm{mm}]\,, \tag{4.1}$$

where n = the number of tippings, $\bar{V}_{\mathrm{B}}$ = the bucket volume [L] and A [m^2] = the paved surface area.

The WTB data was processed as follows: the volume of water collected before the first tipping (V_{FT}) was calculated as difference between the volume before the beginning of runoff and the highest volume detected. The volume of water collected after the last tipping of an event (V_{LT}) is calculated as the difference between the lowest volume of the tipping bucket and the volume at the end of the event.

The beginning of an event is identified as follows: if the previous runoff has completely finished, it is simply the first positive weight change of the balance after a long period of no changes or decreasing weights due to evaporation. If the subsequent rain event is over, but the runoff is still being collected, the two rain events and the associating runoff events cannot be separated and are processed as one event.

When the rain event is over and the runoff from the surface has also stopped, the WTB can still collect water. Such water is the draining of the gutter system than runoff. The runoff detection is delayed due to the measurement set up. A criterion is needed to identify the end of real surface runoff. Based on observations at our lysimeter, this criterion has been chosen to be a flow rate less than 0.002 L/min. Such draining water is still accounted for as runoff, but is no longer accounted in terms of runoff duration (Fig. 4.3).

After the first tipping, every tipping is accounted with $\bar{V}_{\mathrm{B}}$ [L]. The sum of the runoff event measured by the WTB is therefore

$$RO_{\mathrm{WTB}} = \begin{cases} \dfrac{V_{\mathrm{FT}}}{A} \text{ for } n = 0 \\ \dfrac{(n-1)\bar{V}_{\mathrm{B}} + V_{\mathrm{FT}} + V_{\mathrm{LT}}}{A} \text{ for } n \geq 1,\ n \in \mathbb{N} \end{cases} \quad [\mathrm{mm}] \qquad (4.2)$$

where V_{FT} [L] = the volume of water collected before the first tipping and V_{LT} [L] = the volume of water collected after the last tipping of an event.

The runoff sum for the observation period was calculated as the sum of the individual events both for TB and WTB data according to equations 4.1 and 4.2. The surface storage V_{S} was estimated by the maximum rain event sum, at which no runoff was detected, both using TB and WTB data.

4.3 Increased Accuracy of Surface Runoff Measurement using *WTB*

Increased volume resolution

The runoff generation from the permeably paved lysimeter surface was studied using and comparing the data gained from the TB and the WTB. For example, one single runoff event on the 3rd of September 2009 is shown in Fig. 4.3. This rain event started at 10:42 lasted for 33 min and had a sum of 1.2 mm. For this RO event, the TB tipped five times, and a runoff of 0.5 mm and 0.45 mm was detected by the TB and the WTB ,respectively. Note that from 10:43 until 11:03 a total of 0.004 L entered the WTB. This water was left in the gutter system from the previous rain event, which ended 9:45 and was also accounted to the subsequent RO event.

The absolute difference $RO_{\mathrm{WTB}} - RO_{\mathrm{TB}}$ is -0.05 mm. The relative difference U (Eq. 4.3) is -10 %, while the maximum difference would be -17 % (see Eq. 4.4).

This example underscores the great advantage of the WTB system and gives an impression of the reliability of measurements made using solely the TB.

As shown in Fig. 4.3, the weights for the maximum filled and the empty buckets vary. This might be due to differing volumes for the left and the right buckets, as this was estimated during calibration of the system. While the left bucket volume is 0.1029 L, the right bucket only fills up to 0.0955 L before tipping, resulting in a $\bar{V}_{\mathrm{B}}$ of 0.0987 L.

However, this effect is not the only reason for the difference, as the volumes of water at tipping are not reproducible. Further effects are responsible:

(i) water needs some time to flow out of the TB box, which is indicated in Fig. 4.2. In the meantime, water enters the TB box from above. Thus, the WTB detects water entering and leaving the TB box in the same time step. The resulting uncertainty is proportional to the flow intensity. Consequently, the

balance detected the lowest weight for the empty bucket and one of the highest weights for the full bucket, when the flow intensity was the smallest at the end of the runoff event shown in Fig. 4.3 and Fig. 4.4.

(ii) The different maximum and minimum bucket weights are also an artifact of the 3 s measuring interval of the balance. For the runoff event at the 3rd of September 2009 mentioned above, we calculated a flow rate of $3.3{\cdot}10^{-3}$L for the interval between the first and the second tipping of the TB. That results in an uncertainty of ca. 0.01 L for the maximum and minimum filling of the TB at this flow rate and the given temporal resolution of the digital balance.

Because of (i) and (ii), the runoff is calculated from the tipping signals instead of the balance data between the first and the last tipping of the bucket (see Eq. 4.2).

Furthermore, (iii) the buckets of the TB spin along the leverage and not perpendicular to it. For technical reasons in our individual case, it was not possible to mount the tipping bucket in a different way. This means that the similarly filled buckets would lead to different weights detected by the balance due to the different torques. The two buckets have the following leverage factors: 0.50 for the shorter lever and 0.52 for the longer lever. However, the bucket volumes were calculated using the average factor of 0.51 for the first approximation.

Systematic uncertainty of TB compared to WTB

While the discrepancy between runoff measurement by TB and WTB can be high for a single event, it will be smaller after a long observation period with a high number of tippings, as then the relative contribution of the first and the last tippings to the sum of tippings decreases.

In the following description, the maximum relative difference between WTB and TB ($U_{\max}$) for a certain number of tippings of TB is calculated. We consider the WTB data to be more precise than the TB data for the following reasons: the WTB system uses the same tipping information as the TB but also delivers information about the water flow in periods between two tippings. In this period the WTB has a volumetric resolution 200 times higher than that of the TB. A testing of the assumption of the higher precision of the WTB in a physical experiment is not truly possible, because the device can only compared to itself. First, the device is compared to exactly itself. Any test of the weighing function of the WTB must be based on the quantification of a water flow, which would only be possible with another balance. In such a test, one balance would just be compared to another balance. Because measuring the weight is one of the basic physical measurements, and because we employed a calibrated digital balance for the measurement of the mass of the TB, we assume that the weight of the TB is measured as precisely as described above.

The relative detection limit of the digital balance compared to the bucket (x) can be expressed as $x = V_{\min}/\bar{V}_{\mathrm{B}}$. With $V_{\min} = 0.001$L and $\bar{V}_{\mathrm{B}} = 0.1$L x equals

0.01.

Generally, RO_{WTB} can be higher or lower than RO_{TB}, leading to positive or negative differences. In the case of the maximum positive difference, $RO_{\mathrm{WTB}} - RO_{\mathrm{TB}}$, the bucket is almost empty (= 0.001 L) at the beginning of the event and is left almost filled (= 0.099 L) at the end (then, $U_{\max} \rightarrow max$ for $(V_{\mathrm{FT}} + V_{\mathrm{LT}}) \rightarrow 2(V_{\mathrm{B}} - xV_{\mathrm{B}})$). In case of the maximum negative difference, the bucket is almost full at the beginning of the event (= 0.099 L) but left almost empty (= 0.001 L) at the end (then, $U_{\max} \rightarrow min$ for $(V_{\mathrm{FT}} + V_{\mathrm{LT}}) \rightarrow 2xV_{\mathrm{B}}$).

Substituting

$$U_{\max} = \frac{RO_{\mathrm{WTB}} - RO_{\mathrm{TB}}}{RO_{\mathrm{WTB}}} \times 100\,\% \tag{4.3}$$

with Eqs. 4.1 and 4.2 for $V_{\mathrm{FT}} + V_{\mathrm{LT}} \rightarrow 2xV_{\mathrm{B}}$ and $V_{\mathrm{FT}} + V_{\mathrm{LT}} \rightarrow 2(V_{\mathrm{B}} - xV_{\mathrm{B}})$ reveals

$$\frac{-1 + 2x}{n - 1 + 2x} \times 100\,\% \leq U_{\max} \leq \frac{1 - 2x}{n + 1 - 2x} \times 100\,\% \tag{4.4}$$

From Eq. 4.4 one can learn that the maximum systematic uncertainty is highest for small runoff volumes leading to no or only a small number of tippings. $|U_{\max}|$ is lower than 5 % and 1 % for 21 and 99 tippings, respectively, which equals a run off of 2.1 mm and 9.8 mm. The rain distribution in Fig. 4.1 demonstrates that uncertainties higher than 5 % must be assumed at least for 28 % of all rain events (assuming a linear RC of 1) when a TB is used for measurements. However, we know that RC is not linear for different rain intensities and that due to evaporation of rain water from the surface and infiltration, higher maximum systematic uncertainties must be assumed for the quantiles mentioned above.

Increased temporal resolution

Employing WTBs instead of TBs increases the temporal resolution of the runoff observation. The rain event on September, 3rd, 2009 started at 10:42 am, lasted for 33 min and and resulted in a total of 1.2 mm (Fig. 4.3). The associated runoff event lasted from 11:03:01 am until 11:33 am as detected by the WTB, but only from 11:03:13 am until 11:13 am as detected by the TB (Fig. 4.4).

Depending on the water level in the bucket, the starting times of runoff events detected by TB and WTB might be close. This is due to the steep increase of the runoff intensity at the beginning of the event. At the end of the runoff event, the flow intensity tails out slowly. From the TB data, the runoff appears to have already stopped before the end of the rain. That scenario is not impossible: it could be explained by processes like evaporation or infiltration. The low volume resolution of the TB system leads to a very low temporal resolution. In contrast,

the WTB can detect the end of the runoff event much better due to its increased volume resolution and the constant high temporal resolution.

This has important consequences for the measurement of runoff dynamics, e.g. the runoff concentration time (t_c). When measuring with the TB, for a given rain intensity and a given moisture content in the pavement, t_c depends on pavement characteristics such as V_S, rain intensity and other climatic conditions, but also on the level of water in the bucket, left over from the last event. Measuring with the WTB, in contrast, detects a t_c which is almost solely dependent on the pavement, rain intensity and climatic characteristics.

Accuracy of Runoff for a Test Period

During the observation period, 8^{th} of July until $1^s t$ of December 2009, the TB detected a total of 71.6 mm of runoff, while the WTB detected 79.6 mm. This difference is equal to 11 % of the total runoff detected by the TB. Up to 95 % of the difference can be explained by evaporation losses from the TB. During the measurement period, a quantity of 7.6 L evaporated from the TB, as calculated from weight losses from WTB in the periods between the runoff events.

In this study, the individual runoff events, especially those caused by small rain events, were of interest rather than the sum of runoff over a long period. During the observation period, the rainfall gauge detected 154 rainfall events, leading to 121 and 47 runoff events, detected by the WTB and TB respectively. The higher resolution of the WTB compared to the TB led to more observations and will lead to a different description of runoff processes.

This is shown by the following example: although the runoff coefficient (RC) is not constant for different precipitation events, one can calculate an average runoff coefficient (RC) and its standard deviation (SD) for the detected runoff events, in order to compare the data sets: for events detected by the TB, $\bar{RC}_{\text{TB}}$ is 0.38 (SD = 0.21, N=47), while for events detected by WTB $\bar{RC}_{\text{WTB}}$ is only 0.10 (SD = 0.23, N = 121). Using TB data would overestimate the runoff formation compared to WTB data. Additionally, WTB data has higher variation than TB data; thus the first delivers more comprehensive information for process studies than the latter.

Accuracy of Initial Loss from Runoff Measurements

As not all rain events lead to runoff, there must be a retainment of water on or in the pavements. It is not the goal of this work to study this topic in detail, but we can show that the magnitude of V_S measurements strongly depends on the volume resolution of the measuring device.

According to our hypothesis, the storage V_S is the sum of free water retained at the surface of pavements in its micro relief (V_R), the air-filled pore volume of

porous pavements (V_{P}) and the air filled pore volume of the seam material and the underlying soil V_{SM}:

$$V_{\mathrm{S}} = V_{\mathrm{R}} + V_{\mathrm{P}} + V_{\mathrm{SM}} \quad [\mathrm{mm}] \tag{4.5}$$

V_{S} is a function of the initial water content and the material and design characteristics of the pavements and the pavement system, as well as a function of the pore system properties of seam material and the underlying soil. First estimations of the maximum $V_{\mathrm{S\,max}}$ can be derived from the maximum rain events which did not lead to runoff. Analyzing the TB data, $V_{\mathrm{S\,max}}$ is then 2.5 mm, but this value is only 1.7 mm using WTB data. Thus, the lower volume resolution of the TB would lead to an overestimation of the initial loss of 47 %. That would in turn lead to a underestimation of runoff in process-based models, which consider such initial loss.

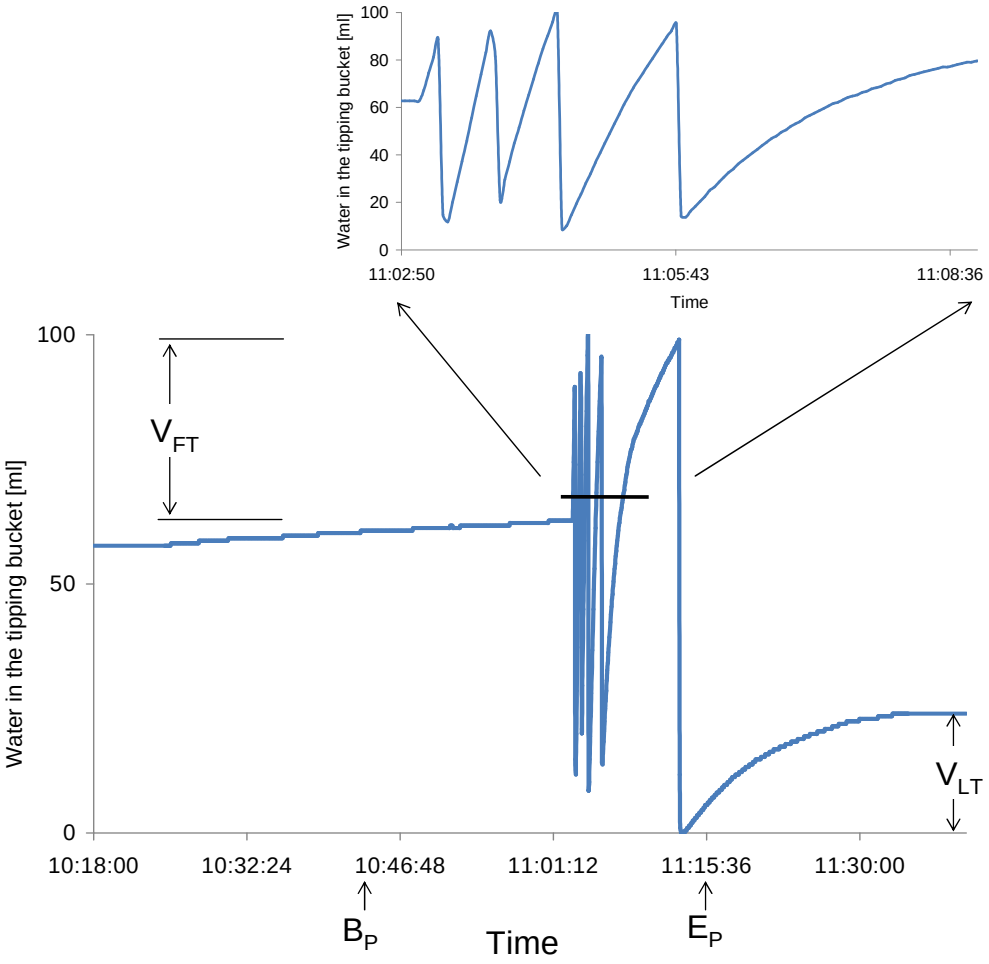

Figure 4.3: Runoff event from concrete paving slab at the 3rd of September 2009 in Berlin-Marienfelde, Germany. The runoff event was studied using the weighable tipping bucket. Indicated are the filled bucket volumes at the beginning (V_{FT}) and at the end of the runoff event (V_{LT}) as well as the beginning (B_{P}) and the end (E_{P}) of the precipitation event.

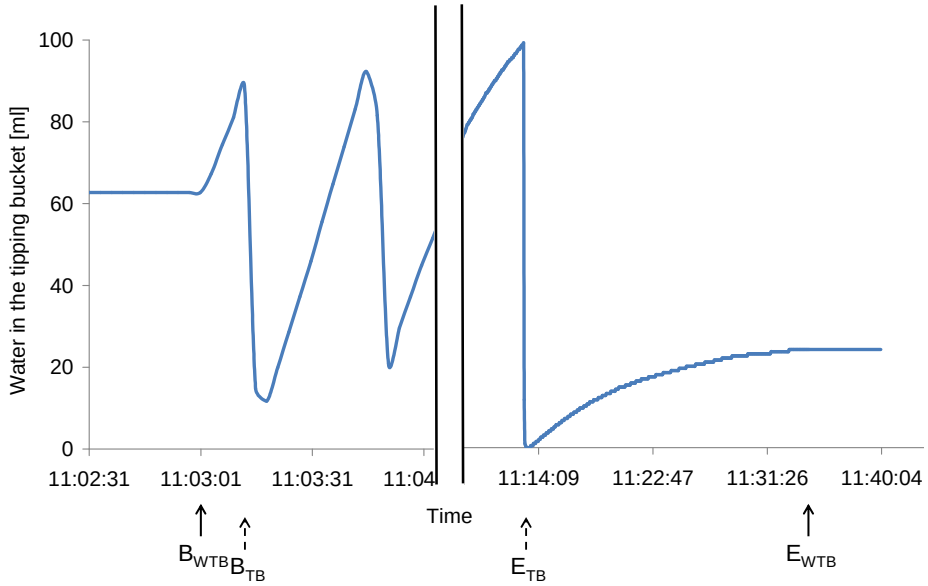

Figure 4.4: Runoff event from concrete paving slab at the 3rd of September 2009 in Berlin-Marienfelde. The dynamics were studied using the traditional tipping bucket (TB) signals compared to the weighable tipping bucket (WTB) data. B_{TB}, B_{WTB}, E_{TB}, and E_{WTB} indicate the beginning and the end of the runoff event as detected by the TB and the WTB, respectively. Note that the time axis is interrupted and scaled differently.

Part III

Results and Discussion

Chapter 5

Water Balance of Paved Soil

In this chapter, the annual water balance process will be analyzed considering the characteristics of the precipitation event frequency. The paved weighable lysimeter and the weighable tipping bucket allow to separate the precipitation event with very precise separation criterion and to obtain the parameters from a broad range of rainfall events.

After the precipitation event separation, the annual precipitation event frequency functions are defined and used to clarify the water balance process. The water balance components are observed throughout rainfall events. The influence of the rainfall-runoff relationship on the water balance process is analyzed.

5.1 Precipitation Event Separation

The goal of this section is to develop the procedure for separating the precipitation-time series into precipitation-event series, as measured by paved lysimeters.

The definition of an event always depends on the objective target. For example, an one-day interval is suitable to assess the average infiltration and evaporation performance during a certain water regime. By contrast, however, the surface hydrological process depends heavily on the interplay between the water balance components during a rainfall event. This makes it necessary to define a precipitation event using a specific and consistent temporal criterion.

In this section, the principle of precipitation event separation is clarified and separation criteria are defined. The temporal accuracy of the lysimeter system regarding runoff measurement is assessed by varying separation criteria. Subsequently, the most suitable criterion is determined. After evaluating the annual precipitation event frequency, the importance of the small events is highlighted.

5.1.1 Precipitation Event Parameters on Small Field Plots of Lysimeter

A precipitation event is characterized by the event sum, event duration, and the timely event pattern. The precipitation event sum is

$$P = \int_{t_o}^{t_p} p\,dt \quad , \tag{5.1}$$

and its real runoff event sum is

$$Q = \int_{t_c}^{t_e} q\,dt \quad , \tag{5.2}$$

where event starts at t_o, generates the first runoff flush at t_c, and then lasts until the time point t_p. Let us define the duration of runoff concentration until the first flush, T_c, as following:

$$T_c = t_c - t_o \quad , \tag{5.3}$$

The total precipitation duration is

$$T = t_p - t_o \quad , \tag{5.4}$$

and the event intensity is therefore

$$r = \frac{P}{T} \quad . \tag{5.5}$$

Theoretically, when the precipitation event itself ends at t_p, no runoff water are possible. However, since the runoff concentration and transportation occur along on the flow way with gutter error of lysimeter, more time is needed until the runoff is completed at t_e, we will define the runoff amount after the event as the *after-flush* (ΔQ) (see Fig. 5.1).

For the separated runoff sum

$$RO = \int_{t_c}^{t_p} q\,dt \quad , \tag{5.6}$$

the after-flush is described as the following:

$$\Delta Q = Q - RO = \int_{t_p}^{t_e} q\,dt \quad . \tag{5.7}$$

The more correctly the concentration time (T_c) can be determined, the greater the separated runoff depth (RO) becomes. Hence, in the end the ΔQ indirectly describes the accuracy of measuring the T_c as well. We introduce the dry duration

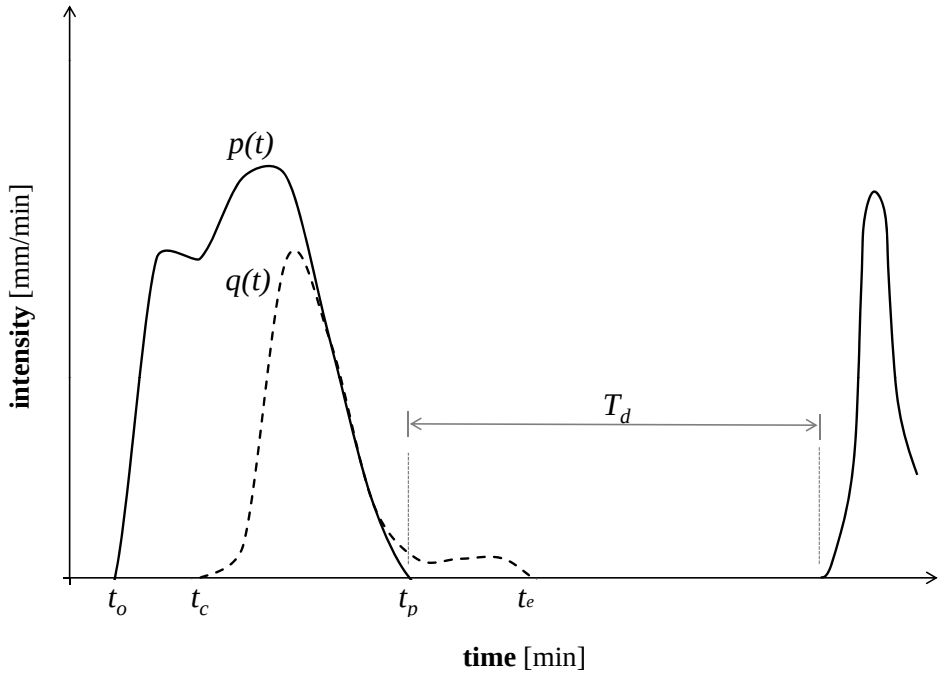

Figure 5.1: Parameters of the runoff-effective precipitation event process. The actual runoff (Q) divides into separated runoff (RO) and after-flush (ΔQ). Each precipitation event is characterized by the depth (P), duration (T), and the event intensity (r). The after-flush ends within the drying period (T_d).

T_d (time span between neighboring events) as a separation criterion. Two rules are important in choosing the T_d:

(i) Quantitatively, as little after-flush as possible should occur after separation.

(ii) Temporally, the runoff should end before the next rainfall event begins.

Fig. 5.3 illustrates a precipitation-event series, observed on Oct. 8th 2009. The time spans between events are varying. After separating the events with T_d for one year, the precipitation event series is obtained with the event number of N.

The collection of rainfall events is formulated as the mathematical set that includes all events $\mathbf{P}_n$ as the set element.

$$\mathbb{P} = \{\mathbf{P}_n \mid T_d, n \in [1, N] : \mathbb{N}\} \quad . \tag{5.8}$$

When the designation of individual events is added with an index n, the distinctive event $\mathbf{P}_n$ then is characterized by the parameters such as rainfall depth (P_n), rainfall event intensity (r_n), duration (T_n), and runoff depth (RO_n).

Now, the annual depths of precipitation and runoff can be denoted as the

following:

$$\begin{aligned} P_{annual} &= \sum_{n=1}^{N} P_n \quad , \\ RO_{annual} &= \sum_{n=1}^{N} RO_n \quad . \end{aligned} \tag{5.9}$$

The size of the set $\mathbb{P}$, N, specifies the total event number of measurement period. N will increase with decreasing T_d. Similarly, the total after-flush ΔQ_{annual} increases with the decreasing T_d as follows.

$$\begin{aligned} N &: f(T_d^{-1}) \quad , \\ \Delta Q_{annual} &: f(T_d^{-1}) \quad . \end{aligned} \tag{5.10}$$

The aim of separation is to determine the smallest T_d, allowed by the measurement system. The simultaneous aim is to minimize the total annual after-flush from the Eq. 5.11:

$$\Delta Q_{annual} = \sum_{n=1}^{N} \Delta Q_n \, , \tag{5.11}$$

5.1.2 Determination of Event Separation Criteria

Both quantitative and temporal separation criteria are needed. As for the quantitative criterion, German Meteorological Service (DWD: Deutsche Wetterdienst) uses 0.1 mm as measurable size of raindrop weight according to the specialist interviews. The lysimeter scale used here is able to balance weight values with a resolution of 100 g, which corresponds to 0.1 mm on a 1 m^2 surface. This agrees with the criterion of DWD. Further, the lysimeters used here can deliver a consistent weighing performance because the unvegetated paved surfaces advantageously were not vibrated as much as the grass lysimeters by wind.

As for the temporal criterion, the rainfall series then have to be separated by the dry duration T_d. Some events are not large enough to produce runoff, and some rain events seem to be separable, but belong together as one runoff event.

From Eq. 5.9 the annual runoff coefficient (RC_{annual}) can be calculated as follows:

$$RC_{annual} = \frac{RO_{annual}}{P_{annual}} = \frac{\sum_1^N RO_n}{\sum_1^N P_n} \tag{5.12}$$

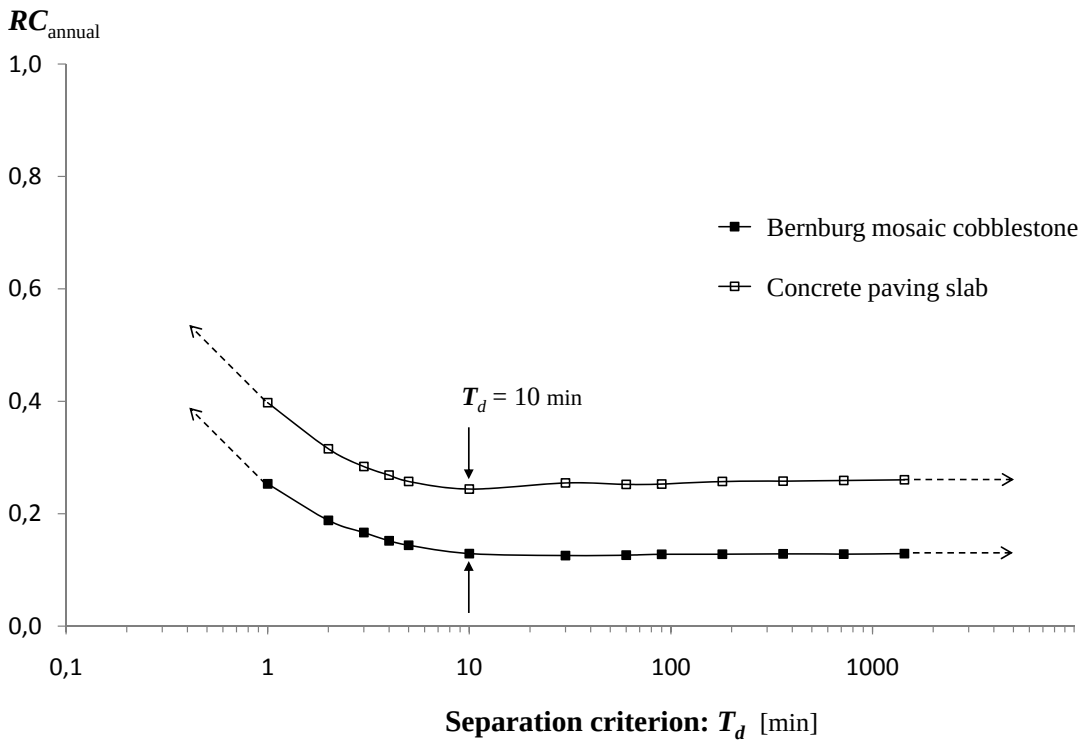

Figure 5.2: Determination of the separation criterion for precipitation events for Bernburg mosaic cobblestones and Concrete paving slabs. $T_d = 10\,\text{min}$ is suggested. For $T_d < 10\,\text{min}$, RC_{annual} presumably converges to the annual average of peak discharge. For $T_d > 10\,\text{min}$, RC_{annual} tends to be constant and presumably corresponds to the real runoff coefficient.

Rearranging Eq. 5.12 using Eq. 5.7 yields

$$RC_{annual} = \frac{\sum_1^N (Q_n - \Delta Q_n)}{\sum_1^N P_n} \quad . \tag{5.13}$$

From the inversal relationship between ΔQ_{annual} and T_d (Eq. 5.10), RC_{annual} is supposed to be a function of T_d. RC_{annual} converges to the real portion of ΔQ_{annual} to P_{annual}, $\Delta Q_{annual}/P_{annual}$, with increasing T_d, whereas RC_{annual} presumably approaches to the annual average of peak discharge with decreasing T_d.

Fig. 5.2 shows the annual runoff coefficient after separating precipitation-time series by varying T_d from 0 min to more than 60 min. Based on these results, Bernburg Mosaic Cobblestones show an RC_{annual} of ca. 15 % while the concrete paving slabs show an RC_{annual} of ca. 25 %.

The RC_{annual} tends to increase exponentially with decreasing T_d. For both pavements, T_d clearly shows very few changes where $T_d > 10\,\text{min}$. This means that every runoff event could be captured within 10 minutes after the precipitation ceased.

5.1.3 Cumulative Precipitation Frequency Functions

For the dynamics of the water balance, the precipitation event frequency may play a large role (Wessolek and Facklam, 1997; Ferguson, 2005; Flötter, 2006). However, the observations of the events were based on less precise temporal resolution. The daily precipitation sum has previously been used to explain the role of event frequency for water balance dynamics. In my study, the separation of events from the paved weighable lysimeter enables a more precise definition of the event parameter.

For the annual water balance, one can describe the set of all rainfall events as a sequence of the random phenomena, caused by uncountable, unpredictable, and complex impact factors in climatic time space. In the Eq. 5.8 (see Chap. 5.1) this random sequence is defined as the population ($\mathbb{P}$) of single rainfall events $\mathbf{P}_n$, which includes parameters like depth (P_n), intensity (r_n), and duration (T_n). Hereby, n denotes the index number of events, and its maximum may be identical to the annual event number N, which is strongly specified by T_d of the monitoring system.

If the subpart of $\mathbb{P}$, in which the events have the same intensity r, is described as the subset

$$\mathbb{P}\,[r] = \{\, \mathbf{P}_n \mid r_n \,=\, r,\; n \,\in\, [1,\; N(r)] \,\}\,, \tag{5.14}$$

the total precipitation sum of population $\mathbb{P}[r]$ can be defined as following:

$$P(r) = \sum_{1}^{N(r)} P_n\,, \tag{5.15}$$

where $N(r)$ = the size of $\mathbb{P}[r]$ and the number of events that have the same intensity r.

From these formulations, the cumulative precipitation $PF\,(r)$ as well as the cumulative event number $NF\,(r)$ are defined as the following:

$$PF(r) = \int_0^r P(r)\,dr\,, \tag{5.16}$$

and

$$NF(r) = \int_0^r N(r)\,dr\,. \tag{5.17}$$

The cumulative precipitation frequency functions give the total sum as well as the total number of events that belong to an arranged class by the event parameters. In Eq. 5.16, rainfall event intensity is chosen as event parameter.

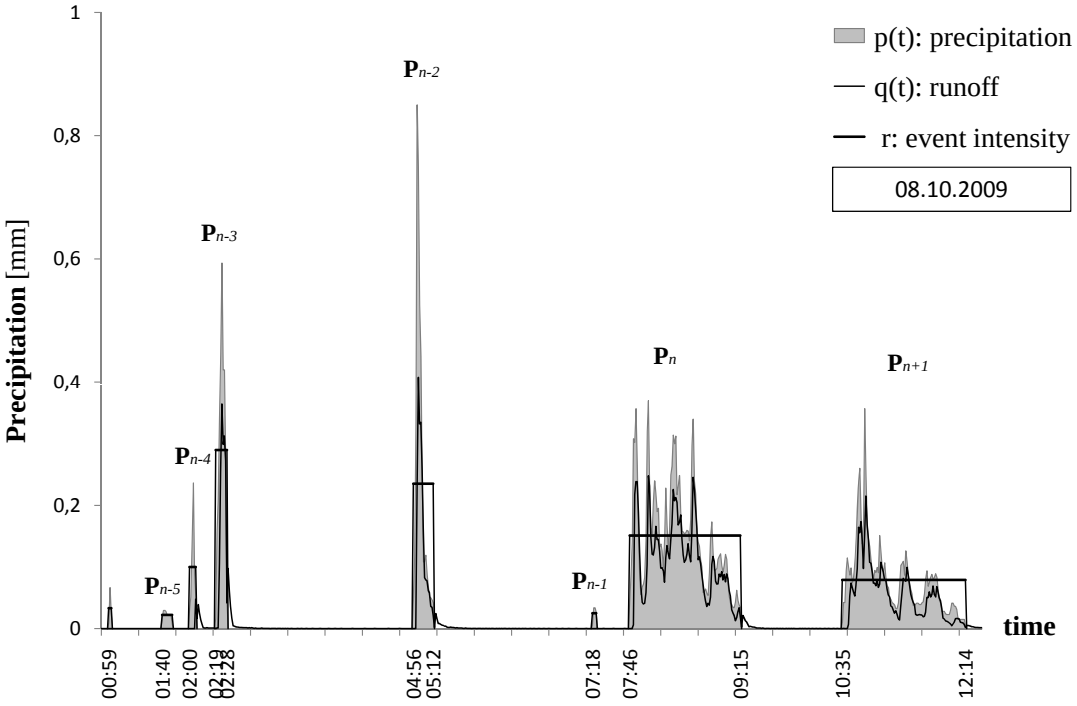

Figure 5.3: An example of precipitation events from Oct. 8^{th} 2009. The precipitation events that are separated from each other have different runoff impacts. A good paved lysimeter system should minimize the ΔQ and T_d.

When r is set on the maximum of event intensities measured during a year, r_m, $PF(r)$ may yield the annual precipitation sum. Similarly, $NF(r)$ indicates the total event number in period and $NF(r)$ equals the total event number of the year, when $r = r_m$.

By means of $PF(r)$ and $NF(r)$ functions, the intensity range of the typical events for a region can be figured out. For the Berlin region, the $r = 0.05$ and 0.1 mm/min are considered pertinent intensity values for interpreting the annual rainfall distribution (Fig. 5.4).

5.2 Annual Precipitation-Event Frequency

The annual precipitation-event frequency is obtained based on the rainfall data between May 2009 and April 2010, using $T_d = 10$ min. On the right vertical axes, Fig. 5.4 shows the curve progress of $PF(r)$ as well as of $NF(r)$. The left vertical axes show the percentages of cumulative sum and number, $PF(r)/PF(r_m)$ and $NF(r)/NF(r_m)$, respectively. During the measurement period of 2009/10, 932 precipitation events were acquired, the total precipitation sum was on 537 mm, and the maximum event intensity, r_m, is ca. 0.45 mm/min.

The smallest events ($r < 0.01$ mm/min) can presumably barely produce runoff and also not massive enough to infiltrate against the wetting capacity of surface. In addition, these small amounts of precipitation likely evaporate immediately after the end of the event. This is particularly true for the urban pavements due to their usual high temperature and dryness. For events with $r < 0.01$ mm/min, although the event frequency was over 60 %, its cumulative precipitation sum was under 10 % of annual precipitation sum.

The strong events presumably have high runoff coefficients, and the infiltration capacity of soil surface can be quickly used up. For flood protection, the runoff coefficient was considered as independent of rainfall intensity and normally assessed as a high value (DWA-A, 2005). The $NF(r)$ has a slow incline after $r > 0.1$ mm/min and $PF(r)$ is about 25 % between $0.1 < r < r_m$. The higher the rainfall event intensity becomes, the more slowly the $PF(r)$ inclines. This means that the normal events play the more considerable role than the storm events for the annual water balance.

The normal events (those with intensities between $0.01 < r < 0.1$ mm/min) may variously impact runoff and infiltration processes. These dynamics may be determined by the rainfall intensity and duration. Because the average events comprise more than 60 % of annual precipitation and more than 40 % of frequency for the measurement period 2009/10, it is important to clarify the role of normal events in the water balance dynamics.

In Tab. 5.2, the monthly cumulative precipitation frequencies are listed using the threshold values of rainfall-event intensity: 0.01, 0.05, and 0.1 mm/min. Flötter (2006) attempted to regulate some event-based specific intensities. His

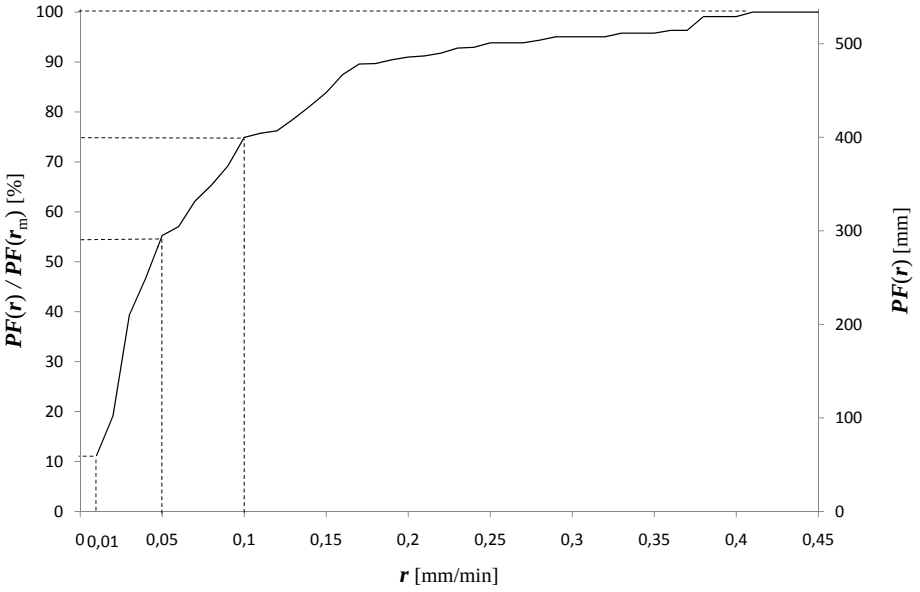

(a) Cumulative precipitation sum.

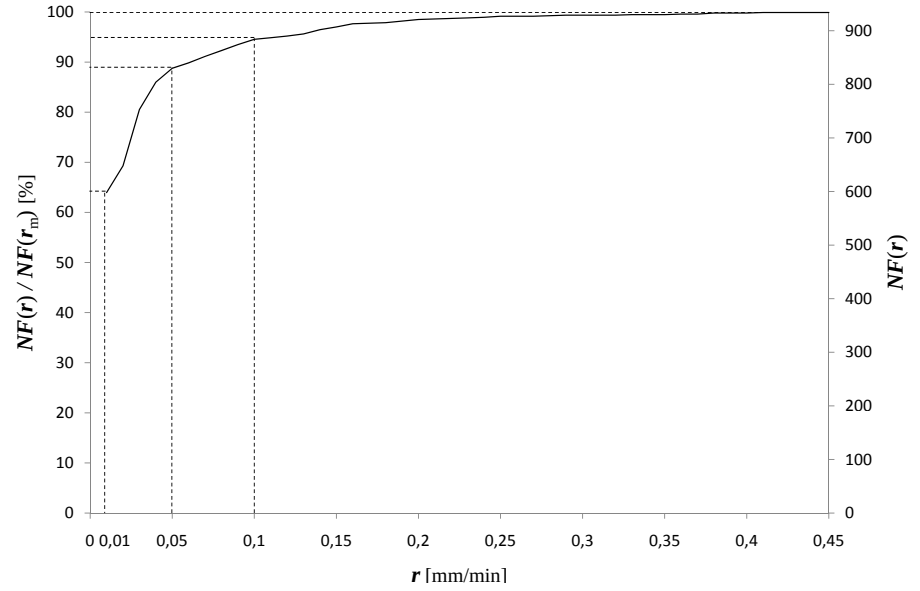

(b) Cumulative precipitation number.

Figure 5.4: The cumulative precipitation depth $PF(r)$ and the cumulative event number $NF(r)$. All are also presented in percent value. The cumulative precipitation sum and number of small events take big percentage of annual frequency.

work used one hour as the reference interval to define a rainfall event. After him, small events have $r < 0.5\,\mathrm{mm/h}$ (corresponding to $0.008\,\mathrm{mm/min}$), normal events $0.5 < r < 4.0\,\mathrm{mm/h}$ ($0.07\,\mathrm{mm/min}$), and storm events have $r > 0.07\,\mathrm{mm/min}$ for Hamburg region, Germany. These almost agree with the thresholds of Tab. 5.2 for the Berlin region. The normal events are supposed to make up the major percentage of annual rainfall.

For summer periods, the $PF(0.1)$ (the cumulative precipitation sum of events with the $r < 0.1$) varies widely. While $PF(0.1)$ is less than ca. 40 % for July and August of 2009, it is about between 70 % and 100 % for the other months. Further, all events had intensity of almost $r < 0.1$ between November 2009 and Feburary 2010, which implies a high frequency of small events during winter time. The water balance process is supposed to progress in a different fashion depending on the precipitation-event frequency. Hence, it is of interest to compare the rainfall-runoffrelathionship of, e.g., July and August of 2009 with that of November 2009 (see Chap. 5.3.2).

5.3 Water Balance 2009–2010

5.3.1 Groundwater Recharge and Evaporation

Using the paved weighable lysimeters, the water budget parameters between May 2009 and April 2010 were measured. The Hellmann rain gauge delivered the annual precipitation of $P_{\mathrm{annual}} = 537\,\mathrm{mm}$.

The annual water balance WB was accumulated by the single measurement values of runoff (RO), seepage (GW), changeable water storage (ΔW), and evaporation (ET), analogous to the Eq. 3.1

Although the water balance (WB) is supposed to near to the P_{annual}, that from the lysimeter with Bernburg mosaic cobblestone (abbreviated as MCS through below), WB_{MCS}, was ca. 457 mm and that of concrete paving slab (abbreviated as CPS throughout below) ca. 452 mm, respectively (Fig. 5.5). The lysimeter with resolution of 0.1 mm was apparently not precise enough to capture the smallest events of $r < 0.01\,\mathrm{mm/min}$, which the Hellmann gauge was able to measure. Therefore, $PF(0.01) = 59.5$ from the Tab. 5.2 can potentially explain the gap between water balances and precipitation for MCS and CPS (80 mm and 75 mm, respectively).

Furthermore, the measurement of snow precipitation during the winter period might have had several failures at very cold and windy conditions because the unheated Hellmann gauge is not able to deliver the accurate snow value. In addition, the frozen lysimeter also cannot react precisely against the long, steady blowing-away of snow layer. Thus, this may be reason for very low precipitation sum of January 2010 (Tab. 5.1).

The annual groundwater recharges for MCS and CPS were ca. 383.3 mm (ca.

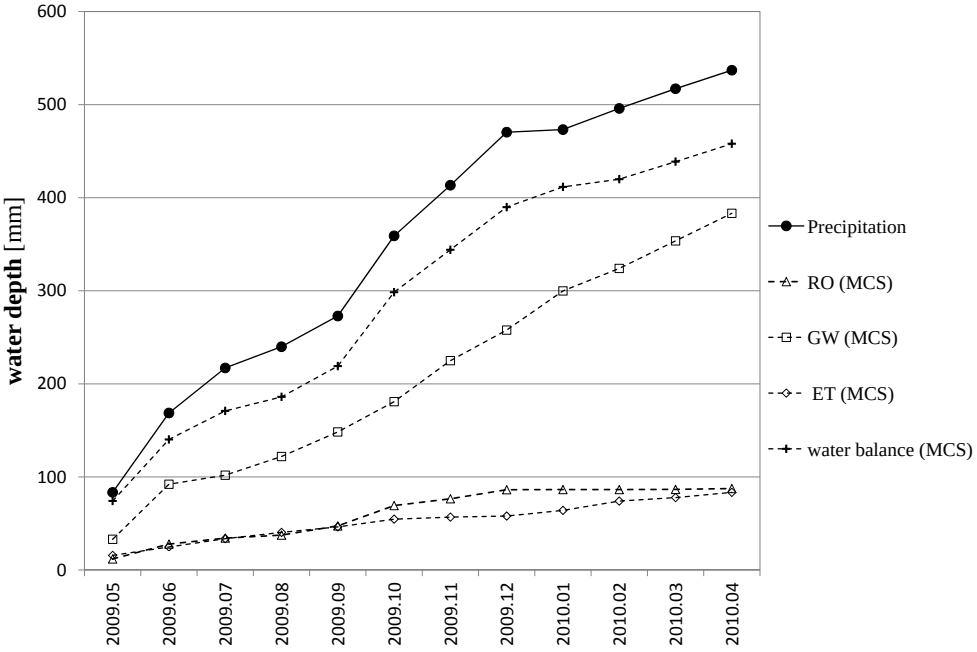

(a) Bernburg mosaic cobblestone.

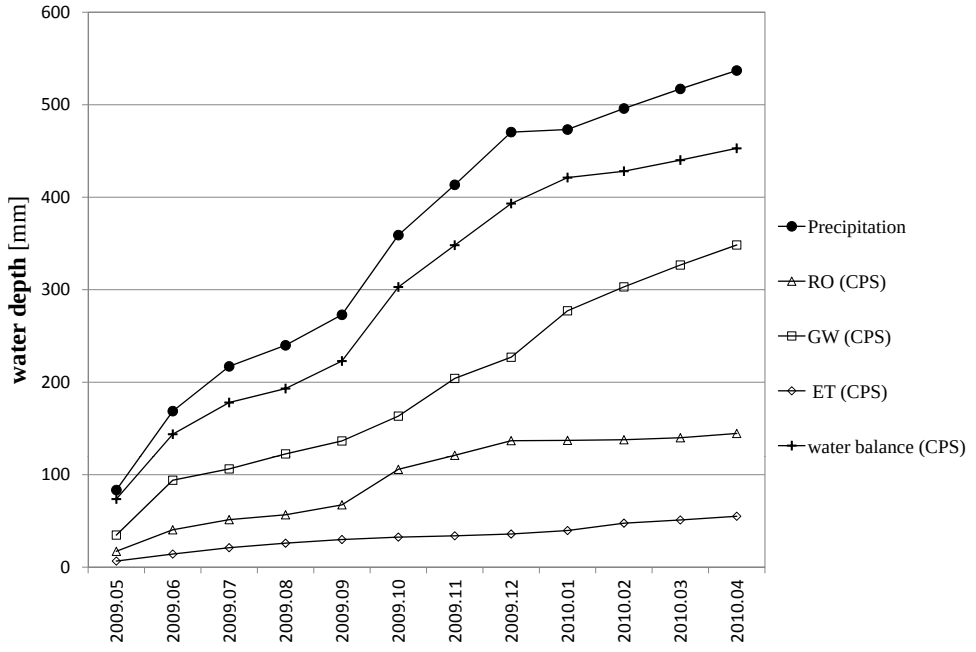

(b) Concrete paving slab.

Figure 5.5: Annual water balance 2009/10.

71.4 % of P_{annual}) and ca. 348.2 mm (64.9 % of P_{annual}), respectively, values that can be classified as surprisingly high.

Wessolek (1993), Senatsverwaltung Berlin für Stadtentwicklung (2001), and Flötter (2006) already specified very high rates of groundwater recharge despite the high degrees of sealing. They concluded that the reason might lie in the high frequency of days with small events. The rainwater of small events could remain within the wetting capacity space without flowing away, and then could infiltrate or evaporate immediately after the end of the event. Hence, the reasonable selection of seam materials and pavement type can positively affect the annual water balance by enhancing the surface storage.

Both surfaces showed higher groundwater recharge in the winter period than in the summer period. The seepage water continuously flowed from groundwater system of both lysimeters. MCS has had slightly higher incline of the groundwater recharge rate than CPS. In sum, there was not a big difference between groundwater recharge beneath both surfaces.

The annual evaporation rates are ca. 83.4 mm (ca. 15.5 % of P_{annual}) from MCS and ca. 55.0 mm (ca. 10.2 % of P_{annual}) from CPS. The periodic evaporation of MCS was always higher than that of CPS. Despite the big difference in the seam portion between MCS (40 %)and CPS (7 %), the difference in their evaporation rates was rarely large. In the winter period they showed almost similar evaporation, while in summer periods the evaporation of MCS was visibly bigger than that of CPS.

Fig. 5.6 illustrates an example of evaporation from MCS and CPS between July 20$^{\text{th}}$ to 25$^{\text{th}}$ 2009, accompanied by grass reference evapotranspiration from FAO lysimeter. The seven rainfall events shown are detected. For every events, all lysimeter surface indicated a rapid increase in evaporation directly after the event. During the warmer daytime temperatures, the evapotranspiration performance of the grass surface is significantly greater than that of the paved surfaces. The actual evaporation from the paved surfaces depends on the surface water supply and climate conditions at the time of day.

During the daytime of July 21$^{\text{st}}$, the evaporation from MCS is much greater than from CPS. It was induced from the storm event late on July 20$^{\text{th}}$. The event was sufficiently intense to store a certain amount of surface water within the surface storage. After the rainfall ceased, the surface water supply of CPS was exhausted through the night, while the surface water of MCS was still not exhausted.

In contrast to that, both paved surfaces showed only a small increase in the afternoon of July 23$^{\text{rd}}$ and 24, because the surface water supply had been already exhausted. The rainfall event at 05:00 am on July 22$^{\text{nd}}$ was not big enough to store sufficient water in the upper paved soil zone. Additionally, for summer relation, the drying duration after this event (between 22$^{\text{nd}}$ and 24$^{\text{th}}$) was too long to save surface water for considerable evaporation during the day time of July 23$^{\text{rd}}$.

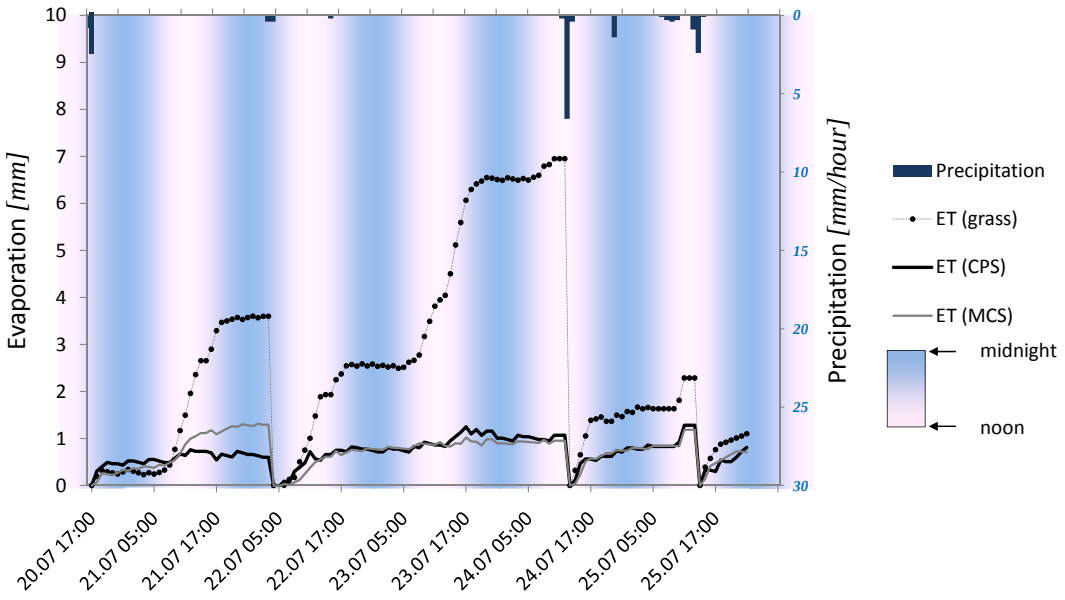

Figure 5.6: Paved surfaces induced a big deficit of evaporation in comparison with the grass reference surface (FAO lysimeter). After various rainfall events, the evaporation behavior of pavements strongly depends on the surface water, supplied from the event. Occasionally, the pavements with small seam portion also can show a slightly high evaporation, because more surface water is available immediately from the wetting capacity for short period. However, there is not a significant difference in the evaporation performance between of MCS and CPS pavements for the annual evaporation.

Table 5.1: Monthly water balance components and runoff coefficients. P = precipitation in [mm], RO = runoff in [mm], RC = runoff coefficient in [%], GW = groundwater recharge in [mm], ET = evapotranspiration in [mm], and ΔW = in [mm]. (*MCS* for Bernburg mosaic cobblestones and *CPS* for Concrete paving slab.)

month	P [mm]	RO [mm]		RC [%]		GW [mm]		ET [mm]		ΔW [mm]	
		MCS	CPS	MCS	CPS	MCS	CPS	MCS	CPS	MCS	CPS
2009.05	83.40	11.84	17.13	14.20	20.54	33.04	34.72	15.68	6.62	13.57	15.18
2009.06	85.30	15.96	23.28	18.71	27.29	59.10	59.28	9.08	7.58	-18.00	-20.05
2009.07	48.40	6.50	11.00	13.43	22.73	9.71	12.27	8.91	6.88	5.50	4.10
2009.08	22.80	3.18	5.20	13.93	22.81	20.09	16.16	6.74	4.85	-14.93	-11.08
2009.09	33.00	7.30	10.79	22.11	32.69	26.40	14.04	5.93	3.95	-9.14	0.96
2009.10	86.10	21.85	38.38	25.38	44.57	32.50	26.84	8.30	2.64	16.79	12.17
2009.11	54.40	7.30	15.20	13.42	27.94	44.09	40.79	2.17	1.38	-8.00	-12.14
2009.12	57.00	9.70	15.80	17.02	27.72	32.83	22.87	1.14	1.94	2.14	4.46
2010.01	2.80	0.20	0.30	7.14	10.71	42.02	50.19	6.10	3.79	-26.57	-26.25
2010.02	22.70	0.00	0.70	0.00	3.08	24.22	25.86	9.97	7.95	-25.93	-27.59
2010.03	21.20	0.20	2.20	0.94	10.38	29.57	23.69	3.75	3.44	-14.71	-17.35
2011.04	19.90	0.90	4.60	4.52	23.12	29.66	21.61	5.63	4.01	-16.93	-17.47
total	537.00	84.93	144.57	15.82	26.92	383.27	348.34	83.40	55.03	-96.21	-95.07

Interestingly, for event-based observation of evaporation, CPS could temporarily have bigger evaporation than MCS, e.g. immediately after the rainfall events. As shown in Fig. 5.6 was there higher actual evaporation from CPS in the morning of July 22$^{\text{nd}}$, during the night time of July 21$^{\text{st}}$., and for the time span after rainfall events on July 25$^{\text{th}}$.

5.3.2 Influence of Rainfall-Runoff Relationship on Water Balance

The total runoff sums were ca. 84.9 mm (annual runoff rate: 15.8 %) from MCS and ca. 144.6 mm (annual runoff coefficient: 26.9 %) from CPS, out of the total precipitation of 537 mm. For months with high precipitation, the monthly runoff sum was also normally high. The annual runoff sum is not as big as the difference in seam portion. Nevertheless, the periodic runoff coefficients of CPS were always bigger than that of MCS (see Fig. 5.5, Tab. 5.1, and Tab. 5.4).

Tab. 5.2 gives an overview of the monthly precipitation frequency classified by the threshold values of rainfall event intensity. From this table, the cumulative precipitation sum ($PF(r)$) and the cumulative number of events ($NF(r)$) are calculated, the maximum event intensity was also added in order to give information about the eventual extreme storm event.

The monthly RC is clearly varying for each pavement through the year. Considering the rainfall event intensity as an impact factor on RC, one can explain

Table 5.2: Monthly precipitation-event frequency. The precipitation-event frequency varies for hydrologic periods. The monthly rainfall event frequency can clarify the water balance dynamics for the annual processes. Events with intensity $0.01\,\mathrm{mm/min} < r < 0.1\,\mathrm{mm/min}$ dominate within the annual precipitation frequency. NF = cumulative event number by given intensity and PF = cumulative precipitation sum by given intensity, % column beside PF is the value of $PF/PF(r_m)$ and gives the monthly percentage of cumulative precipitation sum to the monthly precipitation.

r [mm/min]		≤ 0.01			≤ 0.05			≤ 0.1			≤ r_m	
	r_m	NF	PF	%	NF	PF	%	NF	PF	%	NF	PF
2009.05	0.23	28	2.8	3.36	60	37.5	44.96	68	59	70.74	74	83.4
2009.06	0.38	44	4.4	5.16	66	26.8	31.42	77	58.6	68.70	80	85.3
2009.07	0.41	28	2.8	5.79	42	11.5	23.76	48	20.2	41.74	62	48.4
2009.08	0.17	16	1.6	7.02	25	4.5	19.74	28	7.1	31.14	33	22.8
2009.09	0.3	19	1.9	5.76	26	12.4	37.58	34	25.9	78.48	37	33
2009. 10	0.36	102	10.2	11.85	142	46.7	54.24	148	64.4	74.80	153	86.1
2009.11	0.1	97	9.7	17.83	126	48.4	88.97	129	54.4	100.00	129	54.4
2009.12	0.2	117	11.7	20.53	143	55.2	96.84	147	56	98.25	152	57
2010.01	0.05	14	1.4	50.00	16	2.8	100.00	16	2.8	100.00	16	2.8
2010.02	0.05	74	7.4	32.60	99	22.7	100.00	99	22.7	100.00	99	22.7
2010.03	0.1	43	4.3	20.28	59	19.6	92.45	62	21.2	100.00	62	21.2
2010.04	0.2	16	1.6	8.04	28	8.9	44.72	30	10	50.25	35	19.9
annual value		595	59.5	11.08	832	297	55.31	886	402.3	74.92	**932**	**537**

this dynamic behavior of the RC. May and June of 2009 had a similar precipitation frequency and about the same precipitation sum (83.4 mm and 85.3 mm, respectively). The values of $PF(0.1)$ are nearly the same for both month periods (ca. 59 mm and 70 %). However, the values of $PF(0.05)$ are quite different and this could be the reason for the smaller RC for May than for June, for both pavements.

Interestingly, the RC of July and August, 2009 remained almost unchanged for MCS and CPS, ca. 13.5 % and ca. 23 %, respectively, although the precipitation sums in July (48.4 mm) was more than double that in August (22.8 mm). During these two months, $PF(0.1)/PF(r_m)$ were smaller than 50 %. Based on the assumption that the RC tends to remain constant for the storm events with high event intensity, the small and normal precipitation events of $PF(0.1)$ could not be the primary reason for the difference in the RC. However, the RC of July and August 2009 are supposed to have much higher values than other months, which did not happen because the storm events of $PF(r_m > r > 0.1)$ were either of short duration or of relatively lower intensity. This means that not only the intensity (r) but also the event duration (T) helps the high runoff coefficient. For example, the event of 10.07.2009 15:29:07 lasted only $T = 11$ minutes, with the maximum intensity $r_m = 0.41\,\mathrm{mm/min}$ and that of 21.08.2009 19:13:44 only lasted with $T = ca.\,70\,\mathrm{min}$, $r_m = 0.17\,\mathrm{mm/min}$.

Table 5.3: The distribution of runoff-producing and non-runoff-producing rainfall events in the period of 2009/10. A large proportion of rainfall events without runoff can lead to different dynamics of the annual water balance. This behavior varies according to the kind of pavement. For the mosaic cobble stone, the total number and the sum of events that could produce runoff was significantly less than for the concrete paving slab.

		MCS		**CPS**	
	annual value	$\mathbf{RC_n = 0}$	$\mathbf{RC_n \neq 0}$	$\mathbf{RC_n = 0}$	$\mathbf{RC_n \neq 0}$
N	932 (337*)	274	63	169	168
P [mm]	537 (477.5*)	259.3	218.2	96.2	381.3

* the annual value of r > 0.01 mm/min

In contrast, the RC of September and October 2009 are higher than that of the other months, despite of high value of $PF(0.1)$ over ca. 75 %. The reason is that there were several storm events of long duration with an intensity over 0.1 mm/min (e.g. on Oct. 8$^{\text{th}}$, 2009, see Fig. 5.3).

The behavior of RC during November and December, 2009 were also very similar, presumably because the precipitation frequencies were almost adequate.

Throughout the winter months, runoff behavior might be completely different from that of summer periods, because surface flow then is provided by not falling water, but by melting water. Since melting water may not have any falling intensity, the infiltration rates are very high and the runoff rate is low.

As analyzed above, the periodical rainfall-runoff relationship strongly depends on the precipitation-event frequency. The rainfall-runoff relationship characterized by RC is again strongly dependent on event intensity.

During the nth rainfall event, the rainwater is divided into runoff water and infiltration water at the soil surface as the following:

$$P_n = RO_n + I_n \quad , \tag{5.18}$$

and the runoff coeffcient of the event is

$$RC_n = \frac{RO_n}{p_n} \quad . \tag{5.19}$$

Depending on the surface properties, the infiltration I_n provides the primary source of evaporation and groundwater recharge. If $RC_n = 0$ and, thus, $P_n = I_n$, the rainfall event is denoted as a rainfall event without runoff. Tab. 5.3 lists the total sum and number of rainfall events with ($RC_n \neq 0$) and without runoff ($RC_n = 0$) for both MCS and CPS pavements.

For the annual water balance, the greater the sum of rainfall events without runoff becomes, the more rapidly the RC_{annual} declines. As RC_{annual} declines,

Table 5.4: The average runoff coefficients of event ranges according to the intensity.

		MCS		CPS	
	annual value	$RC_n = 0$	$RC_n \neq 0$	$RC_n = 0$	$RC_n \neq 0$
N	932 (337*)	274	63	169	168
P [mm]	537 (477.5*)	259.3	218.2	96.2	381.3

* the annual value of r > 0.01 mm/min

more water supply is available for other water balance processes such as groundwater recharge, water storage, and evaporation. As for the precipitation sum of events without runoff in 2009/10, the MCS shows a significantly greater value than the CPS.

Fig. 5.7 classifies the rainfall event into runoff-producing and non-runoff-producing events by applying border lines. Precipitation-event sum versus event duration can indirectly state about the rainfall event intensity through the tangent of point (P/T). However, a distinctive selection of such a border line has an uncertainty. The stronger the event intensity is, the better the possibility of it being runoff-producing. For CPS, selecting such an intensity is much clearer than for MCS. Still, some events exist that are runoff-producing but are under dashed line, and that are non-runoff-producing but over the dashed line.

With some exceptions, it is clear that a certain amount of rainfall is needed in order to be effective for runoff. This means, in other words, that pavements have a certain surface space (surface storage, V_s) in which the rain water can be definitely stored without running off. Presumably, the surface storage of MCS is bigger than that of CPS, because MCS simply has more volume space through the higher seam portion and rougher surface.

Fig. 5.8 illustrates the event runoff coefficient acquired in 2009/10. A slight increase of RC with increasing event intensity r is shown for both pavements. On one hand, the fluctuation of the relationship still exists, presumably because the diagram does not consider the surface storage V_s. On the other hand, there are also some events with high rainfall intensity that do not produce runoff, which presumably is due to the insufficient rainfall sum.

Tab. 5.4 shows the average runoff coefficients, where rainfall events are classified into the range intensity. It is clear that CPS generally has a higher RC than MCS. In sum, for the investigation of rainfall-runoff relationship, both surface storage and rainfall event intensity play meaningful roles.

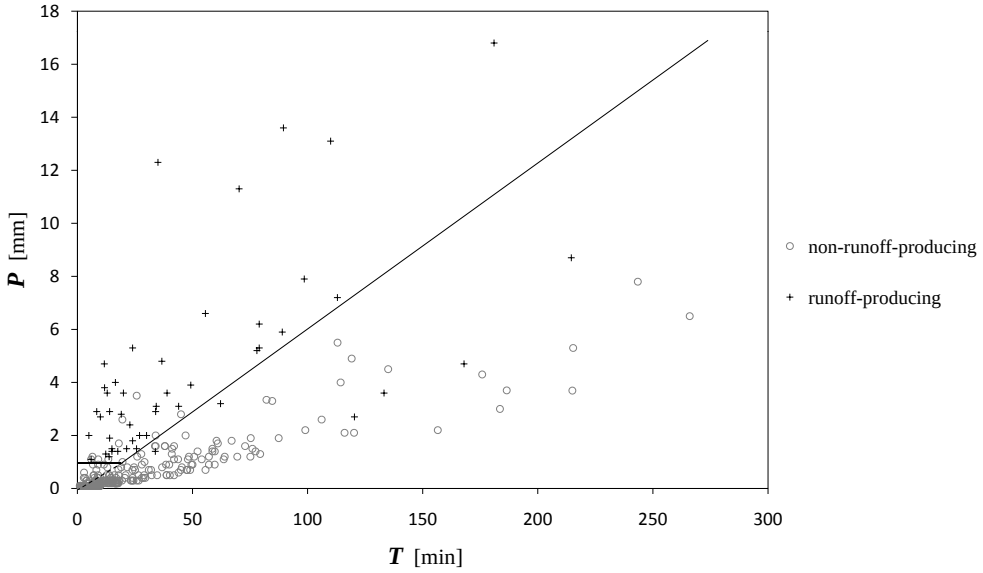

(a) Bernburg mosaic cobblestone.

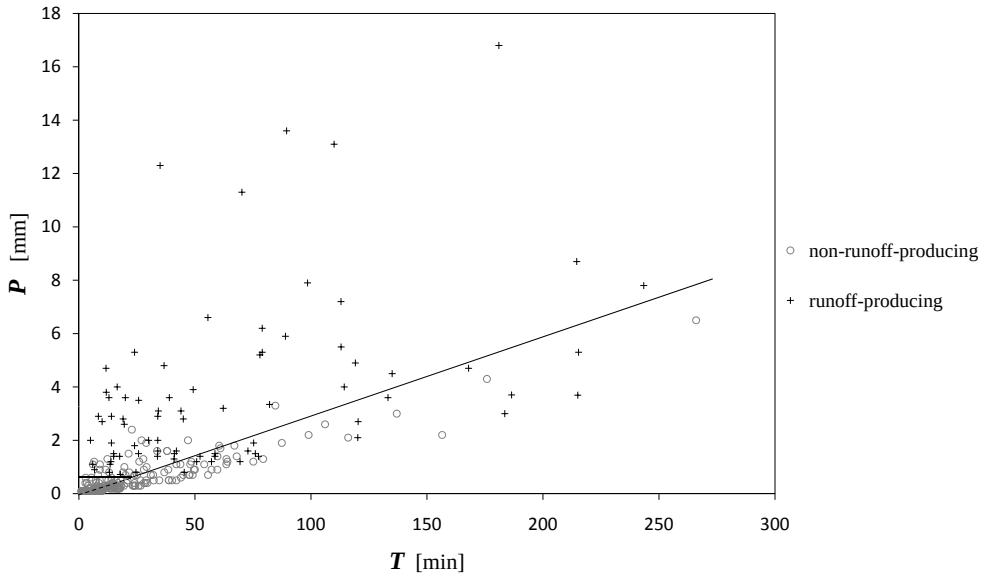

(b) Concrete paving slab.

Figure 5.7: Runoff-producing and non-producing precipitation-events: The rainfall events with lower intensity than runoff-producing intensity are not effective to produce runoff. The events with smaller rainfall sum than a surface storage are also not effective to produce runoff. MCS (Berburg mosaic cobblestone) shows greater runoff-producing intensity and bigger surface storage than CPS (Concrete paving slab).

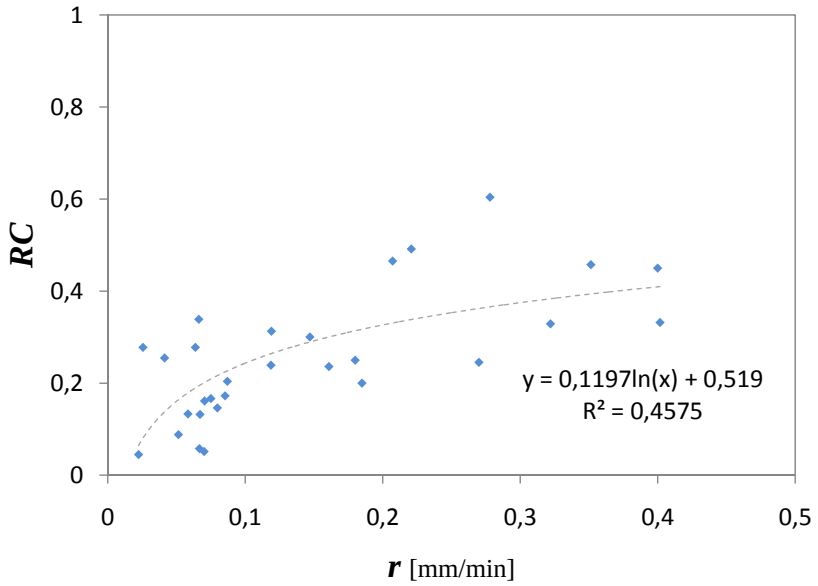

(a) Bernburg mosaic cobblestone

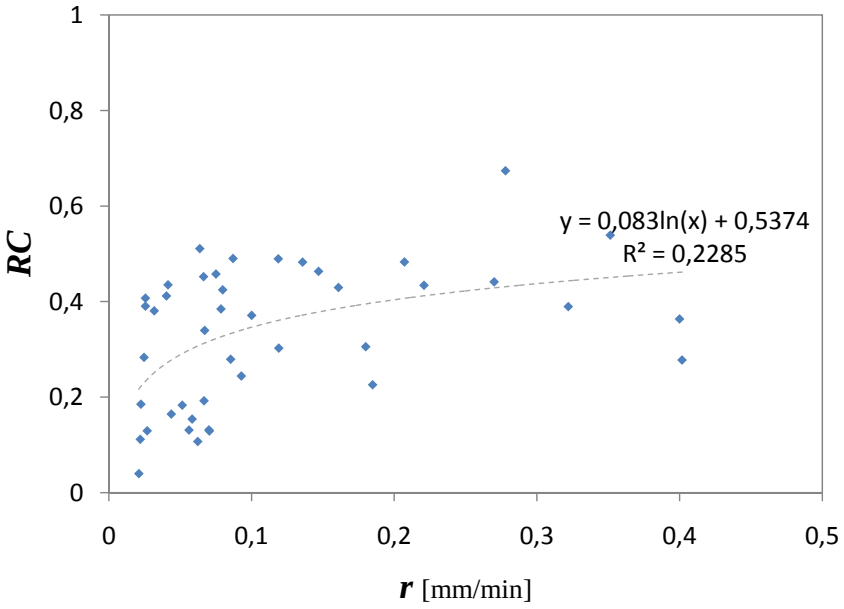

(b) Concrete paving slab

Figure 5.8: Runoff coefficients versus rainfall event intensity.

Chapter 6

Model Concept for Runoff Dynamics of Paved Soil Surface

The most regional runoff models need more appropriate approaches for assessing the impact of urban development on actual runoff behavior, because they do not include variables that typically are used to reflect changes in urban watershed conditions. One of the most widely used basic approaches is the rational concept which was first suggested in 1889 by Kuichiling (McCuen, 2004) and is primarily used for design problems for small urban areas, such as the dimensioning of inlets and culverts. But it is known that the approach of rational methods is not sufficiently adequate for design problems where watershed storage is significant, such as in permeably paved soils. Hence, in the last decades, lots of studies about infiltration properties of soils and porous materials have been done (Green and Ampt, 1912; Philip, 1957a,b; Bear, 1972; Hillel, 1998). For watersheds that are non-homogeneous and undergoing to land use change, especially under urbanization, watershed design work is usually based on hydrograph concept, which does not inherently exclude the involved processes. It is essential to study the runoff dynamics of the paved soil surface for urban hydrograph research.

In this chapter, two models for runoff calculation are suggested: the surface storage model for runoff concentration processes and the intensity-dependent runoff coefficient model for runoff processes, which include both precipitation-event parameters and surface hydrologic parameters. From the profound observation of the rainfall event processes, the runoff concentration process and the runoff process are described in detailed subprocesses.

6.1 Surface Water Process

6.1.1 Phase of Runoff and Infiltration Process

The overall rainfall-runoff relationship during a certain period varies by surface hydrologic parameters of the pavement, e.g. surface storage and infiltration performance, while the runoff dynamics during a certain precipitation event can be clarified by describing rainfall event parameters such as event intensity and event duration.

For comprehending the event-dependent runoff dynamics on small plots, as implemented in our lysimeter system, the rainfall event process can be considered differently than the water-pond hydrologic process.

(i) For the water-pond hydrologic process, the infiltration is only related to the soil-physical properties, controlled by the water head pressure. It does not require any intensity factors. Thus, experiments under water-ponded conditions serve to clarify the soil physical behaviors. Here, it is presumed that the sufficient water supply is provided to demonstrate the potential infiltration capacity.

(ii) For the precipitation event process, the water supply for infiltration does not always sufficiently exist. The high potential infiltration capacity cannot be demonstrated fully. Thus, the precipitation event produces runoff with different effectiveness. For the precipitation events without runoff (non-runoff-producing events), the water is completely taken up in the form of infiltration, evaporation and interception at the paved soil surface.

Depending on the surface storage volume, the runoff-producing event goes through two stages: the runoff concentration process and the runoff process, which can be again separated into two detailed processes (see Fig. 6.1).

During the runoff concentration process, the precipitation sum (called initial loss, denoted as P_a) is affected not only by the infiltration, but also by the interception, the depression storage, the short-term evaporation, and other intensity-kinetic effects.

Interception is a complex interaction of retention and detention processes above the soil surface. This process is a part of initial loss because it occurs at the beginning of a rainfall event and this lost water cannot take part in the groundwater and vegetation water processes. Infiltration describes the seepage of fluid through pore and cavity into the lithosphere (DIN 4049-1, 1989). Water can infiltrate into the soil when the hydraulic potential at the surface is bigger than in the deeper soil zone. Considering interception also as a part of infiltration at the beginning of a rain event, the total infiltration will always have a high rate at the beginning.

In addition, the evaporation is also supposed to play a big role at the beginning of the event. In general, the surface of paved soil has high temperature and a high heat capacity dominates in paving materials, particularly under urban conditions. Once it rains and the paved soil has again enough water supply to

cool the microclimate at the surface, the high heat energy will be released.

Fig. 6.1 shows a rainfall event with a small antecedent event (from the measurement of July 23rd, 2009). As for the antecedent sub-event with the intensity of max. 0.4 mm/5 min, the small first runoff-flush is generated earlier from the concrete paving slab (CPS) than from the Bernburg mosaic cobblestone (MSC). Due to the bigger surface storage of MCS, no considerable runoff was induced from MCS for the first ca. 30 minutes. When the main rainfall event starts, the runoff peak discharge of CPS is much higher than that of MCS.

The graphs clearly show the higher infiltration performance and the lower runoff from MCS than from CPS. For both surfaces the initial infiltration rates have high values, which decline rapidly to a fairly constant rate (final infiltration rate).

For CPS, the final infiltration rate appears to be settling after ca. 70 minutes, with the runoff not stopping. However, the runoff from MCS lasts for ca. 50 minutes much shorter than the runoff from CPS. This is a result of the low initial infiltration capacity of CPS. Essentially all the rain water of MCS infiltrates after the final infiltration rate is reached. After more than four hours of rain, runoff of CPS takes place visibly once again and the infiltration rate tends to remain constant, while MCS has very little runoff and nearly all rain water infiltrates.

It is notable that the observation shows that the infiltration curves, $i(t)$, do not correlate with the precipitation curves, $p(t)$, during final infiltration. The eventual fluctuation of $i(t)$ of final infiltration is caused by the inaccuracy of the temporal measurement. The runoff curves, $q(t)$, clearly change with the precipitation curves, which means these represent the remaining precipitation water after removing the constant final infiltration.

The rainfall-runoff process can be described in 3 consecutive processes affecting the soil infiltration capacity:

(i) the runoff concentration process: as long as the precipitation event is not intense enough, no runoff water occurs. The precipitation up to this point is completely taken up as initial loss;

(ii) the initial infiltration process: after the rainfall intensity exceeds the infiltration capacity, the runoff process takes place. The infiltration rate declines with time elapsing while the soil surface is under the unsaturated state. The upper soil zone still has a high infiltration capacity. The infiltration curve is strongly influenced by the precipitation intensity;

(iii) the final infiltration process: the infiltration rate converges to the constant value of the final infiltration rate and the soil surface reaches the steady infiltration under saturated state. The final infiltration rate may theoretically correspond to the value of the constant hydraulic conductivity of the paved soil. When the precipitation during this process is not intense enough, the rainwater will infiltrate completely without reaching the saturated soil state and no water will run off.

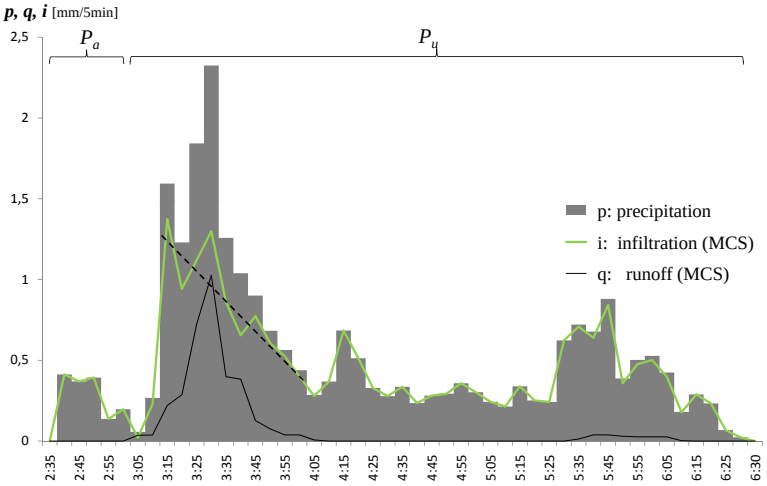

(a) Bernburg mosaic cobblestone (MCS)

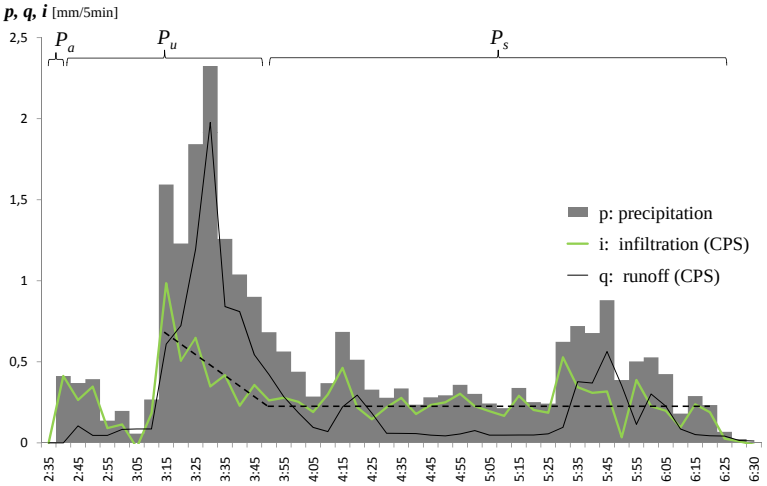

(b) Concrete paving slab (CPS)

Figure 6.1: A precipitation event from Juli 23rd, 2009. The surface water process can be observed in 3 phases: the runoff concentration, the initial infiltration and the final infiltration. The surface water process during these 3 phases has a different relationship with the precipitation due to the changing infiltration behavior of the soil surface.

6.1.2 Runoff Coefficient

The runoff coefficient, RC, is the proportion of the total produced runoff to the total precipitation. This can relate a whole precipitation period, as it is formulated for the annual water balance in Eq. 5.12, or a single event, as in Eq. 5.19. RC is a dynamic function of rainfall intensity and the surface hydrologic parameters.

The rainfall event sum can be described from Fig. 6.1 as follows:

$$P = P_a + P_u + P_s \,, \tag{6.1}$$

where P_a = initial loss, P_u = precipitation sum during initial infiltration ($t < t_s$), and P_s = precipitation sum during final infiltration ($t \geq t_s$), where t_s is the start time of final infiltration. Here, the sum of P_u and P_s makes up the effective precipitation sum (P_e) that directly causes the runoff:

$$P_e = P - P_a = P_u + P_s \,. \tag{6.2}$$

The sums of sub-precipitation P_a, P_u, and P_s are normally calculated as integrals of rainfall rate as follows:

$$\begin{aligned} P_a &= \int_{t_o}^{t_c} p\, dt \quad , \\ P_u &= \int_{t_c}^{t_s} p\, dt \quad , \\ P_s &= \int_{t_s}^{t_p} p\, dt \quad . \end{aligned} \tag{6.3}$$

Let us define the proportion of the runoff to the effective precipitation sum as the effective runoff coefficient, RC_e:

$$RC_e = \frac{RO}{P_e} \quad . \tag{6.4}$$

Rearranging Eq. 5.19 with Eq. 6.4, RC will be restated as follows:

$$RC = \frac{P_e}{P} \cdot RC_e \; = \; (1 \; - \; \frac{P_a}{P}) \cdot RC_e \quad . \tag{6.5}$$

Eq. 6.5 clarifies that the runoff coefficient can be considered a function of both initial loss during runoff concentration and the effective runoff coefficient during the direct runoff process.

During the runoff process, the runoff behavior shows a different intensity-dependency before and after the the saturated time point t_s. The runoff sum can be described in detail with the initial runoff RO_u during $t_c < t < t_s$ and the final runoff RO_s during $t \geq t_s$:

$$RO = RO_u + RO_s \quad , \tag{6.6}$$

where the components of runoff are calculated as follows:

$$\begin{aligned} RO_u &= \int_{t_c}^{t_s} q dt \quad , \\ RO_s &= \int_{t_s}^{t_p} q dt \quad . \end{aligned} \tag{6.7}$$

Let us define the initial runoff coefficient and final runoff coefficient, respectively, as the following:

$$\begin{aligned} RC_u &= \frac{RO_u}{P_u} \quad , \\ RC_s &= \frac{RO_s}{P_s} \quad . \end{aligned} \tag{6.8}$$

From Eq. 6.2 and Eq. 6.4, the runoff coefficient during the direct runoff process is

$$RC_e = \frac{RO}{P_e} = \frac{P_u \cdot RC_u + P_s \cdot RC_s}{P_u + P_s} \quad . \tag{6.9}$$

Finally, from Eq. 6.5, the runoff coefficient of the total precipitation event is defined as the following:

$$RC = (1 - \frac{P_a}{P}) \cdot \frac{P_u \cdot RC_u + P_s \cdot RC_s}{P_u + P_s} \quad . \tag{6.10}$$

It is assumed that the RC_u is strongly dependent on the precipitation event intensity and that no relationship between RC_s and rainfall intensity (r) exists, because the runoff is only the difference between the precipitation and the final infiltration.

When the final infiltration process is not reached during the event and $P_s = 0$ is negligible, as Fig. 6.1 (a) shows, then the runoff coefficient is

$$RC = (1 - \frac{P_a}{P}) \cdot RC_u \quad . \tag{6.11}$$

Fig. 6.2 compares the P-RO-relationship and the P_e-RO-relationship, where the runoff sum more clearly relates to the effective precipitation sum.

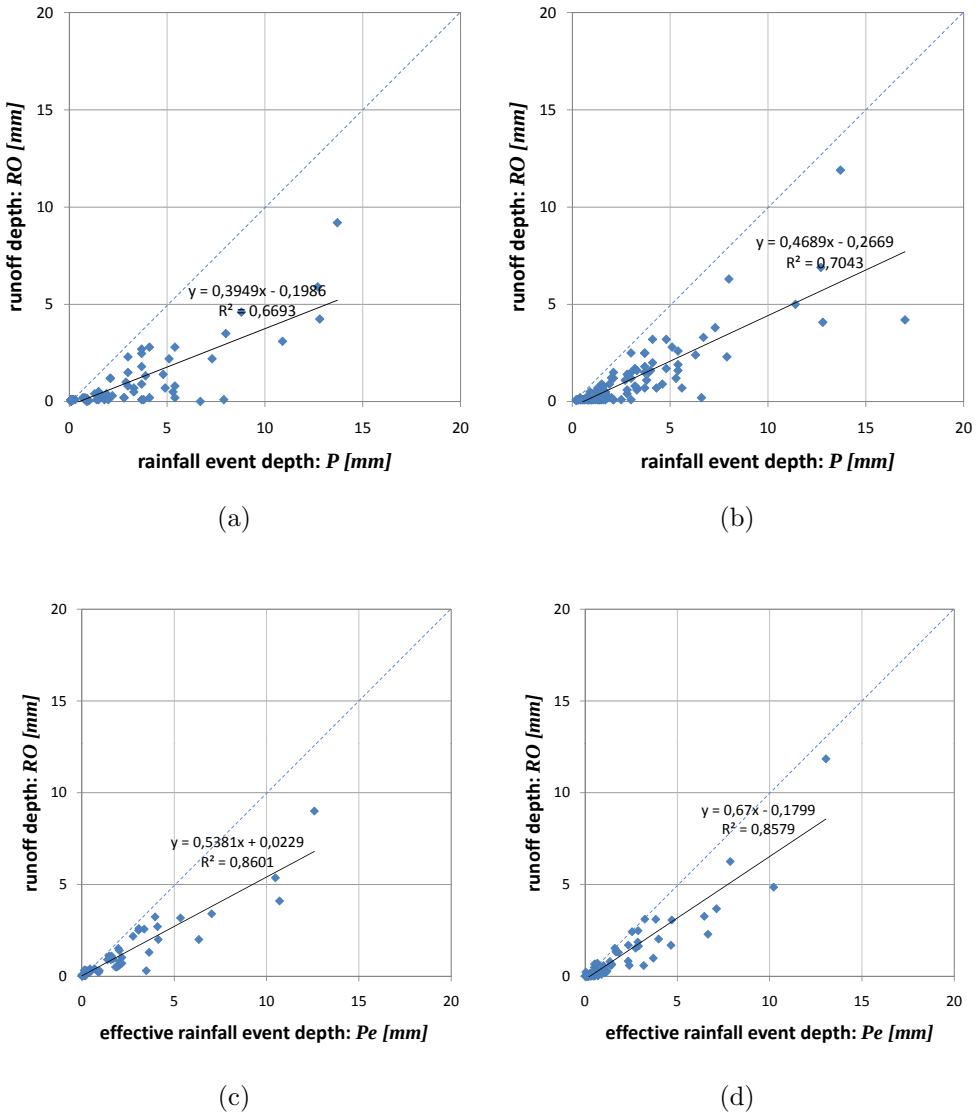

Figure 6.2: Precipitation-runoff Relationship on the paved surfaces from Bernburg mosaic cobblestone and Concrete paving slab: (a) and (b) show the relationship of P vs. RO for MCS and CPS, respectively, while (c) and (d) show the relationship of P_e vs. RO for MCS and CPS, respectively. The runoff sum, RO is more clearly related to the effective precipitation sum, P_e, than to the precipitation event sum, P.

6.2 Surface Storage Model

6.2.1 Runoff Concentration Process

The runoff concentration process is the first phase of the surface water process during a precipitation event. The infiltration capacity during the concentration process is impacted by the soil moisture and the filling state of the surface storage. The runoff concentration is an intensity-controlled process.

In the conventional regional runoff calculation models, it is assumed that a certain portion of regional retention capacity is responsible for initial loss. Based on this approach, runoff can arise without completely using the regional retention capacity that is equivalent to the surface storage capacity for the small field plots. Initial loss was treated as a constant term for the watershed.

Based on the high temporal resolution of the weighable lysimeter and WTB system, the initial loss and runoff concentration duration are obtained precisely for the period between May, 2009 and April, 2010. Fig. 6.3 presents the initial loss (P_a) versus the rainfall event sum (P) for Bernburg mosaic cobblestone and concrete paving slab.

For runoff-producing events, the average value of P_a from MCS accounts for about 1.06 liter, while it is about 0.66 liter for CPS, due to the fact that MCS has a higher seam portion (d) and surface depression volume. The reason for the dissipation of the P_a may lie in the event dependency. The less intense the rainfall event is, the more efficiently the surface storage can take the buffer role for supplying ponding water.

For non-runoff-producing events, the total precipitation water appears completely in form of initial loss. Both pavements showed a maximum P_a of over 5 liters, which is extremely higher than the average initial loss. This has an important meaning for dynamic surface water process.

For small field plots, like the lysimeter surfaces used in the study, the approach assumes that runoff does not occur until the surface storage is used up completely. Predominantly, pavement always has a certain topographical volume (depression volume) built from surface morphology and seam geometry, which makes up a big portion of total surface storage. As the soil of seam materials normally has pores, paving material is also assumed to have a certain volume of pores, especially the concrete products like CPS. These porous volumes also contribute to surface storage volume (Mansell and Rollet, 2009; Starke, 2010). Seam portion is an important indicator for the surface storage V_s.

For pavements with a small seam portion, V_s causes the retention of rainwater at the surface and prevents rainwater from flowing immediately into the soil. However, in case of a large seam portion, more rainwater can fall directly onto the seam space without being stored in surface storage. In such a case the infiltration process becomes more dominant than in the case of a small seam portion. A schematic of surface storage is shown in Fig. 6.4.

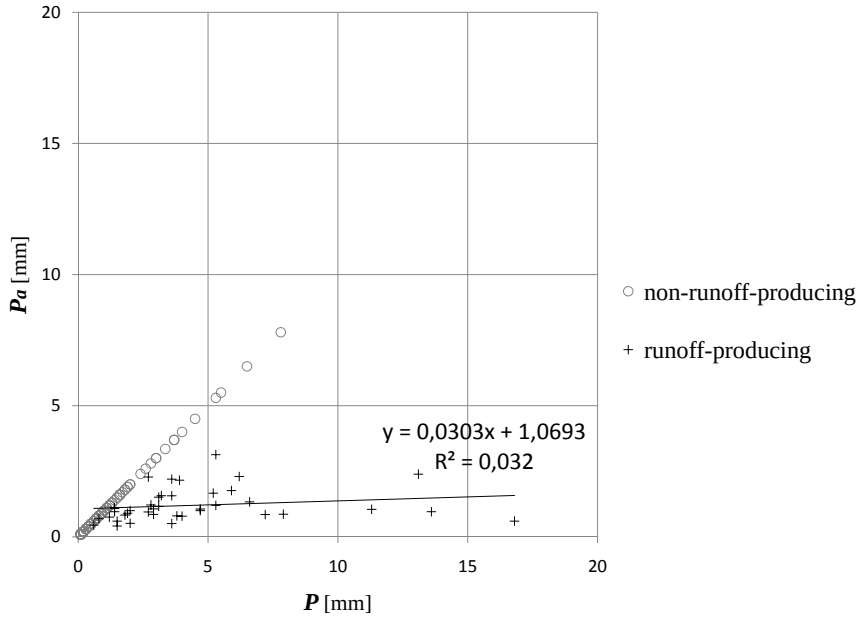

(a) Bernburg mosaic cobblestone

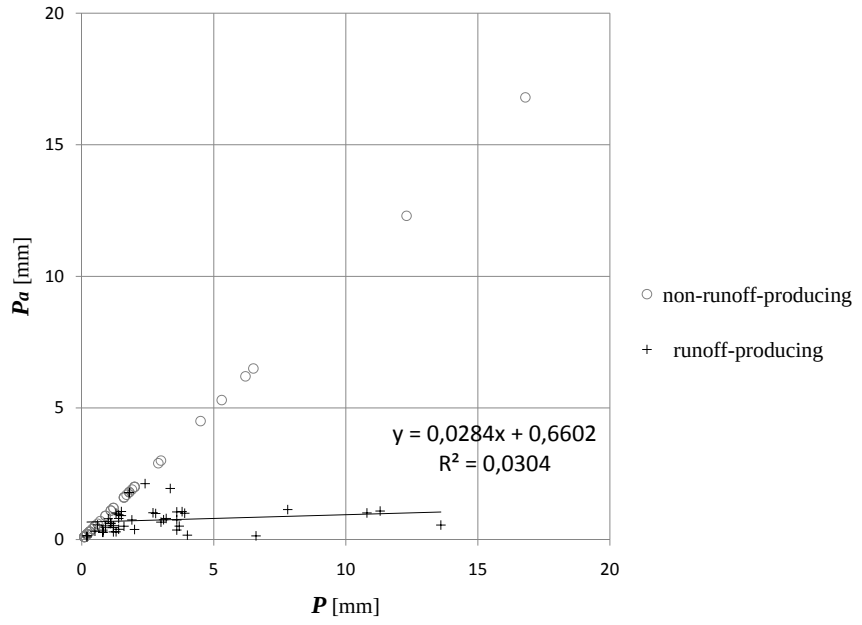

(b) Concrete paving stone

Figure 6.3: Initial loss (P_a) versus precipitation depth (P): the initial loss is not related to P. Permeably paved surfaces have a minimum of initial loss, rainfall event is runoff-effective when the rainfall sum is greater than this minimum of initial loss, which may correspond to the surface storage.

In considering surface storage, two kind of processes are of interest.

(i) Non-ponding process: the soil surface can never be flooded. Rainfall intensity is low enough that the water uptake process is dominant. Rainfall events that do not produce runoff can be classified as such. The infiltration capacity of the soil surface is higher than the precipitation intensity, so the surface storage never gets filled completely;

(ii) Pre-ponding process: immediately before the runoff generation, surface storage is about to be used up. At this stage, the soil surface almost reaches the pond-like state. The rainfall will produce runoff, but has not yet done so;

The non-ponding and pre-ponding process will be skipped when the surface storage has not emptied completely since the previous (e.g. big storm) event; e.g., a storm event is preceded by insufficient drying period. The runoff process can only begin if the rainfall intensity exceeds the infiltration capacity sufficiently enough to build a pond-like water layer on the surface, which will continuously flow down in the form of runoff by gravity along the surface gradient. The amount of runoff is calculated as the remaining amount of the precipitation water that is not involved in the initial loss and infiltration processes.

During the initial loss process, the water uptake at the paved surface is divided into two processes: in the first, one part of the falling rainwater percolates into the soil (infiltration process) while in the second, the remaining rainwater fills up as surface storage (ponding process).

$$P_a = V_s + V_r \,, \tag{6.12}$$

where P_a = initial loss, V_s = volume of surface storage, and V_r = volume of infiltrated water.

In the aspects of intensity, Eq. 6.12 can be restated as below:

$$r = v_s + v_r \,, \tag{6.13}$$

where r = rainfall intensity, v_s = ponding rate, and v_r = infiltration rate.

The ponding rate v_s and infiltration rate v_r are strictly controlled by rainfall intensity r. When r is small enough to sufficiently infiltrate but not high enough to fill the surface storage, then v_r almost equals to r. But, when the rainwater intensity r becomes big enough to quickly fill the surface storage, then the infiltration rate nears a constant maximum r_o. When $r > r_o$, the ponding rate v_s dominates the initial loss process, and runoff is going to be generated after the concentration duration of T_c. Therefore, let us consider the threshold intensity value r_o as *"runoff-producing intensity"*. r_o is an important surface hydrologic parameter for modeling the surface storage process.

The infiltration rate v_r can be described as a function of r, as illustrated in Fig. 6.4:

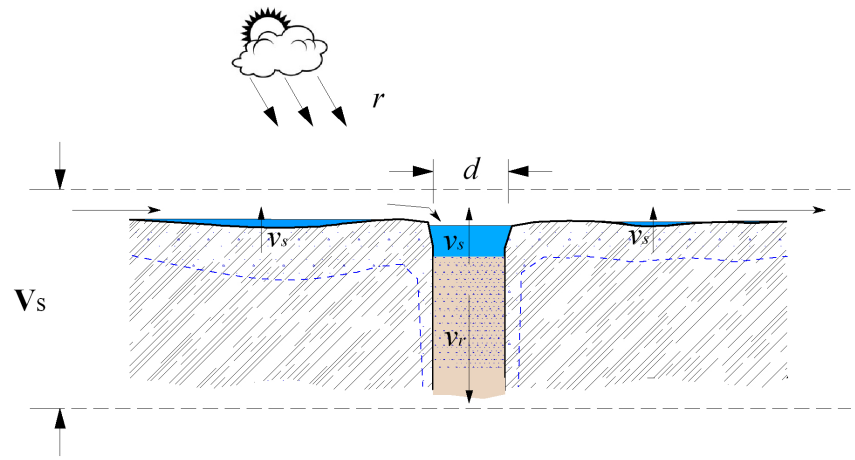

(a) Scheme of Surface Storage (V_s: surface storage volume, d: seam portion).

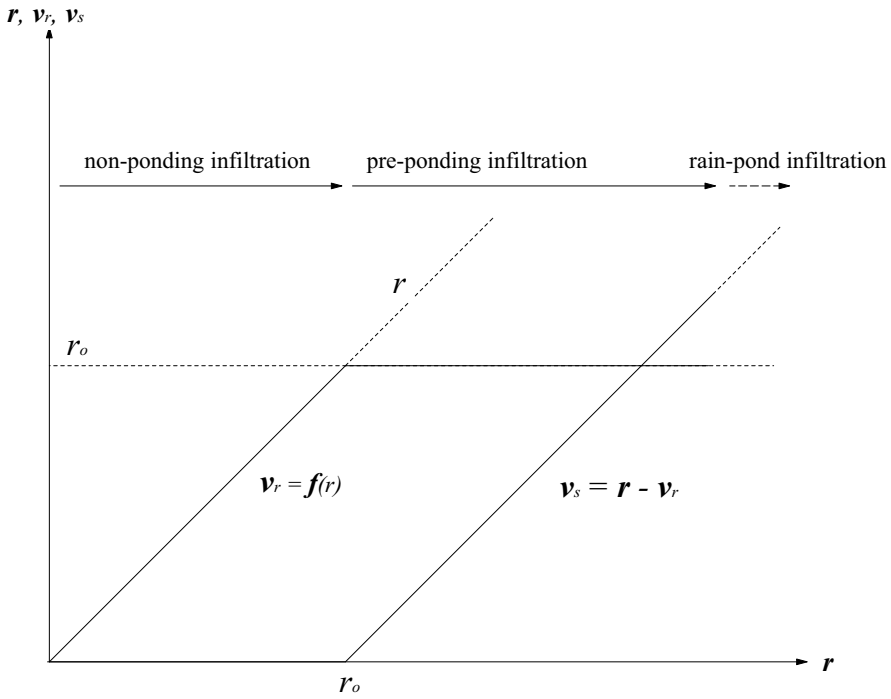

(b) Relationship between the infiltration rate v_r, ponding rate v_s, and the rainfall event intensity r (r_o: runoff-producing intensity).

Figure 6.4: Surface storage is characterized by the seam portion and the soil physical properties of the seam soil and paving material, the topography and the geometry of the pavement structure.

Assuming that the volume value of V_s and the function of v_r by r

$$v_r = f(r) \tag{6.14}$$

are known for the paved soil, the runoff concentration duration T_c is calculated as follows:

$$T_c = \frac{V_s}{v_s} = \frac{V_s}{r - f(r)} \tag{6.15}$$

From Eq. 6.13 and Eq. 6.15, the volume of infiltration water during initial loss can be described as

$$V_r = v_r \cdot T_c \tag{6.16}$$

If v_s is very small, T_c converges to an unlimited value, and V_r also become very big. Therefore, from Eq. 6.12, P_a will increase exponentially.

At the beginning of rainfall, the infiltrability of soil is high. The infiltrability decreases to a certain constant infiltration (final infiltration b) is arrived at by saturation time t_s. . Assuming that the soil surface is completely dried through evaporation prior to precipitation, the lower the beginning intensity r is, the more water will be infiltrated in the form of initial loss P_a (see Figure 6.7). Herein, we can see that the beginning of the rainfall process is critical in determining the ponding of surface storage (ponding time and filling state) and infiltration curve. After the saturated soil state is reached, the runoff is only the rest of the steady infiltration; therefore we cannot say that the runoff coefficient RC in this phase also dependent on rainfall intensity.

6.2.2 Surface Storage Model using Hyperbolic Tangent

The runoff concentration process depends both on the infiltration capacity of the surface and the surface storage. Theoretically, there is not an exact boundary between the non-ponding and preponding process. In Fig. 6.4, r_o indicates the threshold rate by which the transition from non-ponding to pre-ponding will occur during the initial loss. Thus, r_o wil be called the "*pre-ponding infiltration*" rate or the "*runoff-producing intensity*".

In order to simulate the slight transition between non-ponding and pre-ponding process, the "*Tangent Hyperbolic Function* $(tanh)$" ´ is applied.

$$tanh\, x = \frac{e^x - e^{-x}}{e^x + e^{-x}} \tag{6.17}$$

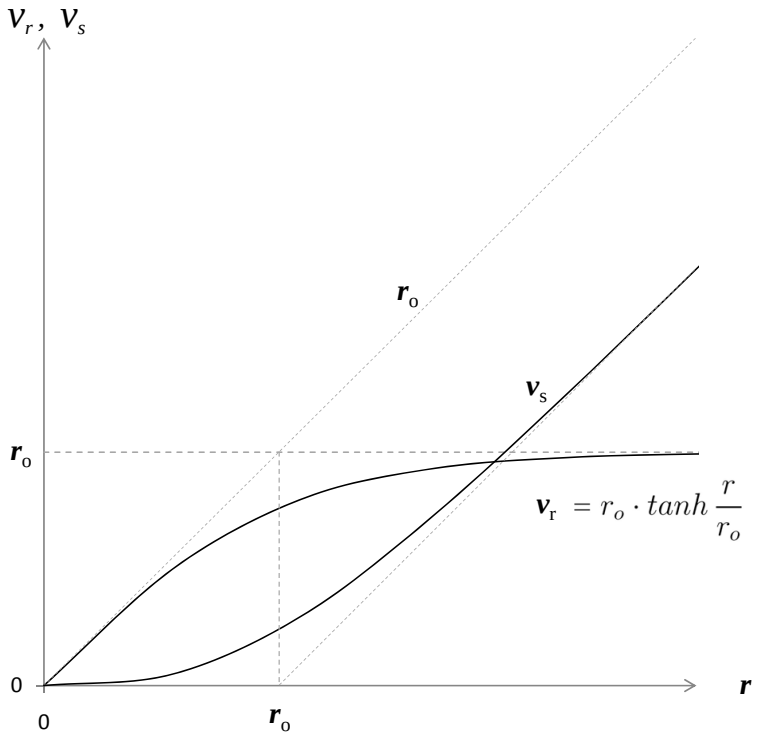

Figure 6.5: The tangent hyperbolic function is suggested for the approximation of the relationship of Eq. 6.14 (compare with Fig. 6.4). Here, v_r = infiltration rate , v_s = ponding rate , r = rainfall event intensity, and r_o = runoff-producing intensity.

By means of the *tanh* function, the relationship between the rainfall intensity and infiltration during runoff concentration can be mathematically described. We can consider 3 phases of the funciont in Fig. 6.5.

(i) The infiltration rate v_r increases together with the rainfall intensity until it is sufficiently smaller than runoff-producing intensity r_o.

(ii) By the range of r_o, v_r starts nearing to r_o.

(iii) After the rainfall intensity r is sufficiently bigger than r_o, v_r remains permanently constant.

The function of Eq. 6.14 is

$$v_r = r_o \cdot tanh \frac{r}{r_o}\,, \tag{6.18}$$

and from Eq. 6.13 and Eq. 6.15, the runoff concentration duration is

$$T_c = \frac{V_s}{v_s} = \frac{V_s}{r - r_o \cdot tanh\,\dfrac{r}{r_o}} \,. \tag{6.19}$$

Therefore, the initial loss can be derived as the following using surface storage, runoff-producing intensity, and rainfall intensity:

$$P_a = r \cdot T_c = V_s \cdot (1 - \frac{r_o}{r} \cdot tanh\,\frac{r}{r_o})^{-1} \quad . \tag{6.20}$$

This relationship clarifies that the initial loss results from the interplay between the rainfall parameter and the surface hydrologic parameters. In Fig. 6.6, the minimum initial loss (P_a) is the surface storage (V_s), which means that the surface storage needs to be completely used up in order to produce runoff. The initial loss can grow to an unlimited value when the rainfall intensity is much smaller than the runoff-producing intensity, due to the indeterminable runoff concentration duration (T_c) for $r \ll r_o$.

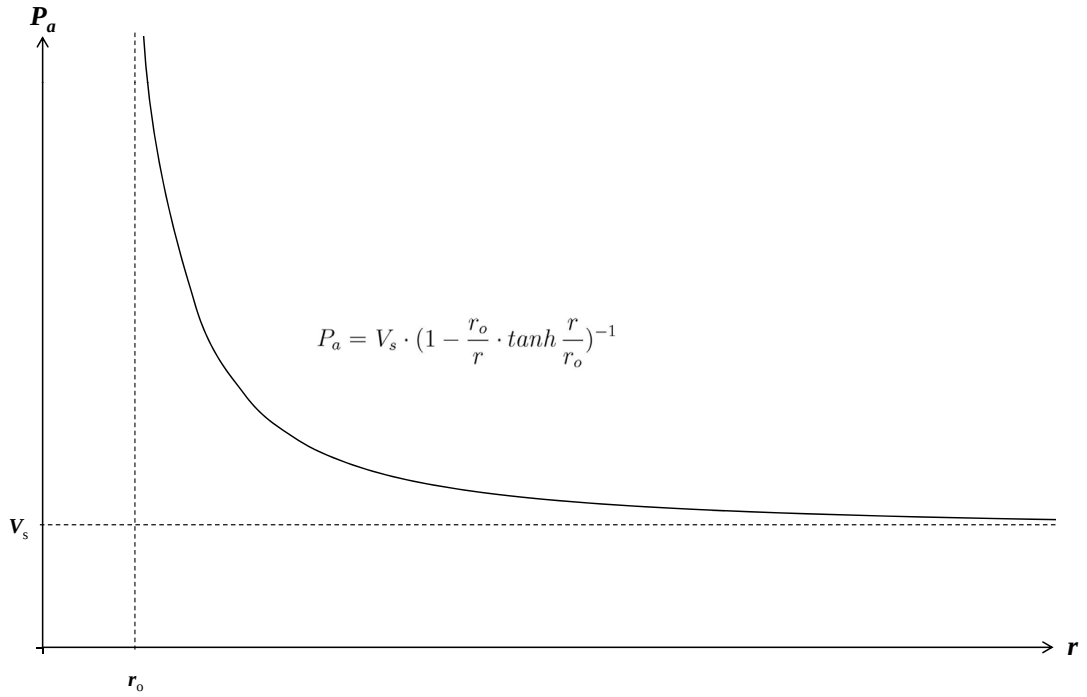

Figure 6.6: Surface storage model for the runoff concentration process: the minimum of initial loss (P_a) is the surface storage (V_s), which means that the surface storage needs to be completely used up in order to produce runoff. The initial loss can grow to an unlimited value when the rainfall intensity is much smaller than the runoff-producing intensity due to the indeterminable runoff concentration duration (T_c) for $r \ll r_o$.

6.3 Runoff Coefficient Model

6.3.1 Description of Rain-pond Infiltration Process

One can determine the infiltration curve when the runoff process can be observed in high temporal resolution. The measurement of runoff is much easier than that of infiltration, because the former process takes place in the visible surface zone, while the latter takes place in time-related (hysteretic) soil moisture in the invisible soil zone, which is afflicted with measurement difficulty and inaccuracy.

The infiltration rate decreases more or less quickly with the time elapsed, depending on the surface properties (Fig. 6.1). At a certain time, the soil surface reaches a saturated state with constant infiltration rate (b). Excepting the possibility that the escaping air bubbles from the soil can further heighten the infiltration rate again, the infiltration rate will arrive at a final constant value that may relate to the constant hydraulic conductivity of the paved soil. In past experiments, many paved surfaces arrived at the final infiltration state more or less within the 60 minutes after rainfall began (Flötter, 2006; Illgen et al., 2007).

In this study, the infiltration approach of Rubin (1966) and Swartzendruber and Hillel (1975) is used for the paved soil surface from Eq. 2.15. Their mathematical suggestion includes the final infiltration as a constant term of the equation for the whole area of validity of the time variable. It is assumed that its universal form can sum up and describe the causal kinetic parameters of paved surfaces and that its simple form form enables easy derivation of the intensity-dependent RC and surface parameters.

Many rainfall events that are runoff-effective do not show the same runoff coefficient. The most important factor of dynamic RC is the rainfall event intensity. Event intensity predominantly influences initial loss and runoff concentration, and even the runoff-effectiveness, if runoff will occur at all. For runoff-effective events, the infiltration curve progress is also decided by rainfall event intensity.

Based on the experiment results of Rubin (1966) and the model approach of Schwartzendruber (1974) about infiltration and runoff for small field plots under constant intensity rainfall, the rainfall event intensity r is considered as a significant factor influencing runoff and infiltration at the paved soil surface. It is assumed that the soil surface has uniform properties and a constant initial soil water content distinctly less than saturated soil moisture and that the intrinsic soil properties remain essentially unchanged with time. After runoff concentration, as the rainfall intensity exceeds its infiltration rate at time t_c and as the infiltrability decreases with time elapsing from $t \geq t_c$ on, if the rainfall intensity (r) is continuously higher than infiltration rate (i) needed to produce runoff, the end infiltration rate b will be arrived at time t_s. After t_s infiltrability will neither decrease nor increase as long as $r > b$. Therefore, the infiltration rate is expressed as follows:

$$i(t) = \begin{cases} r & : t < t_c \\ a \cdot t^{-n}\,,\ (n > 0) & : t_c \leq t < t_s \\ b & : t \geq t_s \end{cases} \tag{6.21}$$

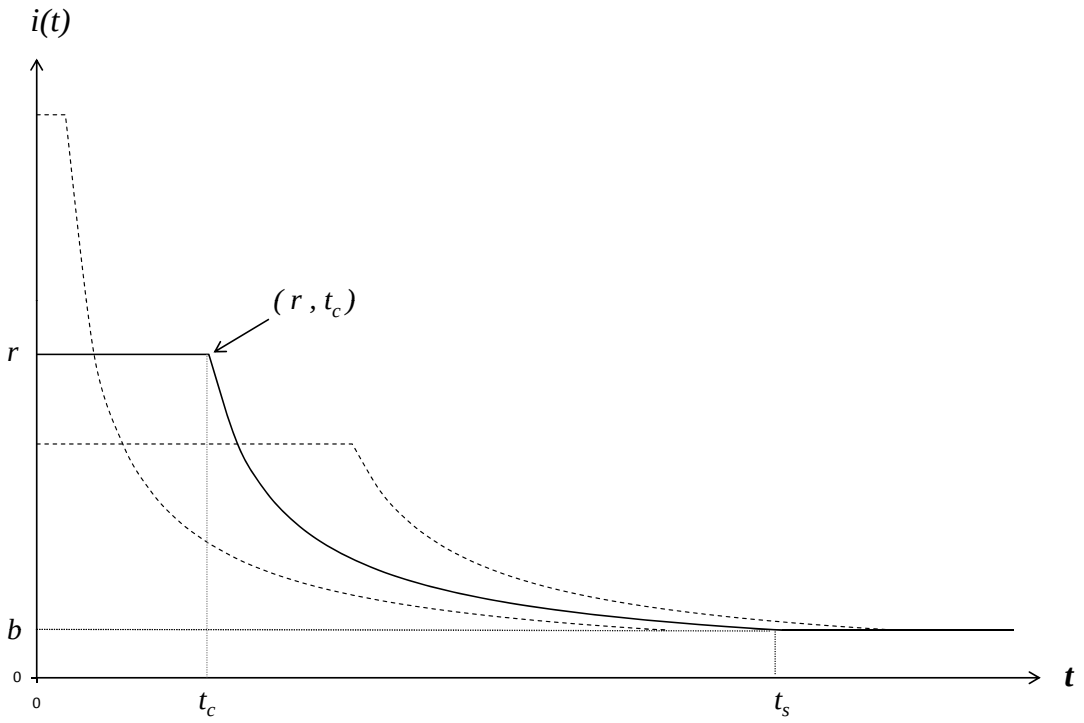

Figure 6.7: Rain-pond infiltration ($i(t)$ = infiltration [mm/min], t = time [min]).

6.3.2 Intensity-dependent Runoff Coefficient for Small Field Plot under Constant Rainfall Flux

Assuming that a rainfall event has constant intensity (or the rainfall intensity is distributed according to the standard rainfall pattern, e.g., as suggested by DVWK (1990) and Dyck and Peschke (1995)), if one makes an explicit use from Eq. 6.21 of the condition $i = r$ at $t = t_c$ and $i = b$ at $t = t_s$, then

$$\begin{cases} r = a \cdot t_c^{-n} & : t = t_c \\ \\ b = a \cdot t_s^{-n} & : t = t_s \end{cases} \tag{6.22}$$

For the initial infiltration during $t_c \leq t \leq t_s$, the infiltration depth can be obtained by

$$I_u = \int_{t_c}^{t_s} a \cdot t^{-n} dt = \frac{a}{1-n} \cdot \left(t_s^{1-n} - t_c^{1-n} \right) \quad . \tag{6.23}$$

Based on the water balance of

$$RO_u = P_u - I_u \tag{6.24}$$

and

$$P_u = r(t_s - t_c)\,, \tag{6.25}$$

the runoff depth during initial infiltration RO_u is formed as

$$RO_u = r(t_s - t_c) \; - \; \frac{a}{1-n} \cdot \left(t_s^{1-n} - t_c^{1-n} \right) \tag{6.26}$$

Therefore, the initial runoff coefficient is, analogous to Eq. 5.19:

$$\begin{aligned} RC_u = \frac{RO_u}{P_u} &= 1 \; - \; \frac{a}{1-n} \cdot \frac{t_s^{1-n} - t_c^{1-n}}{r(t_s - t_c)} \\ \\ &= 1 \; - \; \frac{a}{r(1-n)} \cdot \frac{t_s^{1-n} - t_c^{1-n}}{t_s - t_c}\,. \end{aligned} \tag{6.27}$$

From Eq. 6.22, the following relationship is available:

$$t_c{}^n = \frac{a}{r}\,, \tag{6.28}$$

and Eq. 6.27 yields by applying Eq. 6.28

$$\begin{aligned} RC_u &= 1 - \frac{t_c{}^n}{1-n} \cdot \frac{t_s^{1-n} - t_c^{1-n}}{t_s - t_c} \\ &= 1 - \frac{\dfrac{t_c{}^n}{t_s{}^n} t_c - t_c}{(1-n)(t_s - t_c)}\,. \end{aligned} \tag{6.29}$$

From the Eq. 6.22, one can obtain the relationship between t_c and t_s expressed as

$$t_c = t_s \left(\frac{b}{r}\right)^{\frac{1}{n}}\,. \tag{6.30}$$

The term b/r can be introduced by a new variable R called *relative infiltrability*. R is then

$$R = \frac{b}{r}\,. \tag{6.31}$$

Now we can express RC_u by R as the following:

$$RC_u \quad = \quad 1 - \frac{R - R^{\frac{1}{n}}}{(1-n)\cdot(1 - R^{\frac{1}{n}})}\,. \tag{6.32}$$

In Eq. 6.32, RC cannot be determined analytically for the special case of $n = 1$ that may not exist for the practical soil surface. However, substituting $n = 1$ to Eq. 6.23, the same process of RC_u solution will analytically yield the following result:

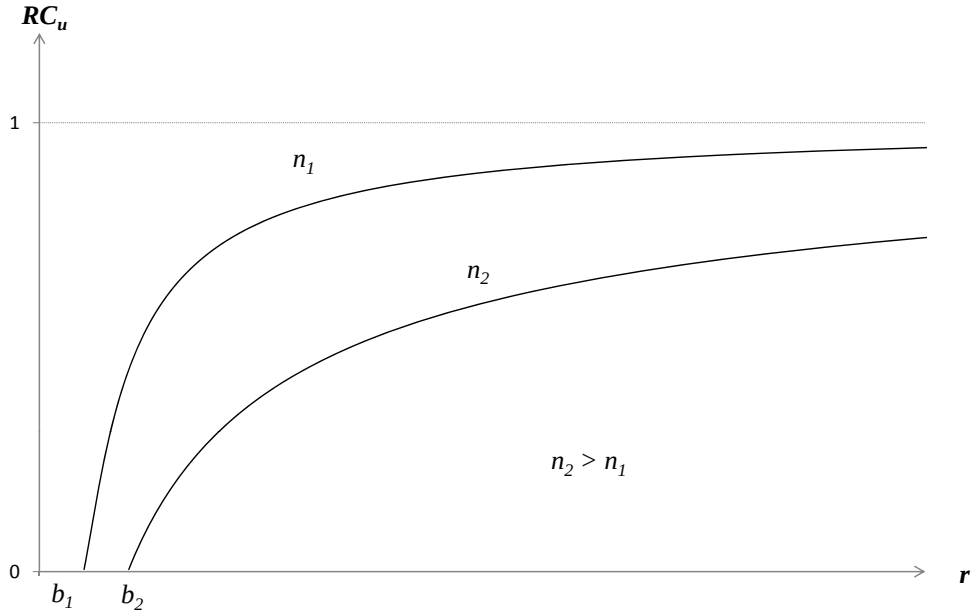

Figure 6.8: The theoretical relationship between the runoff coefficient (RC_u) and the rainfall event intensity (r).

$$RC_u = 1 - \frac{\ln R}{1 - R^{-1}} \quad : \quad n = 1\,. \tag{6.33}$$

Eq. 6.32 clarifies that the runoff coefficient during the initial infiltration process is influenced by the interplay between the rainfall intensity and surface hydrologic parameters, b and n.

Relative Infiltrability

In this study, a definition of the relative infiltrability R is made for describing the surface water process on the paved soil regarding both the soil surface parameter (b) and the rainfall event parameter (r). In the Eq. 6.31 the relative infiltrability R describes the proportion of the end infiltration rate of the soil to the rainfall intensity. R does not occupy any unit and is an important factor of the intensity-dependent runoff coefficient.

The end infiltration rate b is the soil hydrologic parameter that explains the overall infiltration capacity of the soil, while the rainfall intensity r is the parameter that controls the runoff concentration process and the runoff process during the unsaturated infiltration phase. Therefore, the higher the infiltration capacity and the smaller the rainfall intensity is, the bigger the relative infiltrability. R is an important criterion for assessing runoff during both unsaturated and saturated infiltration phases.

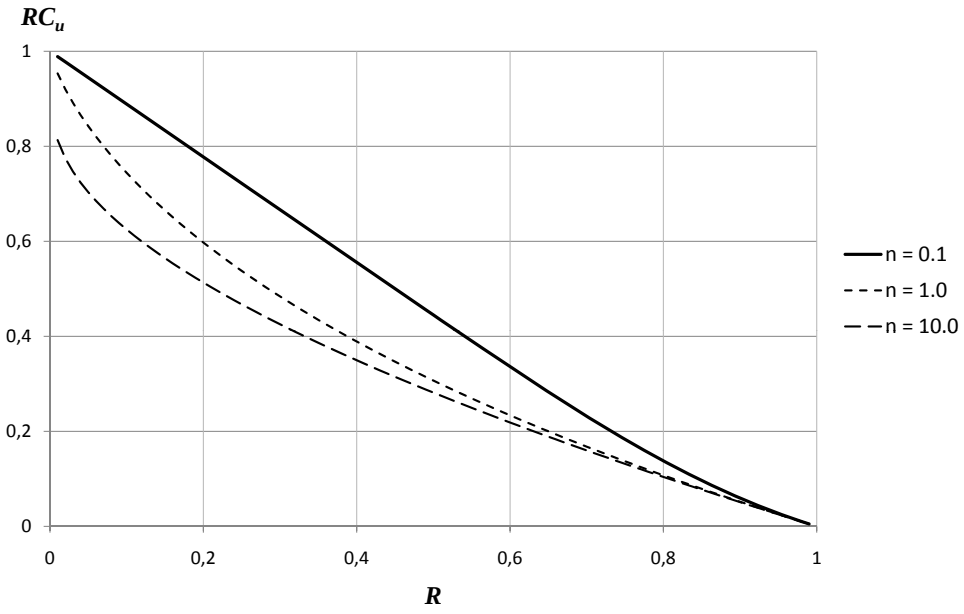

Figure 6.9: The theoretical relationship between the runoff coefficient (RC_u) and the the relative infiltrability (R).

In Fig. 6.9, the relationship between the runoff coefficient and relative infiltrability is shown according to the different infiltration process exponent parameter n. The runoff coefficient is the strictly monotonic decreasing function with increasing relative infiltrability. For the practical circumstances of paved surfaces, the R varies between 0.1 and 1. Here, RC_u decreases almost linearly with increasing R, which respectively varies with n. For $n < 1$, the variation of RC_u is significantly wider than for $n > 1$.

When rainfall events rarely arrive at a saturated infiltration state, the runoff coefficient of precipitation events, RC, can be summarized for practical cases from Eq. 6.11 as the following:

$$RC = \left(1 - \frac{V_s}{P \cdot \left(1 - \frac{r_o}{r} \cdot tanh \frac{r}{r_o} \right)} \right) \cdot \left(1 - \frac{R - R^{\frac{1}{n}}}{(1-n) \cdot (1 - R^{\frac{1}{n}})} \right). \quad (6.34)$$

Chapter 7

Determination of Surface Hydrological Parameters

From the measurement period, the data for precipitation-runoff relationship, such as the event intensity (r), the runoff concentration duration (T_c), the initial loss (P_a), and the runoff coefficient (RC_u), are applied to the runoff dynamics models in Eq. 6.20 and in Eq. 6.32. The surface hydrological parameters, such as surface storage volume, runoff-producing intensity, final infiltration rate, and infiltration exponent, can be obtained through the adaption of model to the event data. Therefore, these models give a method of determination for the surface hydrologic parameters.

In order to apply the data to the model, some requirements were considered for selection and preparation of the event data: The models are developed for the constant flux intensity of the precipitation event; The soil surface is supposed to have a lower water content than the saturated state; Therefore, the events with a drastic fluctuations of rainfall intensity, $p(t)$, were taken away from the data set to exclude the events with eventual hysteresis of soil water content.

The events with very small initial loss were also not considered. In order to obtain the surface storage, such events cannot have the same characteristics like the events that begin with empty V_s. The events with very long duration were also taken away because the relationship between RC and r could not be detected, due to the apparent non-constant flux.

7.1 Results from Surface Storage Model

The pavements of Bernburg mosaic cobblestone (MCS) and Concrete paving slab (CPS) possess different characteristics for surface hydrologic parameters. From the fact that MCS apparently has the higher seam portion and more complex surface roughness than CPS, one can presume a higher surface storage for MCS than for CPS. The results from past studies detected these values for several

pavements more or less through a immediate measurement method. However, such results varied according to the definitions and techniques from each other.

In a big field plots under storm event condition, Schramm (1996) obtained $V_s = 1.6\,\text{mm}$ for concrete cobblestone that has more or less a comparable appearance and properties with MCS, while V_s of a concrete paving slab pavement implemented in his experiment was 1.5 mm (Tab. 2.1). Despite the big difference of the seam portion, both pavements showed a very similar values of V_s. Neverthless, the small difference was to mention up to his imprecise experiment technique of water sprinkling and pumping, only with storm events (see Chap. 2.1).

Meanwhile, Wessolek and Facklam (1997) and Flötter (2006) determined the V_s under the approximately real urban condition. The surface storages for the cobblestone and the paving slab pavement turned out with a contrast to the results by Schramm (1996). From the study of Flötter (2006), the surface storages were 0.24 mm and 0.17 mm for cobblestone and paving slab surface, respectively, which were smaller than the results of Schramm (Tab.2.5).

Wessolek and Facklam (1997) concentrated on the wetting capacity of pavements. From his experiment, the surface storages were 1.5 mm for Bernburg mosaic cobblestone and 0.3 mm for Concrete paving slab, which were between the study results of Flötter and Schramm (see Tab. 2.3).

In my study, the surface storage is estimated through the adaption of the surface storage model from Eq. 6.20 to the data that are measured during the lysimeter experiment in summer months of 2009, other than the previous experiments that attempted to detect the V_s values through direct measurement.

In Fig. 6.3, the values of initial loss remained constant for the runoff-producing events with greater precipitation sum, e.g. $P >$ ca. 7 mm, while that strongly dissipated for the another events with $P <$ ca. 7 mm. That is true for both MCS and CPS. It is notable that the great precipitation event mostly had a great intensity, and for those events, the initial loss remained nearly equivalent. But it is also notable that events with a long duration could have also the great precipitation sum when the rainfall intensity was not too low, and for those events, the initial loss became larger. This dynamic behavior of initial loss can be only explained with the surface storage model as a function of rainfall event intensity.

From the period between May and December 2009, the parameters of runoff concentration (P_a, T_c, r) are obtained for the rainfall events. The models derived in the last chapter consider the rainfall event as constant flux onto the soil surface. However, the events acquired in the lysimeter station showed different rain pattern and could not always show such constant property. Hence, the average intensity of runoff concentration process is considered as r, which may have caused statistical error.

Fig. 7.1 shows the regression result of the initial loss in the relationship with the rainfall intensity. For the high intensity range, the initial loss, P_a, clearly tends to remain constant, while it rapidly increases with decreasing intensity.

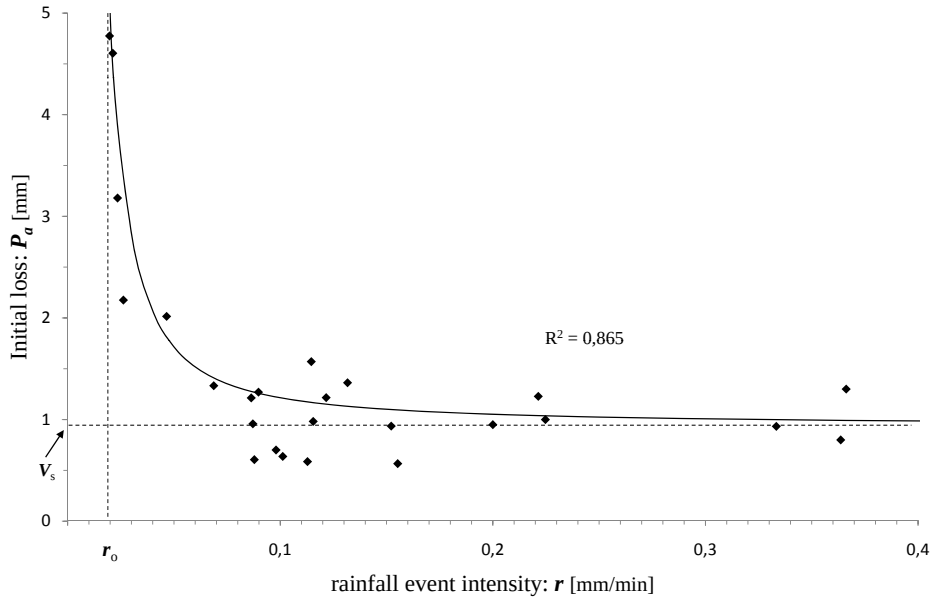

(a) Berburg mosaic cobblestone

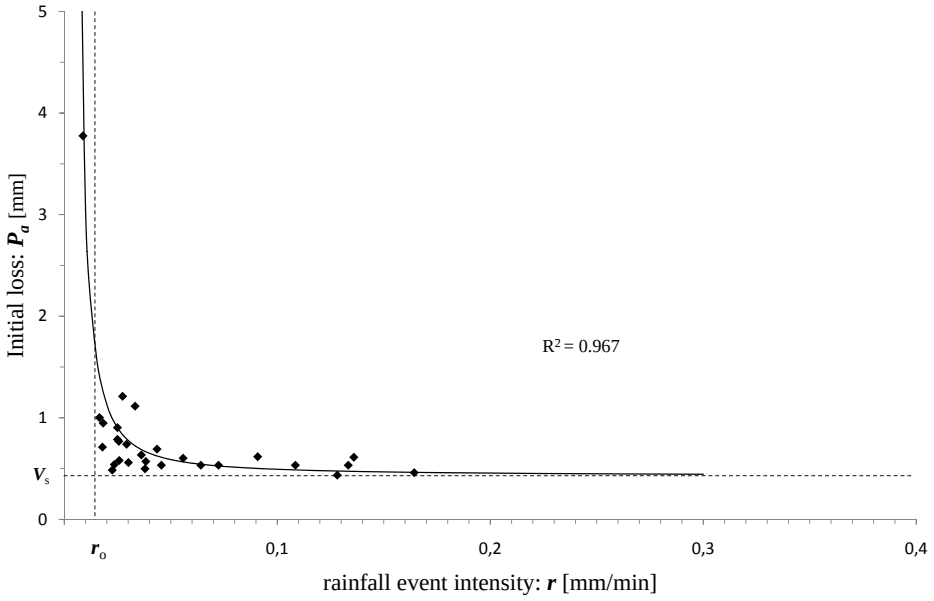

(b) Concrete paving slab

Figure 7.1: Adaption of the surface storage model and determination of the surface storage, V_s, and the runoff-producing intensity, r_o.

The number of runoff-producing events of MCS are less than that of CPS. The dissipation of initial loss was smaller for CPS than for MCS. The middle intensity ranges (between 0.02 and 0.05 mm/min for MCS and between 0.05 and 0.1 mm/min for CPS) are to see as problematic: It was still technically problematic to decide about the filling state of the surface storage despite the event data preparation. Additionally, there were further surface specific parameters like runoff transportation which was not included in the model.

The dashed horizontal line of V_s is tangent with the curve of $P_a - r$ functions, which clarifies that the soil surface always need to be filled completely before the runoff generates from the surface, independent of the rainfall intensity. From the regression with least squares, the surface storages, V_s result in 0.9276 mm for MCS and 0.4235 mm for CPS. The runoff-producing intensity were 0.0236 mm/min for MCS and 0.014 mm/min for CPS (see Tab. 7.1). The dashed vertical line of r_o implies on that the event with $r < r_o$ can store almost unlimited initial loss. The differences of V_s and r_o between MCS and CPS might be not remarkable despite the difference of seam portion. However, Tab. 5.3 shows that this difference made a great difference of the total sum of runoff-producing rainfall events. For MCS, ca. 260 mm (48.4 % of annual precipitation) was completely taken up thanks to the surface storage capacity without producing runoff, while the sum of suce event was only 96 mm (17.9 % of annual precipitation P_{annual}) for CPS.

7.2 Results from Intensity-dependent RC Model

Assuming that the rainfall events never arrived the final infiltration phase in practice, then the runoff coefficient model of Eq. 6.32 does have great sense for the total runoff prognosis. This model clarifies the rainfall-runoff relationship during the initial infiltration process where the infiltration of the paved soil surface decreases with the time. In this model, the interplay between rainfall characteristics and surface characteristics is reflected in the parameter of relative infiltrability R.

Schramm (1996) tried to experimentally obtain the final infiltration rate of a comparable concrete cobblestone and paving slab. After him, the concrete cobblestone and paving slab had the final infiltration rate of 0.1 mm and 0.08 mm, respectively, which were very similar despite of a big difference of seam portion (Tab. 2.1). In his experiment, the variation of the runoff coefficients for different seam portions was small, which implied on the marginal role of seam portion for rainfall-runoff relationship under storm events. His attempt to find the intensity-dependent runoff coefficient was incomplete because no small rainfall events were simulated and included in the analysis of intensity-dependent runoff coefficient.

For the similar materials, Flötter (2006) meaured the final infiltration rate of 0.27 mm/min and 0.01 mm/min, respectively. Since he also could not simulate the small rainfall event, his statement about intensity-dependent runoff coefficient

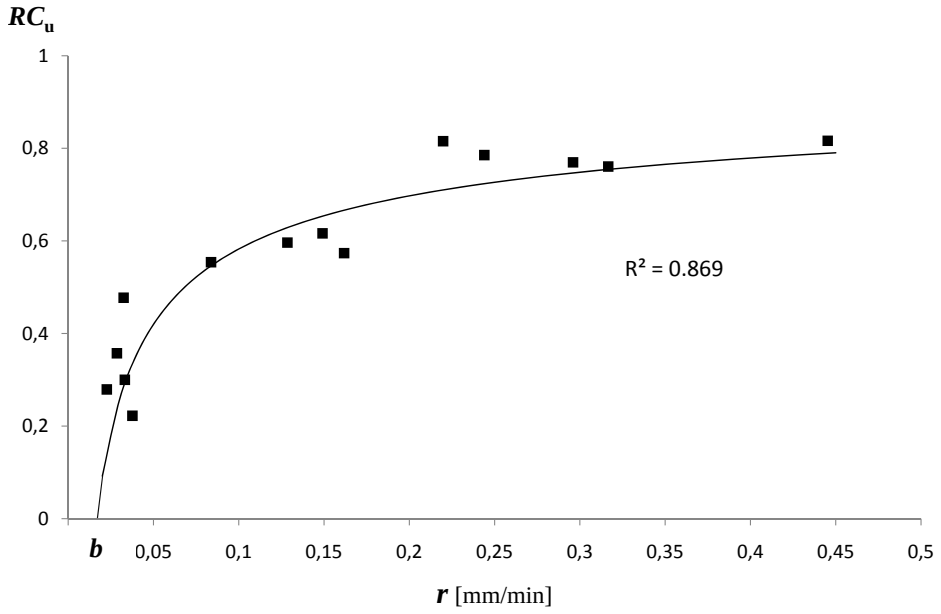

(a) Bernburg mosaic cobblestone

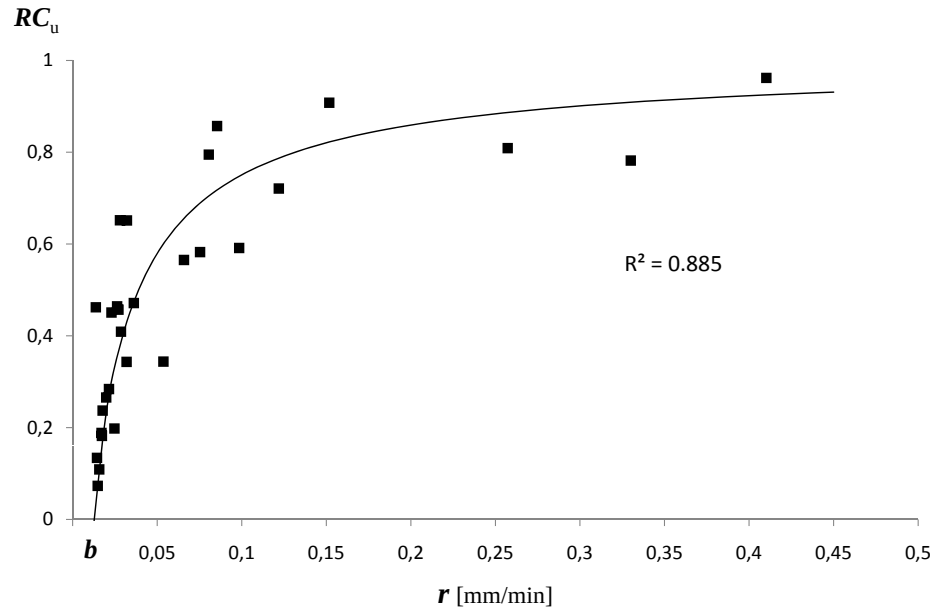

(b) Concrete paving slab

Figure 7.2: Adaption of the intensity-dependent runoff coefficient model and determination of the final infiltration , b, and the infiltration exponent, n.

Table 7.1: Surface hydrologic parameters for pavements of Bernburg mosaic cobblestone and Concrete paving slab.

	Bernburg mosaic cobblestone	Concrete paving slab
r_o [mm/min]: runoff-producing intensity	0.024	0.014
V_s [mm]: surface storage	0.928	0.424
n : infiltration exponent	2.53	0.68
b [mm/min] : final infiltration	0.016	0.012

was developed through operational interpretation (Tab. 2.5).

It was essential to capture the small rainfall event, which was only enabled by the high resolution lysimeters. In addition, the weighable tipping bucket enabled the very high temporal resolution. The high temporal resolution is especially crucial when the paved soil surfaces show negative characteristics as for infiltration performance. Concrete paving slab is a pavement, mostly used for streets with low retention capacity. This is also true for paved surface with cobblestone after a long aging process.

Fig. 7.2 shows the result of the model adaption to the data for the relationship between the runoff coefficient and the rainfall intensity. From the measured rainfall events between May and December 2009, the events are prepared for curve fitting. For runoff coefficient model from Eq. 6.32, the rainfall event was assumed to be constant flux, and the rainfall pattern was required not to have too strong fluctuation. Therefore, similarly to the even data preparation for adaption of surface storage model, events with too long duration was excluded from the process.

The greater the intensity becomes, the more slowly RC_u increases. RC_u can be considered remaining constant if r becomes greater. For instance, the runoff coefficient begin to remain constant for the storm event with $r > 0.2\,\mathrm{mm/min}$ for MCS, while $r > 0.1\,\mathrm{mm/min}$ for CPS. In contrast, the change of rainfall events in the low intensity range can rash increase or decrease RC_u. Tab. 7.1 gives an overview about the result of determination surface hydrologic parameter for both MCS and CPS through statistical regression. When comparing the runoff coefficients between both pavements, RC_u of MCS is always greater than that of CPS. The reason may lie in the fact that MCS has the greater relative infiltrability, R, than CPS. The adaption of the model to the measured data results in $b = 0.016\,\mathrm{mm/min}$ and $n = 2.53$ for MCS as well as $b = 0.012\,\mathrm{mm/min}$ and $n = 0.68$ for CPS.

The final infiltration rate is critical value for the valuablity of RC_u. Rainfall

events with $r < b$ are non-runoff-producing in Fig. 7.2. In addition, the infiltration exponent, n, and the final infiltration rate, b, are related each other. From the rain-pond infiltration model, soils with greater b always show greater infiltration progress, $i(t)$, which requires the greater infiltration exponent. Therefore, n of MCS was greater than that of CPS.

The model gives the statement that the initial loss during the runoff concentration process needs to have the surface storage as minimum and the rainfall events have to exceed the surface storage at least to produce runoff. Also, the initial loss can enormously rise with the decreasing rainfall event because the ponding effect in surface storage can be more effective when the rainfall becomes less intense. If the rainfall intensity is smaller enough than the runoff-producing intensity, the events are non-runoff-producing, which presumably reflects the empiric ponded runoff transportation process without exactly having its parameter. For climate regions, one has to design such pavement materials for urban catchment which does show an slow approach of P_a to V_s for the typical event ranges. Only such pavements can live up to their potential infiltration capacity under the regional hydrologic condition

Conclusions and Outlook

In this study, a process-based model concept for describing the dynamic runoff behaviors of paved soil surfaces was for the first time developed. In order to investigate the water balance process, a paved weighable lysimeter was realized. The lysimeters were constructed with the pavements from Bernburg mosaic cobblestone and Concrete paving slab that together make up so called "Berlin's Walkway". A new measurement setup for runoff dynamics, called the weighable tipping bucket (WTB), was installed in the lysimeter system. The lysimeter surfaces had sufficiently identical properties to the realistic street conditions.

The components, such as precipitation, evaporation, runoff and groundwater recharge were measured in very high resolution. The improvement of the lysimeter technique by using a weighable tipping bucket enabled the high-resolution measurement of runoff processes.

For the representative elementary area of paved soil surfaces, the water balance processes were continuously measured for the climate and hydrologic conditions of Berlin and observed under varying natural precipitation events. The two paved soil surface could show a potential for enhancing groundwater recharge and reducing runoff, depending on the the distribution of small events. In addition, the evaporation from paved surface can be also enhanced, when the surface storage can be effectively controlled. The rainfall event intensity was derived as the main factor for the analysis of runoff-producing rainfall events.

The process-based model of runoff dynamics describes the runoff coefficient in relationship with the rainfall event intensity, the surface storage, the runoff-producing intensity, the final infiltration rate, and the infiltration exponent.

The paved surface can take up the precipitation water as much as the surface storage and the rainfall characteristics allow. The bigger the surface storage and the infiltration capacity becomes, the more the precipitation water can infiltrate. However, the evaporation is problematic. High infiltration does not absolutely leads to a high evaporation. Therefore, the paved surface must be not only permeable, but also enable reconnection between the soil water and the atmosphere, e.g. by improving capillary rising of soil water.

A technical and analytical method could be established to derive the surface hydrologic parameters for further paving materials. This is important for the quantification and improvement of retention capacity for new materials in the

sense of pavement renewing potential.

The model clarified that the surface storage has to be adjusted to the regional precipitation frequency in order to minimize the runoff water. The process-based model allows assessing the uncertainty of the prediction from the simplified empiric models. It can be applied to the various climate conditions.

Bibliography

Akan, A. O. and R. J. Houghtalen (2003). *Urban Hydrology, Hydraulics, and Stromwater Quality. Engineering Applications and Computer Modeling.* John Wiley & Sons, Ltd.

Arnbjerg-Nielsen, K. (2006). Significant climate change of extreme rainfall in Denmark. *Water Science & Technology 54*, 1–8.

Arnbjerg-Nielsen, K. and H. S. Fleischer (2009). Feasible adaption strategies for incresed risk of flooding in cities due to climate change. *Water Science & Technology 60*, 273–281.

ATV-DVWK (1992). *ATV-A 128: Richtlinien für die Bemessung und Gestaltung von Regenentlastungsanlagen in Mischwasserkanälen. ATV-DVWK-Regelwerk.* DWA Deutsche Vereinigung für Wasserwirtschaft, Abwasser und Abfall e. V.

ATV-DVWK (2000). *ATV-DVWK-M 153: Handlungsempfehlungen zum Umgang mit Regenwasser. ATV-DVWK-Regelwerk.* DWA Deutsche Vereinigung für Wasserwirtschaft, Abwasser und Abfall e.V.

Bear, J. (1972). *Dynamics of Fluids in Porous Media.* American Elsevier Publishing Company, Inc., New York.

Berger, S. and P. Cepuder (2007). Lysimeter in Forschung und Lehre - Ergebnisse aus 15 Jahren "Arbeitsgruppe Lysimeter". In *12. Lysimetertagung, Lysimetrie im Kontext zu nationalen und internationalen Regelwerken*, Gumpenstein, Irdning, Austria, 2007.

Beven, K. (2004). Robert E. Horton's perceptual model of infiltration processes. *Hydrol. Process. 18*(17), 3447–3460.

Borgwardt, S. (2006). Long-term in-situ infiltration performance of permeable concrete block pavement. In *8th International Conference on Concrete Block Paving, San Fransisco, California USA.*

Borgwardt, S., A. Gerlach, and K. M. (2000). *Versickerungsfähige Verkehrsflächen. Anforderungen, Einsatz und Bemessung.* Springer, Berlin.

Bronstert, A., S. Krause, and D. Kneis (2006). Niederschlag-Abfluss-Prozess im Flachland: Analyse, Modellierung und Implikationen für die Wasserqualität. In *Symposium zur Analyse und Modellierung der Niederschlags-Abfluss-Prozesse bewährte Techniken und neue Ansätze*. Institut für Hydrologie und Meteorologie. TU Dresden.

Dawson, A. (2008). *Water in road structures. Movement, Drainage and Effects*. Springer.

Diestel, H., N. Markwardt, and J. Moede (1993). Experimentelle Untersuchungen sowie Modellentwicklungen zur Verlagerung von Pflanzenschutzmitteln in der ungesättigten Bodenzone. In H. Bork, M. Renger, F. Alaily, and G. Roth, C. und Wessolek (Eds.), *Bodenökologie und Bodengenese*. FG Bodenkunde und Regionale Bodenkunde, Institut für Ökologie, T U Berlin.

DIN 1986-3 (1986). Drainage systems on private ground. Part III - Specifications for service and maintenance.

DIN 4049-1 (1989). Hydrologie, Begriffe, Grundbegegriffe und Wasserkreislauf.

Dreiseitl, H. and D. Grau (2009). *Recent Water Scapes: Planning, Building and Designing with Water*. Birkhäuser Architektur.

DVWK (1990). *Arbeitsanleitung zur Anwendung von Niederschlag-Abfluss-Modellen in kleinen Einzugsgebieten. Teil 2: Synthese. Heft 113.2*. Verlag Paul Parey.

DVWK (1996). *Ermittlung der Verdunstung von Land- und Wasserflächen*. Wirtschafts- und Verl.-Ges. Gas und Wasser. Bonn. DVWK-Merkblätter zur Wasserwirtschaft.

DWA-A (2005). *Arbeitsblatt DWA-A 138: Planung, Bau und Betrieb von Anlagen zur Versickerung von Niederschlagswasser. DWA-Regelwerk*. DWA Deutsche Vereinigung für Wasserwirtschaft, Abwasser und Abfall e.V.

DWA-A (2006). *Arbeitsblatt DWA-A 117: Bemessung von Regenrückhalteräumen. DWA-Regelwerk.* DWA Deutsche Vereinigung für Wasserwirtschaft, Abwasser und Abfall e.V.

Dyck, S. and G. Peschke (1995). *Grundlagen der Hydrologie*. Verlag für Bauwesen.

Edwards, I., W. Jackon, and P. Fleming (1974, August). Tipping bucket gauges for measuring run-off from experimental plots. *Agricultural Meteorology 13*(2), 189–201.

Endlicher, W. (2008). Heat waves, urban climate and human health. In J. Marzluff, E. Shulenberger, W. Endlicher, M. Alberti, G. Bradley, C. Ryan, C. ZumBrunnen, and U. Simon (Eds.), *Urban Ecology - An International Perspective on the Interaction Between Humans and Nature*, pp. 269–280. Springer.

European Lysimeter Plattform (2008). online: http://www.lysimeter.com.

Fank, J., E. Steinitzer, F. Feichtinger, and P. Cepuder (2004). Messdaten und modellkalibration an der forschungsstation wagna und daraus abzuleitende anforderungen an messstellen zur kalibration von bodenwasserhaushalts- und stofftransportmodellen. In D. Klotz (Ed.), *Untersuchungen zur Sickerwasserprognose in Lysimetern. GSF-Bericht 02/04.*, pp. 79–86. Klotz, D.

Faram, M., R. Ashley, C. P.R., and R. Andoh (2010). Appropriate drainage systems for a changing climate. *Proceedings of the ICE - Engineering Sustainability 163*, 107–116.

Ferguson, B. (2005). *Porous Pavements - integrated studies in water management and land development*, Chapter 4. Porous Pavement Hydrology, pp. 119–170. Taylor & Francis, New York.

Flötter, O. (2006). Wasserhaushalt gepflasterter Strassen und Gehwege: Lysimeterversuche and drei Aufbauten unter praxisnahen Bedingungen unter Hamburger Klima. In *Hamburger Bodenkundliche Arbeiten*, Volume 58, pp. 330. Institut für Bodenkunde. Universität hamburg.

Geiger, W., H. Dreiseitl, and J. Stemplewski (2009). *Neue Wege für das Regenwasser*, Volume 3. Oldenbourg Industrie Verlag.

Glugla, G. and P. Krahe (1995, March). Abflussbildung in urbanen gebieten. In *Verfügbarkeit von Wasser, 8. Wissenschaftliche Tagung des DVWK*. Deutscher Verband f'ur Wasserwirtschaft und Kulturbau: DVWK.

Göbel, P., C. Dierkes, H. Kories, J. Messer, E. Meissner, and W. Coldewey (2007). Impacts of green roofs and rain water use on the water balance and groundwater levels in urban areas. *Grundwasser 12*(3), 189–200.

Green, H. W. and G. A. Ampt (1912). Studies on soil phyics. Part II - the permeability of an ideal soil to air and water. *The Journal of Agricultural Science 4*(01), 1–24.

Green, I. R. A. (1986). An explicit solution of the modified horton equation. *Journal of Hydrology 83*(1-2), 23–27.

Habib, E., W. F. Krajewski, and A. Kruger (2001). Sampling errors of tipping-bucket rain gauge measurements. *Journal of Hydrologic Engineering 6*(2), 159–166.

Heinzmann, B. (1998). Improvement of the surface water quality in the berlin region. *Water Science & Technology 38*(6), 191–200.

Hillel, D. (1998). *Environmental Soil Physics*. London: Academic Press.

Illgen, M., K. Harting, T. Schmitt, and A. Welker (2007). Runoff and infiltration characteristics of pavement structures-review of an extensive monitoring program. *Water Science & Technology 56*(10), 133–140.

IPS (2005). *STROM Handbuch*. Ingenieurgesellschaft Prof. Dr. Sieker.

Khan, A. and C. Ong (1997). Design and calibration of tipping bucket system for field runoff and sediment quantification. *Journal of Soil and Water Conservation 52*, 437–443.

Klingelmann, E. (2009, April). Sorption and leaching of glyphosate on partly sealed urban areas. Master's thesis, Technische Universität Berlin.

Kuttler, W. (1998). Stadtklima. In H. Sukopp and R. Wittig (Eds.), *Stadtökologie*, pp. 125–167. Stuttgart: Gustav Fischer Verlag.

Kwon, K.-H. (2008). *Ein Entscheidungshilfesystem für die Planung dezentraler Regenwasserbewirtschaftungsmaßnahmen in Siedlungsgebieten Koreas*. Ph. D. thesis, von der Fakultät VI - Planen Bauen Umwelt der Technische Universität Berlin.

Lanthaler, C. (2006). Updated information about lysimeter and soil hydrology measuring sites in europe. European Lysimeter Plattform. online http://www.lysimeter.at.

Mansell, M. and F. Rollet (2009). The effect of surface texture on evaporation, infiltration and storage properties of paved surfaces. *Water Science & Technology 60*(1), 71–76.

McCuen, R. (2004). *Hydrologic analysis and design*. Pearson Education.

Meissner, R., H. Rupp, J. Seeger, G. Ollesch, and G. Gee (2010). A comparison of water flux measurements: passive wick-samplers versus drainage lysimeters. *European Journal of Soil Science 61*, 609–621.

Nakayama, T. and T. Fujita (2010, May). Cooling effect of water-holding pavements made of new materials on water and heat budgets in urban areas. *Landscape and Urban Planning 96*(2), 57–67.

Nehls, T. (2007, January). Water and heavy metal fluxes in paved urban soils. Master's thesis, Technische Universität Berlin.

Nehls, T., G. Jozefaciuk, Z. Sokolowska, M. Hajnos, and G. Wessolek (2007). Filter properties of seam material from paved urban soils. *Hydrology and Earth System Sciences Discussions 4*(4), 2625–2657.

Nehls, T., G. Jozefaciuk, Z. Sokolowska, M. Hanjos, and G. Wessolek (2006, January). Pore-system characteristics of pavement seam materials of urban sites. *J. Plant Nutr. Soil Sci. 169*, 16–24.

Niemczynowicz, J. (1999, March). Urban hydrology and water management - present and future challenges. *Urban Water 1*(1), 1–14.

Niesel, A. (2002). *Bauen mit Grün. Die Bau- und Vegetationstechnik des Landschafts- und Sportplatzbaus.* Parey. Berlin.

Pecher, K. and H. Hoppe (2011). Künftige bemessung von kanalisationen. *Korrespondenz Abwasser Abfall 58*(2), 121–127.

Philip, J. R. (1957a). The theory of infiltration: 1. the infiltration equation and its solution. *Soil Science 83*(5), 345–358.

Philip, J. R. (1957b). The theory of infiltration: 4. sorptivity and algebraic infiltration equations. *Soil Science 84*(3), 257–264.

Pillsbury, A., J. Osborn, R. Pelishek, and S. Te (1962). Effects of vegetation manipulation on disposition of precipitation on chaparral-covered watersheds. *Journal of Geophysical Research 67*, 695–699.

Rim, Y.-N. (2008). Untersuchungen zum Abflusverhalten Flächenbefestigungen in Lysimetern. Master's thesis, Institut für Ökologie. TU Berlin.

Rim, Y.-N., S. Trinks, T. Nehls, N. Litz, and G. Wessolek (2009). Eine wägbare teilversiegelte Lysimeteranlage in Berlin. In *13. Gumpensteiner Lysimetertagung - Lysimeters - Perspectives in research and application.* Gumpenstein, Irdning, Austria, 2009.

Rubin, J. (1966). Theory of rainfall uptake by soils initially drier than their field capacity and its applications. *Water Resour. Res. 2*(4), 739–749.

Schmidt, M. (2001, Mai). Untersuchungen an der lysimeteranlage zur ermittlung von versickerungs- und oberflächenabflusspenden für unterschiedliche gehwegbefestigungen. 2. Zwischenbericht zum Forschungsprojekt. Institut für Landschafts- und Umweltplanung. TU Berlin.

Schramm, M. (1996). Kennzeichnung von unterschiedlichen flächenbefestigungen hinsichtlich ihrer hydraulisch-physikalischen eigenschaften. In J. Breuste, T. Kleidel, T. Meinel, B. Münchow, M. Netzband, and M. Schramm (Eds.), *Erfassung und Bewertung des Versieglungsgrades befestigter Flächen*, Number 12 in UFZ-Bericht, Chapter 3, pp. 1–59. Umweltforschungszentrum Leipzig-Halle.

Schwartzendruber, D. (1974). Infiltration of constant-flux rainfall into soil as analyzed by the approach of green and ampt. *Soil Science 117*(5), 272–281.

Sen, Z. and A. Altunkaynak (2006). A comparative fuzzy logic approach to runoff coefficient and runoff estimation. *Hydrol. Process. 20*(9), 1993–2009.

Senatsverwaltung Berlin für Stadtentwicklung (2001). Umweltatlas berlin. online: http://www.stadtentwicklung.berlin.de, Senatsverwaltung Berlin für Stadtentwicklung.

Sieker, F., H. Sieker, and S. Bandermann (2003). *Naturnahe Regenwasserbewirtschaftung in Siedlungsgebieten*. Expert Verlag.

Sieker, F., H. Sieker, U. Zweynert, and P. Schlottmann (2009). *Konzept für bundeseinheitliche Anforderungen an die Regenwasserbewirtschaftung*, Volume 19/2009. UBA (Umwelt Bundes Amt).

Starke (2011). Effects of different water-permeable pavement designs on evaporation rates (submitted). *Water Science & Technology*.

Starke, P. (2010). Urban evaporation rates for water-permeable pavements. *Water Science & Technology 62*(5), 1161–1169.

Swartzendruber, D. and D. Hillel (1975). Infiltration and runoff for small field plots under constant intensity rainfall. *Water Resour. Res. 11*(3), 445–451.

Tol, R. S. J. (2002). Estimates of the damage costs of climate change - Part I. Benchmark Estimates. *Environmental and Resource Economics 21*, 47–73.

Townsend, M., M. Mahoney, J. A. Jones, K. Ball, J. Salmon, and C. F. Finch (2003). Too hot to trot? exploring potential links between climate change, physical activity and health. *Journal of Science and Medicine in Sport 6*(3), 260–265.

Wessolek, G. (1993). Erarbeitung eines Schlüssels zur Einschätzung von Versickerung und Oberflächenabfluss versiegelter Flächen Berlins. Im Auftrag der Bundesanstalt für Gewässerkunde, Aussenstelle Berlin, unpublished.

Wessolek, G. (1994). Auswertung von Versuchen zur Ermittlung der Abflussverhältnisse unterschiedliche versiegelter und kanalisierter Flächen Berlins. Im Auftrag der Bundesanstalt für Gewässerkunde, Aussenstelle Berlin, unpublished.

Wessolek, G. (2001). Bodenüberformung und -versiegelung. In H.-P. Blume, P. Felix-Henningsen, W. R. Fischer, H.-G. Frede, R. Horn, and K. Stahr (Eds.), *Handbuch der Bodenkunde*, Volume 11, pp. 29. Landsberg/Lech: ecomed.

Wessolek, G. (2008). Sealing of soils. In J. Marzluff, E. Shulenberger, W. Endlicher, M. Alberti, G. Bradley, C. Ryan, U. Simon, and Z. C. (Eds.), *Urban Ecology: An International Perspective on the Interaction Between Humans and Nature*, Chapter 3, pp. 161–179. Springer.

Wessolek, G. and M. Facklam (1997). Standorteigenschaften und wasserhaushalt von versiegelten flächen. *Journal of Plant Nutrition and Soil Science 160*(1), 41–46.

Wessolek, G. and M. Facklam (1999). Aspekte zur wasserbilanz versiegelter standorte. In W. Burghardt, B. Mohs, and B. Winzig (Eds.), *Regenwasserversickerung und Bodenschutz*, Chapter Bodenkundliche Grundlagenuntersuchungen, pp. 50–56. Bundesverband Boden.

White, E. and P. Rhodes (1970). A tipping bucket recorder for use in stem flow studies. *Journal of Applied Ecology 7*, 349–351.

W.M.O. (2006). *Guide to Meteorological Instruments and Methods of Observation*, Volume 7. Edition. online: http://www.wmo.int.

Yu, B., C. Ciesiolka, C. Rose, and K. Coughlan (1997). Note on sampling errors in the rainfall and runoff data collected using tipping bucket technology. *Transactions of the Asae 40*, 1305–1309.